

001
002
003
004
005
006
007
008
009
010
011
012
013
014
015
016
017
018
019
020
021
022
023
024
025
026
027
028
029
030
031
032
033
034
035
036
037
038
039
040
041
042
043
044
045
046

Microbial symbionts buffer hosts from the demographic costs of environmental stochasticity

Joshua C. Fowler^{1,2*}, Shaun Ziegler³, Kenneth D. Whitney³,
Jennifer A. Rudgers³, Tom E.X. Miller¹

¹*Department of BioSciences, Rice University, Houston, 77005, TX, USA.

²Department of Biology, University of Miami, Miami, 33146, FL, USA.

³Department of Biology, University of New Mexico, Albuquerque, 87131, NM, USA.

*Corresponding author(s). E-mail(s): jcf221@miami.edu;

Contributing authors: shaun.ziegler@gmail.com; whitneyk@unm.edu;

jrudgers@unm.edu; tom.miller@rice.edu;

Phone: 719-359-2960

Author Contributions

J.C.F. contributed to data collection, data analysis, and led manuscript drafting. S.Z. contributed to data collection and manuscript revisions. K.D.W. contributed to research conception, data collection, and manuscript revisions. J.A.R. established transplant plots, contributed to research conception, data collection, and manuscript revisions. T.E.X.M. contributed to research conception, data collection, data analysis, and manuscript revisions.

Data and Code Accessibility

Data will be made accessible as an Environmental Data Initiative package online
DOI: [updated here when available](#). Code for all analysis is available through
<https://github.com/joshuacfowler/Grass-Endophyte-Stochastic-Demography>

Article Type: Letter

Running Title: Symbiont-mediated demographic buffering

Keywords: stochastic demography, plant-microbe interactions, environmental variability, symbiosis, mutualism, long-term data, life history, Epichloë, Poaceae

This file contains: Abstract (150 words), Main Text (5000 words), Figures (1-5); Supporting Information - Supplemental Methods, Supplemental Figures S1-S89, Supplemental Tables S1-S3, References (84)

047
048
049
050
051
052
053
054
055
056
057
058
059
060
061
062
063
064
065
066
067
068
069
070
071
072
073
074
075
076
077
078
079
080
081
082
083
084
085
086
087
088
089
090
091
092

Abstract

Species' persistence in increasingly variable climates will depend on resilience against the fitness costs of environmental stochasticity. Most organisms host microbiota that shield against stressors. Here, we test the hypothesis that, by limiting exposure to temporally variable stressors, microbial symbionts reduce hosts' demographic variance. We parameterized stochastic population models using data from a 14-year symbiont-removal experiment including seven grass species that host *Epichloë* fungal endophytes. Results provide novel evidence that symbiotic benefits arise not only through improved mean fitness, but also through damped inter-annual variance. Hosts with "fast" life history traits benefited most from symbiont-mediated demographic buffering. Under current climate conditions, contributions of demographic buffering were modest compared to benefits to mean fitness. However, simulations of increased stochasticity amplified benefits of demographic buffering and made it the more important pathway of host-symbiont mutualism. Microbial-mediated variance buffering is likely an important, yet cryptic, mechanism of resilience in an increasingly variable world.

Introduction	093
Global climate change involves heterogenous changes in environmental variability, including an increasing frequency of extreme weather events and of “whiplash events” that alternate between climate extremes [? ? ? ?]. Yet, the ecological consequences of changing variability are less well understood than those of changing means, such as long-term warming or drying. Incorporating realistic variability into forecasts of population dynamics can improve predictive ability [?].	094
Classic theory predicts that long-term population growth rates (equivalently, population mean fitness) will decline under increased environmental stochasticity because costs of bad years outweigh benefits of good years – a consequence of nonlinear averaging [? ?]. For example, in unstructured populations, the long-term stochastic growth rate in a fluctuating environment (λ_S) will always be lower than the arithmetic mean of annual growth rates ($\bar{\lambda}_t$) by an amount proportional to the environmental variance (σ^2):	095
$\log(\lambda_S) \approx \log(\bar{\lambda}_t) - \frac{\sigma^2}{2\bar{\lambda}_t}$	096
Populations structured by size or stage experience similar costs of temporal variability [? ?]. There are accordingly two pathways to increase population viability in variable environments: increase the arithmetic mean growth rate and/or dampen temporal fluctuation in growth rates, also called “demographic buffering”.	097
Both inherent characteristics of species and the environments they experience can buffer demographic fluctuations. Inherent characteristics include life history traits [?], trade-offs among vital rates [?], and transient shifts in population structure [?]. For example, theory predicts long-lived species, those on the slow end of the slow-fast life history continuum, to be less sensitive to environmental variability than short-lived species [?], a pattern with empirical support across plants [? ?] and animals [? ?]. Demographic variance is also determined by external abiotic factors, such as the magnitude of environmental variability [?] or environmental autocorrelation [? ?]. The complex interplay of these factors determines populations’ risk of extinction [1] and underlies management strategies promoting ecosystem resilience [?]. Yet, little is known about how inter-specific interactions contribute to demographic buffering [?].	100
Most multicellular organisms host symbiotic microbes that affect growth and performance [? ?], many of which are vertically transmitted from maternal hosts to offspring [?]. Vertical transmission links the fitness of hosts and symbionts in a feedback loop that selects for mutual benefits [?]. These mutualistic microbes can protect hosts from stressful environmental conditions including drought, extreme temperatures, or natural enemies [? ?]. Some well studied examples include bacterial symbionts of insects that provide hosts with thermal tolerance through the production of heat-shock proteins [?], and fungal symbionts of plants that produce anti-herbivore and drought-protective compounds [? ? ?]. However, these diverse protective symbioses are context-dependent: the magnitude of benefits depends on environmental conditions [? ?] and thus will vary temporally in stochastic environments [?]. We hypothesized that context-dependent benefits from symbionts may buffer host populations against variability through strong benefits during harsh periods and neutral or even costly outcomes during benign periods, reducing the impacts of host exposure to extremes	101
	102
	103
	104
	105
	106
	107
	108
	109
	110
	111
	112
	113
	114
	115
	116
	117
	118
	119
	120
	121
	122
	123
	124
	125
	126
	127
	128
	129
	130
	131
	132
	133
	134
	135
	136
	137
	138

139 and dampening inter-annual variance relative to non-symbiotic hosts (Fig. 1A). Vari-
140 ance buffering is a previously unexplored mechanism by which symbionts may benefit
141 their hosts instead of or in addition to elevating average fitness (Fig. 1C), the focus
142 of most previous research.

143 To test the hypothesis that context-dependent benefits of symbiosis dampen inter-
144 annual variance in host fitness, we used a combination of long-term field experiments
145 and stochastic demographic modeling. We used cool-season grasses and *Epichloë* fun-
146 gal endophytes, a tractable experimental model in which non-symbiotic plants can be
147 derived from naturally symbiotic plants through heat treatment, providing a contrast
148 of symbiont effects that controls for the confounding influence of host genetic back-
149 ground. *Epichloë* endophytes are specialized symbionts growing intercellularly in the
150 aboveground tissue of ~ 30% of *C₃* grass species [?]. These fungi are primarily trans-
151 mitted vertically from maternal plants through seeds [?]. They produce a variety of
152 alkaloids that can protect host plants from natural enemies [?] and drought stress [?].

153 Over 14 years (2007–2021), we collected longitudinal demographic data on the
154 survival, growth, reproduction, and recruitment of all plants within replicated
155 endophyte-symbiotic and endophyte-free populations at our field site in southern Indi-
156 ana, USA. Through taxonomic replication (seven host-symbiont species pairs) we
157 aimed to understand whether host life history traits could explain inter-specific vari-
158 ation in the magnitude of demographic buffering through symbiosis. We used this
159 long-term data to parameterize Bayesian stochastic population projection models.
160 Specifically, we (1) quantified the effect of symbiosis on the mean and variance of host
161 vital rates (survival, growth and reproduction) and fitness, (2) evaluated the relation-
162 ship between host life history traits and the magnitude of symbiont-mediated variance
163 buffering, (3) determined the relative contributions of symbiont-mediated mean and
164 variance effects to host fitness, and (4) projected how increased environmental stochas-
165 ticity (expected under future climates) changes the importance of variance buffering
166 as a pathway of host-symbiont mutualism.

167

168 Materials and Methods

169

170 Study site and species

171

172 This study was conducted at Indiana University's Lilly-Dickey Woods Research and
173 Teaching Preserve (39.238533, -86.218150) in Brown County, Indiana, USA. This
174 site is part of the Eastern broadleaf forests of southern Indiana, where the ranges
175 of many understory cool-season grass species overlap. We focused on seven of these
176 grasses (*Agrostis perennans*, *Elymus villosus*, *Elymus virginicus*, *Festuca subverticil-*
177 *lata*, *Lolium arundinaceum*, *Poa alsodes*, and *Poa sylvestris*), each of which hosts a
178 unique species of *Epichloë* endophyte (Table S1). All are native to eastern North
179 America except the Eurasian species *L. arundinaceum*.

180

181 Seeds from local, naturally symbiotic populations of the seven focal host species
182 were collected during summer-fall 2006. Seeds were disinfected with a heat treatment
183 or left untreated to generate symbiont-free (S-) and symbiotic (S+) plants from the
184 same genetic lineages. In fall of 2007 and spring of 2008, we established 10 3x3 m plots
for *A. perennans*, *E. villosus*, *E. virginicus*, *F. subverticillata*, and *L. arundinaceum*

and 18 plots for *P. alsodes* and *P. sylvestris*. Each plot was randomly assigned to be planted with 20 evenly spaced symbiotic (S+) or symbiont-free (S-) plants. Full details of endophyte removal, plant propagation and field set-up are provided in *Supporting Information - Supplemental Methods and Table S1*.

Long-term demographic data collection

Each summer (2008–2021) we censused all individuals in each plot for survival, growth and reproduction. Plots contained 13.3 individuals/m² on average during the study. Each census year was a sample of inter-annual variation (n = 14 years, comprising 13 demographic transition years). We censused each species during its peak fruiting stage (May: *Poa alsodes*, *Poa sylvestris*; June: *Festuca subverticillata*; July: *Elymus villosus*, *Elymus virginicus*, *Lolium arundinaceum*; September: *Agrostis perennans*), such that the censuses were pre-breeding and new recruits came from the previous years' seed production (Fig. S1 shows a generalized life cycle diagram). Leaf litter was cleared out of each plot before the census, to aid in locating plants. For each tagged plant, we determined survival, measured size as a count of tillers, and collected reproductive data as counts of reproductive tillers and seed-bearing spikelets on up to three reproductive tillers. We also tagged all unmarked recruits from the previous years' seed production and collected the same demographic data. New recruits typically had one tiller and were non-reproductive. In 2008 through 2010, we took counts of seeds per inflorescence for all reproducing individuals in the plots to relate inflorescence and spikelet counts to seed production. In 2018, we stopped collecting data for *L. arundinaceum*, which had very high survival and low recruitment, and consequently low variation in population size across years. In total, the dataset included demographic information for 16,789 individual host-plants and 31,216 transition-year observations.

Vital rate modeling

Equipped with demographic data, we fit statistical models for adult survival, seedling survival, adult growth, seedling growth, reproductive status (flowering or vegetative), fertility of flowering plants (number of inflorescences), production of seed-bearing spikelets (number per inflorescence), the average number of seeds per spikelet, and the recruitment of seedlings from the preceding year's seed production. We fit vital rates as generalized linear mixed models in a hierarchical Bayesian framework using RStan [?] which allowed us to isolate endophyte effects on vital rate means and variances, borrow strength across species for some variance components, and propagate uncertainty from individual-level vital rates to population projection models [?]. All size-structured models included the same linear predictor, including two key parameters for each species: one which described the effect of endophyte symbiosis on the mean of that vital rate, and another which described inter-annual variance in the vital rate for symbiotic and symbiont-free plants, estimated using random year effects specific to each species and endophyte status. This species- and endophyte status-specific random year effect allowed us to quantify effects of endophytes on inter-annual variance for each vital rate. Other parameters accounted for size structure in the

231 data (defined as the number of tillers) as well as differences between originally trans-
 232 planted plants (started in a greenhouse) and those which recruited naturally into the
 233 plots. Each vital rate model included a random effect for plot variance shared across
 234 species. Full details of the statistical analyses are included in *Supporting Information*
 235 - *Supplemental Methods*.

236

237 Stochastic population model

238

239 We built stochastic matrix projection model for each host species. We parameter-
 240 ized the models using the fitted statistical vital rate models in a manner similar to
 241 continuous IPM models [?], while accounting for the discrete data representing our
 242 focal species' growth [?]. Each matrix projection model included two state variables:
 243 r_t (the number of newly recruited individuals in year t which we assume to be non-
 244 reproductive), and \mathbf{n}_t (a vector including all non-seedling individuals of discrete sizes
 245 $x \in \{1, 2, \dots, U\}$ ranging from one to the maximum number of tillers U). We use these
 246 two state variables to avoid assuming demographic equivalence between seedling and
 247 non-seedling one-tiller plants. We used the same model structure, corresponding to
 248 a pre-breeding census, for each species and endophyte status (not shown in model
 249 notation for readability; Fig. S1).

250 The number of recruits in year $t + 1$ is given by:

251

$$252 \quad r_{t+1} = \sum_{x=1}^U P(x; \boldsymbol{\tau}_P) F(x; \boldsymbol{\tau}_F) K(x; \boldsymbol{\tau}_K) D R(\boldsymbol{\tau}_R) n_t^x \quad (2)$$

253

254 The total number of seeds produced by a maternal plant of size x is the product of
 255 the size-specific probability of flowering P , the number of inflorescences conditional
 256 on flowering F , the number of spikelets per inflorescence K , and the number of seeds
 257 per spikelet D . Multiplying by the probability of transitioning from seed to seedling
 258 R gives a per-capita seedling production rate, which is multiplied by the number of
 259 plants of size x (n_t^x , the x^{th} element of \mathbf{n}_t) and summed over all sizes. Each function
 260 also depends on species- and endophyte-specific year random effects for that vital rate
 261 ($\boldsymbol{\tau}$, a vector of year-specific values).

262 The number of y -sized plants in year $t + 1$ is given by:

263

$$264 \quad n_{t+1}^y = Z(y; \boldsymbol{\tau}_Z) B(\boldsymbol{\tau}_B) r_t + \sum_{x=1}^U S(x; \boldsymbol{\tau}_S) G(x, y; \boldsymbol{\tau}_G) n_t^x \quad (3)$$

265

266

267 where n_{t+1}^y is the y^{th} element of vector \mathbf{n}_{t+1} . The first term on the right hand
 268 side of Eqn. 3 represents growth (Z) and survival (B) of seedling recruits. The second
 269 term includes survival of previously x -sized plants and the growth of survivors from
 270 size x to y , summed over all x . To avoid predictions of unrealistic growth outside of
 271 the observed size distribution, we capped the growth function for plants at the 97.5th
 272 percentile of observed sizes for each host species [?]. We analyzed projection models
 273 constructed from parameters representing the dynamics of naturally recruited plants.

274 Each vital rate function in Eqns. 2 and 3 has separate intercepts and year ran-
 275 dom effects for symbiotic and symbiont-free populations, allowing us to calculate the

effect of endophyte symbiosis on the mean, variance, and coefficient of variation (CV) of λ_t , the dominant eigenvalue of the year- and endophyte-specific projection matrix.	277
This model treats climate drivers implicitly through year-specific random effects. We also developed a climate-explicit version with additional parameters defining the relationship between either annual or growing season drought index and each vital rate (<i>Supporting Information - Supplemental Methods</i>).	278
	279
	280
	281
	282
To calculate stochastic population growth rates (λ_S) for each host species and endophyte status we simulated population dynamics for 1000 years by randomly sampling from the 13 annual transition matrices, discarding the first 100 years to minimize the influence of initial conditions. Sampling observed transition matrices (rather than independently sampling regression coefficients) produces models that realistically capture inter-annual variation by preserving vital rate correlations [?]. We tallied total population size at each time step as $N_t = r_t + \sum_{x=1}^U n_t^x$ and calculated the stochastic growth rate as $\log(\lambda_S) = E[\log(\frac{N_t}{N_{t+1}})]$ [? ?]. We calculated total effects of endophyte symbiosis as the difference in λ_S between S+ and S- populations. We propagated uncertainty from the vital rates to the calculation of λ_S using 500 draws from model posteriors.	283
	284
	285
	286
	287
	288
	289
	290
	291
	292
	293
	294
Life History Analysis	295
We collected metrics describing each host species' life history to test the relationship between pace of life and variance buffering (Table S2). We recorded seed size as the average lemma length from the Flora of North America [?]. We calculated the 99th percentile of maximum observed age for symbiont-free plants from the census data for each species. Using the Rage package [?], we calculated generation time, longevity, net reproductive rate R_0 , Keyfitz entropy (describing survivorship across lifespan), and Demetrius entropy (describing reproduction across lifespan) from the mean transition matrix for symbiont-free populations. Next, we fit Bayesian phylogenetic mixed-effects models using the brms package [?] to test the relationship between each life history trait and the effect of symbiosis on the CV of λ_t (a measure of variance buffering) while controlling for phylogenetic non-independence. We pruned species-level phylogenies of plants [?] and <i>Epichloë</i> fungi [?] to include the focal species (or a congener for one host), and defined separate phylogenetic covariance matrices from these pruned trees for host and symbiont species. We propagated uncertainty in the estimated variance buffering effect with a measurement error model. The statistical analysis is described in full in the <i>Supporting Information - Supplemental Methods</i> .	296
	297
	298
	299
	300
	301
	302
	303
	304
	305
	306
	307
	308
	309
	310
	311
	312
	313
Mean-variance decomposition	314
We decomposed total endophyte effects on λ_S into contributions from effects on vital rate means, and variances. Specifically, we repeated the calculation of S+ and S- λ_S described above for two additional "treatments": (1) endophyte effects on mean vital rates only, with inter-annual variances shared between S+ and S- at the S- reference level for all vital rates, and (2) endophyte effects on vital rate variances only, with vital rate means shared between S+ and S- at the S- reference level. The combination of all four λ_S treatments (S+ vital rate means and variances, S- means and variances,	315
	316
	317
	318
	319
	320
	321
	322

323 S+ means with S- variances, S- means with S+ variances) allowed us to quantify
324 the extent that overall effects of symbiosis derive from changes in vital rates means,
325 variances, and their interaction. The interaction occurs because the variance penalty
326 to stochastic growth is proportional to the arithmetic mean of annual growth rates
327 (as in Eq. 1, for example) such that variance is more detrimental for populations with
328 lower average growth rates. To quantify how mean and variance effects of symbionts
329 arise through effects on different vital rates, we performed an additional decomposition
330 described in *Supporting Information Supplemental Methods* that isolates symbiont
331 effects on growth and survival from effects on fertility and recruitment.

332 We simulated scenarios of increased variance relative to that observed during our
333 study by sampling subsets of the 13 observed annual transition matrices. We created
334 two scenarios of increased environmental variance by sampling the transition matrices
335 associated with the set of either six or two most extreme λ_t values for S- populations.
336 These extreme λ_t values represent the best and worst years experienced by symbiont-
337 free populations. By sampling away from an average year in both directions, the six-
338 and two- years scenarios increased standard deviation of annual host growth rates by
339 1.3 and 2.1 times, respectively, without changing mean growth rates (< 2.1% difference
340 in $\bar{\lambda}_t$ between simulation treatments, Fig. S80). We performed the same mean-variance
341 decomposition for these scenarios as described above.

342

343 Results

344

345 Symbionts buffer host demographic variance

346

347 Across 14 census years, endophytes reduced inter-annual variance for 66% (37/56) of
348 host species-vital rate combinations (average Cohen's D for effects on vital rate stan-
349 dard deviation: -0.15) (Fig. 2A; Fig. S22 - Fig. S29). Endophytes also increased mean
350 vital rates for the majority (36/56) of host species-vital rate combinations (average
351 Cohen's D for effects on vital rate mean: 0.15), and benefits were particularly strong
352 for host survival, plant growth and recruitment (Fig. 2A; Fig. S2 - S11). The mag-
353 nitude of mean and variance effects differed among hosts and vital rates. Symbiont
354 effects on vital rate variance were as large and even exceeded mean effects for certain
355 species. For example, endophytes modestly increased mean adult survival (Fig. 2C)
356 and strongly reduced variance in survival (Fig. 2D) for *Festuca subverticillata*, while
357 for *Poa alsodes*, variance buffering was more apparent in seedling growth and inflores-
358 cence production (Fig. 2E). Additionally, some vital rates showed costs of symbiosis.
359 Symbiotic individuals of *A. perennans* grew larger than symbiont-free hosts (Fig. 2B),
360 yet endophytes also reduced this species' mean recruitment (Fig. 2A). Similarly, endo-
361 phytes increased variance for certain species' vital rates, including seedling growth for
362 *Elymus villosus* and *Festuca subverticillata* (Fig. 2A).

363 Because not all vital rates contribute equally to fitness, we used stochastic matrix
364 models to integrate diverse vital rate effects described above into comprehensive mea-
365 sures for the arithmetic mean and variance of year-to-year fitness (λ_t). On average
366 across host species, mean fitness of S+ populations increased by more than 10%
367 (> 92% confidence that endophytes increased $\bar{\lambda}_t$) and inter-annual variability in fitness
368

was 26% lower ($> 86\%$ confidence that endophytes decreased the coefficient of variation of λ_t) than S- populations (Fig. 3). For some host species, the CV of λ_t declined by more than 62% (*P. alsodes*, *F. subverticillata*), while for others, endophyte effects on variance were substantially smaller (5% lower for *E. villosus*, 13% lower for *A. perennans*), or even positive (37% increase for *E. virginicus*). Considering mean and variance effects together, none of the host-symbiont pairings were antagonistic (i.e., with endophytes that both decreased mean fitness and increased variance) (Fig. 3C)

369
370
371
372
373
374
375
376

Faster life histories predict stronger symbiont-mediated variance buffering

377
378
379

Hosts with slow life history trait values experienced weaker variance buffering from endophytes than those with fast life histories (Fig. 4). Variance buffering was stronger for host species with shorter lifespan (Fig. 4A; 67% probability of positive relationship with empirically observed maximum plant age) and smaller seeds (Fig. 4B; 65% probability of positive relationship with seed length). Other life history traits similarly had weak, positive support for the prediction that faster life history traits correlate with stronger variance buffering (Fig. S83-S85). Models indicate moderate phylogenetic signal in the effect of variance buffering (average Pagel's λ of 0.22 (90% CI: 0-0.8) and of 0.56 (90% CI: 0-0.9) from models including host and symbiont phylogeny respectively (Table S2)).

380
381
382
383
384
385
386
387
388
389
390
391
392
393
394
395
396
397
398
399
400
401
402
403
404
405
406
407
408
409
410
411
412
413
414

Contributions from variance buffering are weak relative to mean effects

391
392
393

To evaluate the relative importance of mean fitness benefits and variance buffering as alternative pathways of mutualism, we decomposed the overall effect of the symbiosis on stochastic growth rates λ_S using simulations including either the full symbiosis effect (both mean and variance effects), mean effects alone, variance effects alone, or neither mean nor variance effects. Overall, the full effect of symbiosis on λ_S , averaged across host species, provided strong evidence of grass-endophyte mutualism (99% certainty of a positive total effect on λ_S) (Fig. 5; see Fig. S81 for individual host species). Contributions to this full effect derived from both mean and variance buffering effects, as well as a slightly negative interaction (i.e., the combined influence of mean and variance effects was smaller than the sum of their individual effects). Endophytes' contributions to λ_S from mean effects were four times greater, averaged across species, than contributions from variance buffering (Fig. 5), suggesting that, under the regime of environmental variability represented by our 14-year study, dampened fluctuations in fitness via variance buffering was a less important element of symbiont benefits than increased mean fitness. Decomposing this result further into contributions through different vital rates demonstrated that demographic buffering arose primarily from symbionts' effects on host survival and growth, rather than from effects on reproduction (Fig. S82). Results for individual host species were largely consistent with cross-species trends (Fig. S71). The full effect of symbiosis on λ_S was positive for five out of seven host species, with statistical confidence ranging from 78% to $> 99\%$

415 certainty. The exceptions were *P. sylvestris* and *A. perennans*, for which our analy-
416 sis indicated effectively neutral symbionts in their overall fitness effect (42% and 57%
417 posterior probability of positive effects respectively; Fig. S71).

418

419 **Variance buffering strengthens under increased environmental 420 variability**

421

422 To simulate increased variability, we repeated the decomposition of λ_S for two alterna-
423 tive scenarios, randomly sampling transition matrices that represented either the six or
424 two most extreme years, subsets of the thirteen transition matrices across the 14-year
425 study period. Increased variability elicited stronger mutualistic benefits of endophyte
426 symbiosis than ambient variability (Fig. 5; overall effect of the symbiosis increased by
427 ~ 2 fold). This increase was driven by increased contributions from variance buffering
428 (from a 16% contribution in the ambient scenario to a 54% contribution in the most
429 variable scenario) rather than from greater mean effects. In the most variable scenario,
430 the relative importance of mean and variance effects reversed, with variance buffering
431 contributions that were 1.2 times greater than mean contributions, averaged across
432 species (Fig. 5).

433

434 **Discussion**

435

436 Across seven host species, eight vital rates, 14 years, and 16,789 individuals, our anal-
437 ysis provided the first empirical evidence, to our knowledge, of demographic buffering
438 conferred by microbial symbionts. Our taxonomically-replicated, long-term field exper-
439 iments that manipulated the presence/absence of fungal symbionts in plants revealed
440 that heritable microbes can commonly benefit hosts not only through improved mean
441 fitness – the focus of most previous research – but also through buffering against envi-
442 ronmental variance (Fig. 1). Benefits to mean fitness dominated the overall fitness
443 advantage of endophyte symbiosis under observed environmental variability. However,
444 the strongest symbiotic benefits derived from the combination of both mean effects
445 and variance buffering (Fig. 1B), and simulation experiments point to an increasing
446 role for demographic buffering under increased temporal environmental stochastic-
447 ity (Fig. S81-S82). There is growing interest in demographic buffering as a potential
448 source of resilience against increased stochasticity under global change [?]. Our results
449 suggest that biotic interactions, and microbial mutualisms in particular, may be an
450 under-appreciated mechanism of demographic buffering. In fact, any interaction that
451 is subject to context-dependence – where the magnitude of cost or benefit depends on
452 harshness of the environment – holds potential to modify demographic variance across
453 years. However, long-term experimental data required to detect such an influence are
454 rarely available.

455 Taxonomic replication of host-symbiont pairs enabled us to generalize beyond the
456 focal taxa and facilitated inference about the *types* of species in which demographic
457 buffering may be more or less likely. Because host taxa with “slow” life history traits,
458 such as long lifespan, may be intrinsically buffered from environmental variability [?
459 ? ?], we predicted that buffering effects of endophyte symbiosis would be stronger
460

in hosts with faster pace of life. Supporting this prediction, we found that shorter-lived and smaller-seeded host species experienced stronger reductions in demographic variance through endophyte symbiosis. Thus, microbial symbiosis may compensate for the lack of intrinsic tolerance of variability conferred by slow life history traits. Future studies may consider fungal life history traits, such as diversity in biologically-active alkaloids, or the production of stromata - fruiting bodies capable of horizontal (contagious) transmission. The host species for which the net mutualism benefit was greatest (*F. subverticillata* and *L. arundinaceum*) (Fig. S81) were among those never observed to produce fungal stromata (Table S2), supporting theoretical expectations that strict vertical transmission drives evolution of strong host-symbiont mutualism [? ?]. We caution that inferences on trait correlates of demographic buffering were subject to large uncertainties (Fig. S83-S84), reflecting relatively narrow taxonomic breadth (closely related grass species in the sub-family Pooideae and their co-evolving symbionts). Understanding of how life history variation modulates the fitness consequences of microbial symbiosis would profit from tests across a wider span of plant and animal groups [?]. We also found relatively consistent, positive effects of endophyte symbiosis on stochastic fitness (Fig. S78-S79), suggesting that variation across host species and vital rates in mean and variance effects (Fig. 3C) may reflect alternative strategies that yield similar net benefits.

While our results highlight symbiont-mediated demographic buffering as a potential source of resilience against increased environmental stochasticity, much work remains to connect symbiont effects on mean and variance to quantitative forecasts of host-symbiont dynamics under global change. Like most temporally stochastic population projection models, our approach quantified demographic variance across years (and simulated increasing variance) without attributing its cause(s). Realistic forecasts for host-symbiont dynamics under environmental change will require explicit connections between driver variables and demographic responses. Reduced sensitivity to drought, as is common in *Epichloë* symbioses [? ? ? ?], is a candidate mechanism that could generate a signature of variance buffering: drought conditions may less costly for S+ hosts, dampening the effects of drought years and reducing fluctuations in fitness through time (Fig. 1). Preliminary climate-explicit analyses indicated that symbionts reduced sensitivity to drought indices for five of seven host taxa (Supporting Information Text; Fig. S88-S89; Table S3). However, we did not find a strong relationship between magnitude of variance buffering and relative drought sensitivities, suggesting that other climatic factors or temporally-varying aspects of the environment may elicit benefits of symbiosis, including documented resistance to herbivory for six of these host taxa [? ?]. Identifying the type and timescale of relevant drivers would allow more direct connections between demographic models and outputs from global climate models.

Symbiont-mediated demographic buffering is a potential target of selection for improved holobiont fitness [?] and carries implications for the evolution of bet-hedging strategies in variable environments. Demographic buffering may be considered a bet-hedging strategy if reduced temporal variance comes at the cost of arithmetic mean fitness [?]. This may be unlikely in this system, where most host species exhibited both reduced variance and elevated mean fitness through symbiosis (Fig. 3C). However,

507 the context-dependent fitness effects that underlie demographic buffering may favor
508 other forms of evolutionary bet-hedging. Theory suggests that imperfect transmission
509 (the production of S- offspring from S+ parent) may be an adaptive host strategy
510 in spatially or temporally varying environments when fitness effects of symbionts are
511 environment-dependent by extending phenotypic variance of offspring and improving
512 the odds of some having the optimal symbiont status for their environment [? ? ?].
513 Imperfect vertical transmission is well-documented in grass-endophyte symbioses [?
514], including our focal taxa (Table S2), and could be incorporated into our model by
515 dynamically linking S+ and S- populations [? ?]. A further step could incorporate
516 diverse symbiont partners (e.g. different strains of *Epichloë* fungi or multiple species
517 within the microbiome) to understand how microbial diversity contributes to host
518 genotypic and phenotypic variance [?].

519 Several limiting features of our study point to new directions and valuable next
520 steps. We focused explicitly on temporal variation and intentionally averaged over
521 spatial heterogeneity. Endophytes may dampen spatial heterogeneity in host fitness
522 in ways that parallel their effects on temporal variance, and this hypothesis could be
523 explored by leveraging the plot replication in our experiment. At larger spatial scales,
524 buffering effects of symbionts may vary across the broad geographic distributions of
525 these eastern North American grass species, especially since historical and projected
526 trends in climate variability are geographically heterogeneous [?]. Finally, our demo-
527 graphic modeling framework could be further “unpacked” to explore other elements
528 of fitness in stochastic environments. We identified damping variance in survival and
529 growth as the key avenue by which symbionts’ variance effects contributed to host
530 fitness (Fig. S82). Elasticity analyses could explore the selection that drives diverse
531 symbiont effects across host vital rates. Small changes in variance of vital rates that
532 are highly important to population growth (i.e. those with high elasticities) may be
533 more strongly selected for than larger changes in less important vital rates [?], and
534 symbionts may even provide an adaptive advantage by increasing temporal variance in
535 certain vital rates (i.e. demographic lability) [?]. Further, our simulations assumed an
536 independently distributed environmental distribution through time, but environmental
537 auto-correlation can be an important component of stochastic population projections
538 [?] and might modify the fitness consequences of symbiont-mediated variance buffer-
539 ing. Similarly, correlated responses of multiple vital rates could amplify or dampen
540 demographic variance [? ? ?]. Our “matrix sampling” approach accounted for vital
541 rate correlations implicitly [?] but exploring whether and how endophyte symbiosis
542 alters the correlation structure of host vital rates could add nuance to understanding
543 of symbionts’ contributions to variance buffering.

544

545 Conclusion

546

547 Ecologists increasingly recognize the importance of symbiotic microbes for host organ-
548 isms and the populations, communities, and ecosystems in which their hosts reside
549 [? ? ? ?]. Despite awareness of these ubiquitous interactions, long-term studies of
550 microbial symbiosis are rare. Our results provide an important advance to improve
551 forecasts of the responses of populations (and symbionts) to increasing environmental
552

stochasticity under global change. We found that, relative to mean fitness benefits, symbiont-mediated variance buffering made weak contributions to host-symbiont mutualism under observed environmental variability. However, demographic buffering is likely to become the dominant benefit that fungal endophytes confer to grass hosts in more variable future environments. Thus, demographic buffering – a cryptic microbial influence that manifests only over long time scales – is poised to become the dominant benefit of symbiosis. This result emerges from the context-dependent nature of grass-endophyte interactions, combined with the observation that environmental stochasticity generates fluctuation in context. These key ingredients, and thus the potential for symbiont-mediated variance buffering, similarly apply to the diverse host-microbe symbioses across the tree of life.

553
554
555
556
557
558
559
560
561
562
563
564
565
566
567
568
569
570
571
572
573
574
575
576
577
578
579
580
581
582
583
584
585
586
587
588
589
590
591
592
593
594
595
596
597
598

599 **Acknowledgments** We thank Mark Sheehan, Ali Campbell, Kyle Dickens, Blaise
600 Willis, and Sar Lindner for contributions to field data collection. We also thank Volker
601 Rudolf, Daniel Kowal, Lydia Beaudrot and Judie Bronstein for helpful comments on
602 and discussion of this project. This research was supported by the National Science
603 Foundation (grants 1754468 and 2208857).

604 **Supplementary information** Supplementary information for this paper includes
605 Supplementary Methods, Figs. S1 to S89, and Tables S1 to S3.
606

607 **References**
608

- 609 [1] Menges, E. S. Applications of population viability analyses in plant conservation.
610 *Ecological Bulletins* 73–84 (2000).
611

612
613
614
615
616
617
618
619
620
621
622
623
624
625
626
627
628
629
630
631
632
633
634
635
636
637
638
639
640
641
642
643
644

Figures

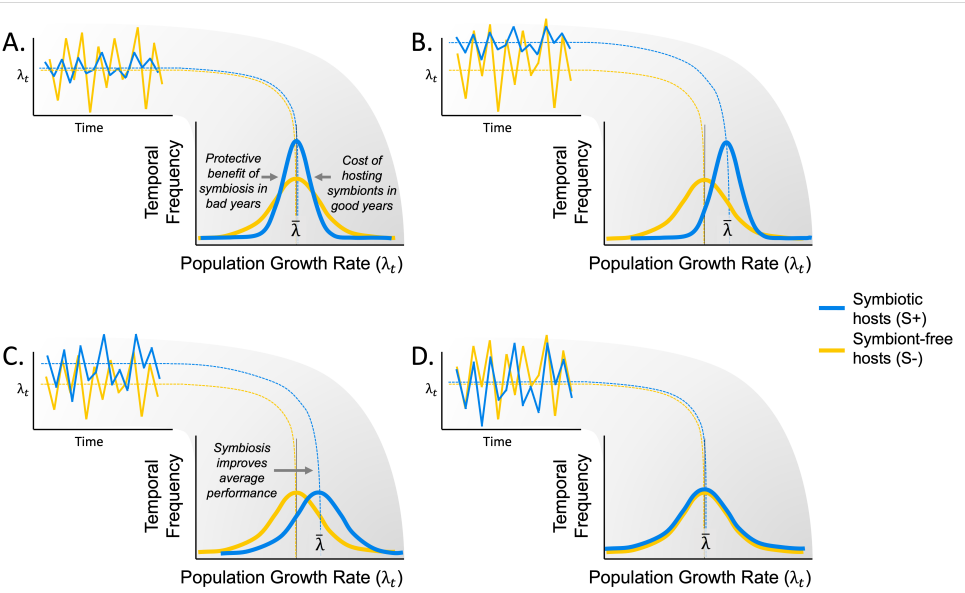
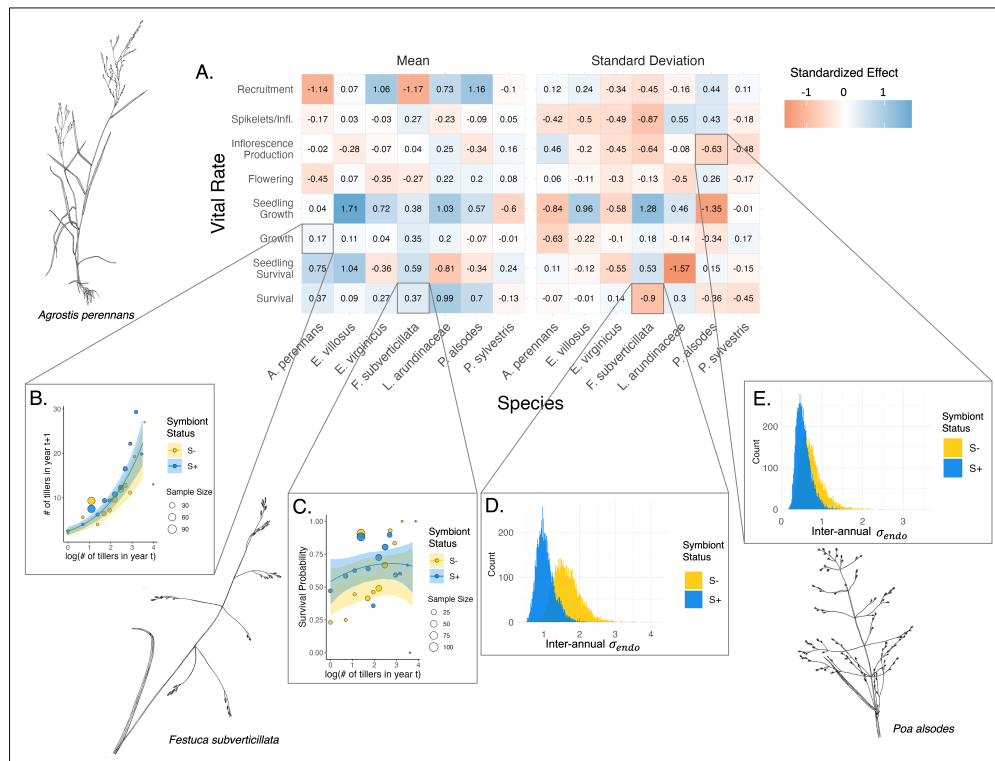


Fig. 1: Hypothesized effects of symbiosis on the mean and variance of annual population growth rates. (A) Context-dependent symbiosis may provide benefits to hosts during harsh years while being neutral or costly during benign years. Temporal variance in populations growth rates of symbiotic host populations (S+; blue lines) is expected to decrease relative to symbiont-free hosts (S-; yellow lines). (B) Symbiosis may improve average performance across years in addition to reducing temporal variance. (C) Consistent benefits of symbiosis could improve average performance across years with no influence on temporal variance. (D) Symbiosis may have an effectively neutral effect on population growth rates.

645
646
647
648
649
650
651
652
653
654
655
656
657
658
659
660
661
662
663
664
665
666
667
668
669
670
671
672
673
674
675
676
677
678
679
680
681
682
683
684
685
686
687
688
689
690

691
692
693
694
695



718
719
720
721
722
723
724
725
726
727
728
729
730
731
732
733
734
735
736

Fig. 2: Endophyte symbiosis altered host vital rates. (A) Shading represents the posterior mean standardized effect size (Cohen's D) of endophyte symbiosis on mean or standard deviation of host vital rates (blue indicates that symbiosis increased the mean or standard deviation and red indicates a reduction). Endophytes' diverse vital rate effects include increased (B) mean growth of *A. perennans* and (C) mean survival probability of *F. subverticillata*. Endophyte presence also reduced inter-annual standard deviation in (D) the survival of *F. subverticillata* and (E) the fertility of *P. alsodes*. In panels B-C, expected mean vital rates that average across years and plots are shown with 80% credible intervals along with points representing data binned by size for symbiotic (S+) and symbiont-free (S-) plants. Panels D-E show estimated posterior distributions of endophyte-status specific inter-annual standard deviation ($\sigma_{\tau_{e,h}}^2$) for each vital rate for S+ (blue) and S- (beige) populations. Organism silhouettes modified from "Festuca subverticillata" by Cindy Roché and "Agrostis hyemalis" and "Poa alsodes" by Sandy Long ©Utah State University.

737
 738
 739
 740
 741
 742
 743
 744
 745
 746
 747
 748
 749
 750
 751
 752
 753
 754
 755
 756
 757
 758
 759
 760
 761
 762
 763
 764
 765
 766
 767
 768
 769
 770
 771
 772
 773
 774
 775
 776
 777
 778
 779
 780
 781
 782

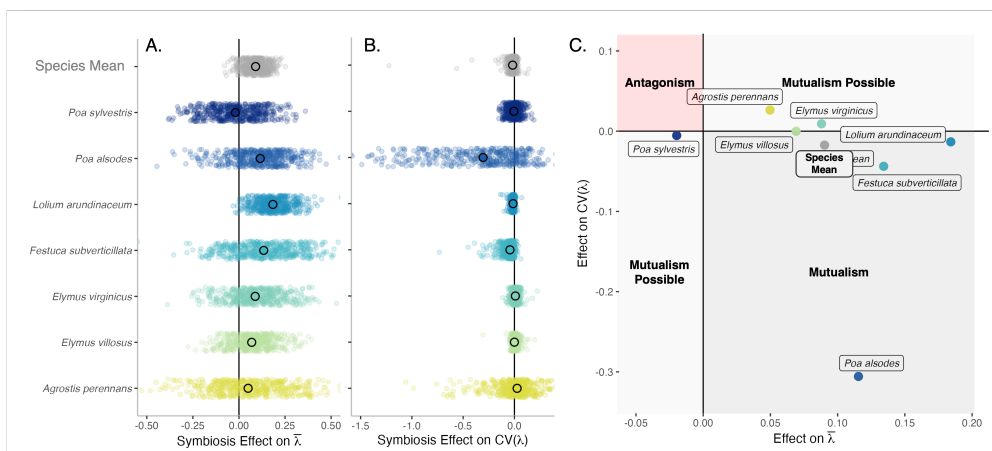


Fig. 3: Mean and variance-buffering effects on fitness. Black circles indicate the posterior median effect of endophytes along with 500 posterior draws (smaller colored circles) on the (A) mean and (B) coefficient of variation in λ_t for each host species as well as a cross species mean. (C) For all hosts, endophytes either reduce variance, increase the mean, or both, and consequently when considering stochastic environments, the interactions are always at least potentially mutualistic.

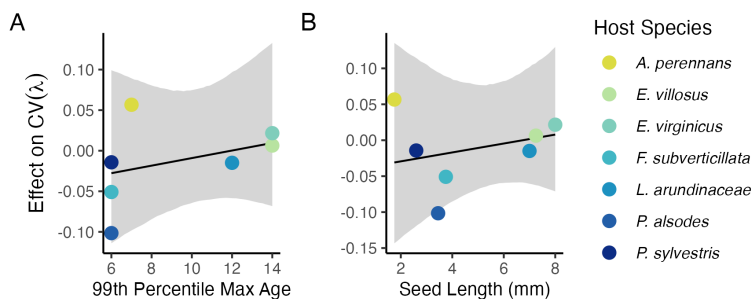
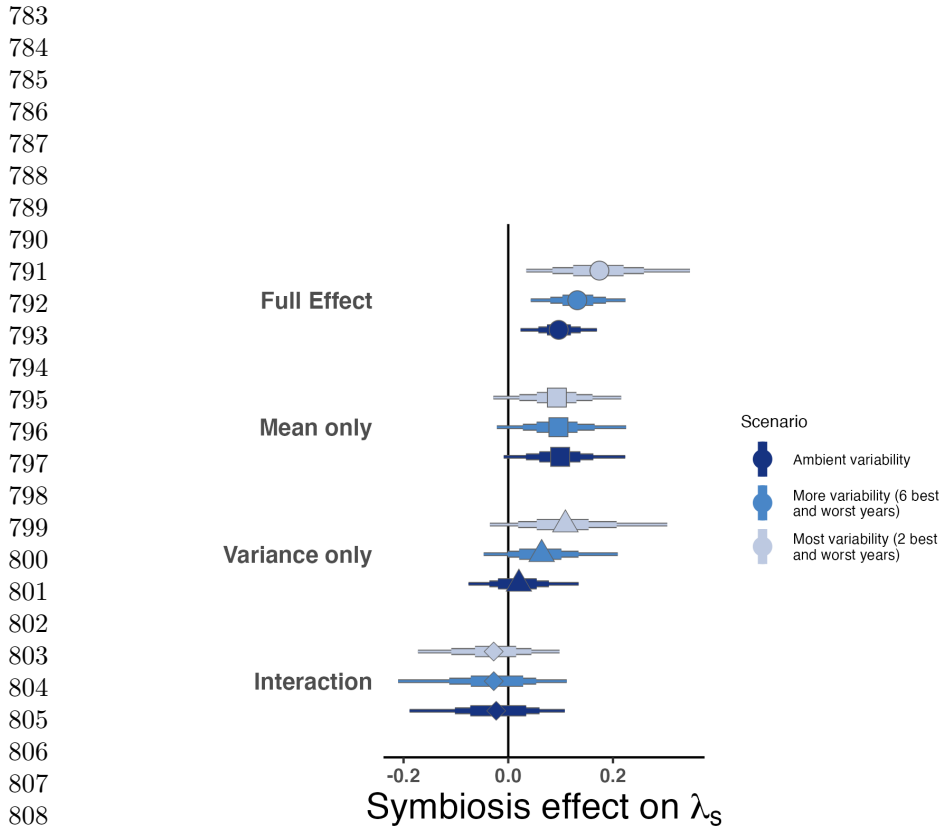


Fig. 4: Host species with faster life history traits experience stronger effects of symbiont-mediated variance buffering. Regressions between life history traits describing the fast-slow life history continuum ((A) 99th percentile maximum age observed during long term censuses in years; (B) Seed size) and the effect of endophyte symbiosis on the coefficient of variation in annual population growth rate (λ_t). Each panel shows the fitted mean relationship (line) along with the 95% credible interval.



810 **Fig. 5:** Cross-species average endophyte contributions to stochastic growth rates under
811 observed and elevated variance. Endophyte symbiosis contributes to the total effect of
812 mutualism on λ_s through benefits to mean growth rates and through variance buffering
813 as well as the interaction between mean and variance effects. Shapes indicate the
814 posterior mean of each contribution averaged across the seven focal symbionts, along
815 with bars for the 50, 75 and 95% credible intervals. The full effect of the symbiosis
816 (circles) becomes more mutualistic under scenarios of increased variance (represented
817 by color shading). Relative to the ambient scenario sampling transition matrices for
818 all 13 transition years during the study period, simulations increased variance by
819 sampling the most extreme six or two years years, leading to increased contributions
820 from variance buffering effects (triangles) and a constant contribution from mean
821 effects (squares).

Supporting Information	829
	830
	831
	832
	833
	834
	835
	836
	837
List of Supp. Figures	
S1 Life cycle diagram depicting the generalized structure of matrix population model	26
	838
S2 Effect of endophyte symbiosis on mean adult survival - Original	27
	839
S3 Effect of endophyte symbiosis on mean adult survival - Recruits	28
	840
S4 Effect of endophyte symbiosis on mean adult growth - Original	29
	841
S5 Effect of endophyte symbiosis on mean adult growth - Recruits	30
	842
S6 Effect of endophyte symbiosis on mean flowering - Original	31
	843
S7 Effect of endophyte symbiosis on mean flowering - Recruits	32
	844
S8 Effect of endophyte symbiosis on mean fertility - Original	33
	845
S9 Effect of endophyte symbiosis on mean fertility - Recruits	34
	846
S10 Effect of endophyte symbiosis on mean spikelet production - Original	35
	847
S11 Effect of endophyte symbiosis on mean spikelet production - Recruits	36
	848
S12 Effect of endophyte symbiosis on yearly adult survival - Original	37
	849
S13 Effect of endophyte symbiosis on yearly adult survival - Recruits	38
	850
S14 Effect of endophyte symbiosis on yearly adult growth - Original	39
	851
S15 Effect of endophyte symbiosis on yearly adult growth - Recruits	40
	852
S16 Effect of endophyte symbiosis on yearly flowering - Original	41
	853
S17 Effect of endophyte symbiosis on yearly flowering - Recruits	42
	854
S18 Effect of endophyte symbiosis on yearly fertility - Original	43
	855
S19 Effect of endophyte symbiosis on yearly fertility - Recruits	44
	856
S20 Effect of endophyte symbiosis on yearly spikelet production - Original	45
	857
S21 Effect of endophyte symbiosis on yearly spikelet production - Recruits	46
	858
S22 Posterior distributions of the standard deviations of inter-annual year effects for survival	47
	859
S23 Posterior distributions of the standard deviations of inter-annual year effects for seedling survival	47
	860
S24 Posterior distributions of the standard deviations of inter-annual year effects for growth	47
	861
S25 Posterior distributions of the standard deviations of inter-annual year effects for seedling growth	48
	862
S26 Posterior distributions of the standard deviations of inter-annual year effects for flowering probability	48
	863
S27 Posterior distributions of the standard deviations of inter-annual year effects for fertility	48
	864
S28 Posterior distributions of the standard deviations of inter-annual year effects for spikelets per inflorescence	49
	865
	866
	867
	868
	869
	870
	871
	872
	873
	874

875	S29 Posterior distributions of the standard deviations of inter-annual year effects for recruitment	50
876		
877	S30 Graphical posterior predictive check for mean and higher moments of <i>A. perennans</i> growth model across size	51
878		
879	S31 Graphical posterior predictive check for mean and higher moments of <i>E. villosus</i> growth model across size	52
880		
881	S32 Graphical posterior predictive check for mean and higher moments of <i>E. virginicus</i> growth model across size	53
882		
883	S33 Graphical posterior predictive check for mean and higher moments of <i>F. subverticillata</i> growth model across size	54
884		
885	S34 Graphical posterior predictive check for mean and higher moments of <i>L. arundinacea</i> growth model across size	55
886		
887	S35 Graphical posterior predictive check for mean and higher moments of <i>P. alsodes</i> growth model across size	56
888		
889	S36 Graphical posterior predictive check for mean and higher moments of <i>P. sylvestris</i> growth model across size	57
890		
891	S37 Graphical posterior predictive check for mean and higher moments of <i>A. perennans</i> survival model across size	58
892		
893	S38 Graphical posterior predictive check for mean and higher moments of <i>E. villosus</i> survival model across size	59
894		
895	S39 Graphical posterior predictive check for mean and higher moments of <i>E. virginicus</i> survival model across size	60
896		
897	S40 Graphical posterior predictive check for mean and higher moments of <i>F. subverticillata</i> survival model across size	61
898		
899	S41 Graphical posterior predictive check for mean and higher moments of <i>L. arundinacea</i> survival model across size	62
900		
901	S42 Graphical posterior predictive check for mean and higher moments of <i>P. alsodes</i> survival model across size	63
902		
903	S43 Graphical posterior predictive check for mean and higher moments of <i>P. sylvestris</i> survival model across size	64
904		
905	S44 Graphical posterior predictive check for mean and higher moments of <i>A. perennans</i> inflorescence production model across size	65
906		
907	S45 Graphical posterior predictive check for mean and higher moments of <i>E. villosus</i> inflorescence production model across size	66
908		
909	S46 Graphical posterior predictive check for mean and higher moments of <i>E. virginicus</i> inflorescence production model across size	67
910		
911	S47 Graphical posterior predictive check for mean and higher moments of <i>F. subverticillata</i> inflorescence production model across size	68
912		
913	S48 Graphical posterior predictive check for mean and higher moments of <i>L. arundinacea</i> inflorescence production model across size	69
914		
915	S49 Graphical posterior predictive check for mean and higher moments of <i>P. alsodes</i> inflorescence production model across size	70
916		
917	S50 Graphical posterior predictive check for mean and higher moments of <i>P. sylvestris</i> inflorescence production model across size	71
918		
919		
920		

S51	Graphical posterior predictive check for mean and higher moments of <i>A. perennans</i> spikelet model across size	921
		72
S52	Graphical posterior predictive check for mean and higher moments of <i>E. villosus</i> spikelet model across size	922
		923
S53	Graphical posterior predictive check for mean and higher moments of <i>E. virginicus</i> spikelet model across size	924
		925
S54	Graphical posterior predictive check for mean and higher moments of <i>F. subverticillata</i> spikelet model across size	926
		927
S55	Graphical posterior predictive check for mean and higher moments of <i>L. arundinacea</i> spikelet model across size	928
		929
S56	Graphical posterior predictive check for mean and higher moments of <i>P. alsodes</i> spikelet model across size	930
		931
S57	Graphical posterior predictive check for mean and higher moments of <i>P. sylvestris</i> spikelet model across size	932
		933
S58	Graphical posterior predictive check for mean and higher moments of <i>A. perennans</i> flowering model across size	934
		935
S59	Graphical posterior predictive check for mean and higher moments of <i>E. villosus</i> flowering model across size	936
		937
S60	Graphical posterior predictive check for mean and higher moments of <i>E. virginicus</i> flowering model across size	938
		939
S61	Graphical posterior predictive check for mean and higher moments of <i>F. subverticillata</i> flowering model across size	940
		941
S62	Graphical posterior predictive check for mean and higher moments of <i>L. arundinacea</i> flowering model across size	942
		943
S63	Graphical posterior predictive check for mean and higher moments of <i>P. alsodes</i> flowering model across size	944
		945
S64	Graphical posterior predictive check for mean and higher moments of <i>P. sylvestris</i> flowering model across size	946
		947
S65	Posterior predictive check for statistical model of Seedling Survival . .	948
		949
S66	Posterior predictive check for statistical model of Seedling Growth . .	950
		951
S67	Posterior predictive check for statistical model of Mean Seeds/Spikelet	952
		953
S68	Posterior predictive check for statistical model of Recruitment	954
		955
S69	Posterior distributions of the vital rate regressions for Adult Survival .	956
		957
S70	Posterior distributions of the vital rate regressions for Seedling Survival	958
		959
S71	Posterior distributions of the vital rate regressions for Adult Growth .	960
		961
S72	Posterior distributions of the vital rate regressions for Seedling Growth	962
		963
S73	Posterior distributions of the vital rate regressions for Flowering Probability	964
		965
S74	Posterior distributions of the vital rate regressions for Inflorescence Production	966
		966
S75	Posterior distributions of the vital rate regressions for Spikelets/Inflo- rescence	967
		968
S76	Posterior distributions of the vital rate regressions for Seeds/Spikelet .	969
		970
S77	Posterior distributions of the vital rate regressions for Recruitment . .	971
		972
S78	Annual growth rate values (λ_t) over thirteen years	973

967	S79 Stochastic population growth rates (λ_S) for symbiotic and symbiont-free populations	100
968		
969	S80 Mean and standard deviation of annual growth rate values during simulation scenarios	101
970		
971	S81 Endophyte contributions to stochastic growth rates under observed and elevated variance across species	102
972		
973	S82 Vital rate decomposition of endophyte contributions to stochastic growth rates under observed and elevated variance across species	103
974		
975	S83 Relationship between variance buffering and life history traits describing the fast-slow life history continuum accounting for phylogenetic covariance between <i>Epichloë</i> symbionts	104
976		
977	S84 Relationship between variance buffering and life history traits describing the fast-slow life history continuum accounting for phylogenetic covariance between <i>Epichloë</i> symbionts	105
978		
979	S85 Posterior estimates of life history trait effects on variance buffering	106
980		
981	S86 Posterior distributions of the life history trait regressions	107
982		
983	S87 Faithfulness of experimental plots to assigned endophyte status	108
984		
985	S88 Weather station time-series for Bloomington, IN	109
986		
987	S89 Predicted population growth rates across drought indices	110
988		

List of Supp. Tables

989	S1 Summary of host-endophyte propragation and transplant methods	112
990		
991	S2 Summary of focal life history traits	113
992		
993	S3 Summary of host-endophyte drought sensitivities	114
994		
995		
996		
997		
998		
999		
1000		
1001		
1002		
1003		
1004		
1005		
1006		
1007		
1008		
1009		
1010		
1011		
1012		

Supplemental Methods	1013
Endophyte removal, plant propagation, and field set-up	1014
Seeds from naturally symbiotic populations of the seven focal host species were collected during summer-fall 2006 from Lilly-Dickey Woods and the nearby Bayles Road Teaching and Research Preserve (39.220167, -86.542683). To generate symbiotic (S+) and symbiont-free (S-) plants from the same genetic lineages, seeds from each species were disinfected with a heat treatment described in Table S1 or left untreated. The heat treatment created symbiont-free plants by warming seeds to temperatures at which the fungus becomes inviable but the host seeds can still germinate.	1015
Both heat-treated and untreated seeds were surface sterilized with bleach to remove epiphyllous microbes, cold stratified for up to 4 weeks, then germinated in a growth chamber before transfer to the greenhouse at Indiana University where they grew for ~ 8 weeks. We confirmed endophyte status by staining thin sections of inner leaf sheath with aniline blue and examining tissue for fungal hyphae at 200X magnification [?]. We established experimental populations with vegetatively propagated clones of similar sizes (ranging from one to six tillers).	1016
During the fall of 2007 and spring of 2008, we established 10 3x3 m plots for <i>A. perennans</i> , <i>E. villosus</i> , <i>E. virginicus</i> , <i>F. subverticillata</i> , and <i>L. arundinaceum</i> and 18 plots for <i>P. alsodes</i> and <i>P. sylvestris</i> . Half of the plots were randomly assigned to be planted with either symbiotic (S+) or symbiont-free (S-) plants, and initiated with 20 evenly spaced individuals labeled with aluminum tags. In spring 2008, we placed plastic deer net fencing around each plot to limit deer herbivory and disturbance; damaged fences were regularly replaced.	1017
We expected plots to maintain their endophyte status (S+ or S-) because these fungal symbionts are almost exclusively vertically transmitted, and plots were spaced a minimum of 5 m apart, limiting seed dispersal or horizontal transmission of the symbiont between plots. We regularly confirmed endophyte treatment throughout the lifetime of the experiment by opportunistically taking subsets of seeds from reproductive individuals and scoring them for their endophyte status with microscopy as above. Overall, these scores reflected 98% faithfulness of recruits to their expected endophyte status across species and plots (Fig. S87; Supplement data). Additionally, we have rarely observed fungal stromata, the fruiting bodies by which <i>Epichloë</i> are potentially transmitted horizontally, provided the fly vector is also present [?]. For <i>A. perennans</i> , <i>F. subverticillata</i> , <i>L. arundinaceum</i> , and <i>P. alsodes</i> , we never observed stromata. We observed stromata only infrequently for <i>E. villosus</i> , and even more rarely for <i>E. virginicus</i> and <i>P. sylvestris</i> (Table S2). For these species, stromata have only been observed irregularly across years on 35, 4, and 6 plants respectively, making up < 0.3% of all censused plants.	1018
Detailed vital rate modeling	1019
We fit vital rates models in a Bayesian hierarchical framework. Statistical models for adult survival, seedling survival, adult growth, seedling growth, flowering (yes or no), fertility of flowering plants (number of flowering tillers), production of seed-bearing	1020
	1021
	1022
	1023
	1024
	1025
	1026
	1027
	1028
	1029
	1030
	1031
	1032
	1033
	1034
	1035
	1036
	1037
	1038
	1039
	1040
	1041
	1042
	1043
	1044
	1045
	1046
	1047
	1048
	1049
	1050
	1051
	1052
	1053
	1054
	1055
	1056
	1057
	1058

1059 spikelets (number per inflorescence), the average number of seeds per spikelet, and the
 1060 recruitment of seedlings from the preceding year's seed production, were constructed
 1061 as follows:

1062 *Survival* - We modeled survival as a Bernoulli process, where the survival (S) of
 1063 an individual i in plot p and census year t was predicted by the plot-level endophyte
 1064 status (e), host species (h), size in the preceding census, and the plant's origin status
 1065 (o ; whether it was initially transplanted or naturally recruited into the plot).

1066

1067

$$1068 \quad S_{i,p,e,h,t} \sim \text{Bernoulli}(\hat{S}_{i,p,e,h,t}) \quad (\text{S4a})$$

$$1069 \quad \text{logit}(\hat{S}_{i,p,e,h,t}) = \beta_{0_{h,o}} + \beta_{1_h} * \text{endo}_e \quad (\text{S4b})$$

$$1070 \quad + \beta_{2_{h,o}} * \text{size}_{i,t-1} + \beta_{3_{h,o}} * \text{size}_{i,t-1}^2 + \tau_{e,h,t} + \rho_p \quad (\text{S4c})$$

$$1072 \quad \tau_{e,h,t} \sim \text{Normal}(0, \sigma_{\tau_{e,h}}^2) \quad (\text{S4d})$$

$$1073 \quad \rho_p \sim \text{Normal}(0, \sigma_\rho^2) \quad (\text{S4e})$$

1075

1076 Here, \hat{S} is the survival probability, $\beta_{0_{h,o}}$ is an intercept specific to each host species
 1077 and recruitment origin, β_{1_h} is the endophyte effect, $\beta_{2_{h,o}}$ is the effect of plant size
 1078 specific to each species and recruitment origin, $\beta_{3_{h,o}}$ is a quadratic plant size effect
 1079 specific to each species and recruitment origin, $\tau_{e,h,t}$ is a normally distributed year
 1080 effect for each species and endophyte status with variance $\sigma_{\tau_{e,h}}^2$, and ρ_p is a normally
 1081 distributed plot effect with variance σ_ρ^2 ($p(e)$ indicates that plot identity is uniquely
 1082 associated with an endophyte status). We assume that the plot-to-plot variance σ_ρ^2 was
 1083 shared across host species, allowing us to "borrow strength" across the multi-species
 1084 dataset; other model parameters are unique to host species. We separately modeled
 1085 the survival of newly recruited seedlings with a similar model but omitting previous
 1086 size dependence and origin status.

1087 *Growth* - We modeled plant size in census year t (G) with the same linear pre-
 1088 dictor for the mean as described for survival. Because we measured size as positive
 1089 integer-valued counts of tillers, we modeled it with a zero-truncated Poisson-inverse
 1090 Gaussian distribution. This distribution includes a shape parameter λ_G to account for
 1091 overdispersion in the data. We additionally modeled the growth of newly recruited
 1092 seedlings separately with a Poisson-inverse Gaussian model omitting size structure
 1093 and the plants' origin status as with seedling survival.

1094 *Flowering* - We modeled whether or not a plant was flowering during the census (P)
 1095 as a Bernoulli process, with the same linear predictor for the mean as described above
 1096 for survival except that size dependence for reproductive vital rates was determined
 1097 by the individual's size during the same census year as opposed to its size during the
 1098 previous year.

1099 *Fertility* - For a plant that was flowering during the census, its fertility was the
 1100 number of reproductive tillers produced (F), which we modeled as a function of size in
 1101 the same census period with a zero-truncated Poisson-Inverse Gaussian distribution,
 1102 with the same linear predictor for the mean as described above.

1103

1104

<i>Spikelets per Inflorescence</i> - Spikelet production (K) was recorded as integer counts on up to three inflorescences per reproducing plant. We modeled these data with a negative binomial distribution, with the same linear predictor for the mean as described above.	1105
	1106
	1107
	1108
	1109
<i>Seed Production per Spikelet</i> - For individuals with recorded counts of seed production, we calculated the number of seeds per spikelet from our counts of seeds and spikelets per inflorescence, and then modeled seeds per spikelet (D) as means of a Gaussian distribution for each species and endophyte status. Because we had less detailed data across years and plants for seed production than for other reproductive vital rates, we omitted both plot and year random effects.	1110
	1111
	1112
	1113
	1114
	1115
<i>Seedling Recruitment</i> - We used a binomial distribution to model the recruitment of new seedlings (R) into the plots from seeds produced in the preceding year, assuming no long-lived seed bank. We included an intercept specific to each host and endophyte status and the same random effects structure as in other models. We estimated the number of seeds per plot in the preceding year by multiplying the total number of reproductive tillers per plant by the mean number of spikelets per inflorescence and mean number of seeds per spikelet (D). For plants with missing fertility or spikelet data, we used the expected number of reproductive tillers (F) or of spikelets per inflorescence from (K), drawing from the full posteriors of our models. We rounded this value to get the estimated seed production for each individual, and finally summed across all reproductive plants in each year and plot to get the total number of seeds produced.	1116
	1117
	1118
	1119
	1120
	1121
	1122
	1123
	1124
	1125
	1126
	1127
Model assessment	1128
All parameters were given vague priors [?]. We ran each vital rate model for 2500 warm-up and 2500 MCMC sampling iterations with three chains. We assessed model convergence with trace plots of posterior chains and checked for \hat{R} values less than 1.01, indicating low within- and between-chain variation [? ?]. For those models that showed poor convergence, we extended the MCMC sampling to include 5000 warm-up and 5000 sampling iterations, which was only necessary for seedling growth. We visualized the interactions between plant size, origin status, and endophyte status for both the interannual mean expected value for each vital rate (averaging over year and plot variance) (Fig. S2 - S11) and for the expected vital rate values specific to each year (averaging over plot variance) (Fig. S12 -S21). We graphically checked vital rate model fit with posterior predictive checks comparing simulated and observed data (Fig. S30-S68). Initial analyses including only linear effects of size produced estimates of endophytes' effects on vital rate means and inter-annual variances that were similar to those from the more flexible quadratic models, but provided worse fit to size-structure in the data in some cases. We therefore proceeded with the more flexible quadratic models. Results from subsequent matrix model analyses were qualitatively similar regardless of this choice.	1129
	1130
	1131
	1132
	1133
	1134
	1135
	1136
	1137
	1138
	1139
	1140
	1141
	1142
	1143
	1144
	1145
Estimating climate drivers of environmental context-dependence	1146
To connect the variance buffering effects of endophytes with inter-annual variability in climate, we built climate-explicit stochastic matrix population models from the	1147
	1148
	1149
	1150

1151 vital rate data in addition to the climate-implicit model described in the main text.
1152 Identifying the potentially complex relationships between vital rates and environmental
1153 drivers remains a key challenge for accurate forecasts of the ecological impacts of
1154 environmental stochasticity [?]. We first downloaded temperature and precipitation
1155 data from a weather station in Bloomington, IN, approx. 27 km from our study site,
1156 using the rnoaa package [?]. Compared to other weather stations in the area, the
1157 measurements from Bloomington contain the most complete climate record across the
1158 study period and are correlated with more local measurements from Nashville, IN for
1159 years in which local data are available (total daily precipitation: $R^2 = .76$; mean daily
1160 temperature: $R^2 = .94$). The mean annual temperature across the study period was
1161 $11.9 C^\circ$ (SD: $1.05 C^\circ$) and the average annual precipitation was 1237.9 mm/year (SD:
1162 204.89 mm/year) (Fig. S88). Given the known role of endophytes in promoting host
1163 drought tolerance, we calculated the Standardised Precipitation-Evapotranspiration
1164 Index (SPEI) for 3 and 12 months preceding each annual censuses, reflecting drought
1165 during the growing season and across the year [?]. To calculate SPEI, we used the
1166 Thornthwaite equation to model potential evapotranspiration as implemented in the
1167 SPEI R package [?]

1168 We repeated the process of fitting statistical models for each vital rate as described
1169 above with the inclusion of a parameter describing the influence of SPEI. We fit
1170 separate vital rate models incorporating either the growing season or annual drought
1171 index for each vital rate, except for the model describing the mean number of seeds
1172 per inflorescence. This model was fit without climate effects because the data came
1173 from only a few years. Initial analyses indicated similar fits for models including only a
1174 linear term and those with both linear and quadratic terms describing the relationship
1175 between the climate driver and the vital rate response, and so we proceeded with
1176 models including only the linear term. We expected that including climate predictors
1177 into the models would explain some inter-annual variance in vital rates, shrinking the
1178 variance associated with the fitted year random effects. We assessed model fit with
1179 graphic posterior predictive checks and convergence diagnostics as described for the
1180 climate-implicit analysis. Finally, we next built matrix projection models incorporating
1181 the climate-dependent vital rate functions to assess the response of symbiotic (S+) vs
1182 symbiont-free (S-) populations to drought. The model is as described in **Materials**
1183 and **Methods** with the inclusion of parameters describing the slope of the relationship
1184 with SPEI. We compared the sensitivity of λ to either annual or seasonal SPEI of S+
1185 populations ($\frac{\Delta\lambda^+}{\Delta SPEI}$) with those of S- populations ($\frac{\Delta\lambda^-}{\Delta SPEI}$) (Fig. S89; Table S).

1186 Most species were slightly more responsive to growing season rather than annual
1187 drought conditions, and for most species symbiotic populations were less sensitive to
1188 SPEI than symbiont-free populations (Fig. S89; Table S3). However, these drought
1189 indices did not explain the full extent of inter-annual variability in demographic vital
1190 rates. For example, flowering in *A. perennans* had one of the strongest climate signals
1191 (82% probability of a positive relationship with SPEI), yet the estimated inter-annual
1192 variance $\sigma_{\tau_{e,h}}^2$ for symbiont-free plants shrank from 6.7 to 6.1 after including 3-month
1193 SPEI as a covariate, suggesting that other factors contribute to inter-annual variability.

1194

1195

1196

Detailed statistical analysis of life history traits	1197
We fit Bayesian phylogenetic mixed-effects models using the brms package [?] to test the relationship between each life history trait and the effect of symbiosis on the CV of λ_t (a measure of variance buffering) while controlling for phylogenetic non-independence. We pruned species-level phylogenies of plants [?] and <i>Epichloë</i> fungi [?] to include the focal species. <i>Agrostis perennans</i> was not included in the published tree, and so we used the congener <i>A. hyemalis</i> . We defined separate phylogenetic covariance matrices for the pruned tree for host and symbiont species.	1198
We propagated uncertainty in the estimated variance buffering effect V with a measurement error model:	1199
$V_{MEAN,h} \sim Normal(V_{EST,h}, V_{SD,h})$	1200
$V_{EST,h} \sim Normal(\mu_h, \sigma)$	1201
$\mu = \alpha + \beta * trait + \pi_j$	1202
$\alpha \sim Normal(0, .1)$	1203
$\beta \sim Normal(0, .1)$	1204
$\sigma \sim Half - Normal(.05, .01)$	1205
$\pi_h \sim MVN(0, \sigma_\pi \mathbf{A})$	1206
$\sigma_\pi \sim Half - Normal(0, .1)$	1207
	1208
	1209
	1210
	1211
	1212
	1213
	1214
	1215
	1216
	1217
	1218
	1219
	1220
	1221
	1222
	1223
	1224
	1225
	1226
	1227
	1228
	1229
	1230
	1231
	1232
	1233
	1234
	1235
	1236
	1237
	1238
	1239
	1240
	1241
	1242
Here, V_{EST} is the variance buffering effect for host species h , estimated from the posterior mean (V_{MEAN}) and standard deviation (V_{SD}), propagating uncertainty associated with the effect of symbiosis. The model includes an intercept (α) and slope (β) defining the relationship between variance buffering effect and the life history trait. The residual standard deviation is given by (σ). We used weakly informative priors to aid model convergence. Each prior was centered at zero, except for the residual standard deviation, which we centered at the standard deviation of the estimated variance buffering effect, .05. The phylogenetic random effect (π), modeled as a multivariate normal distribution, has a between-species standard deviation (σ_π) structured by the phylogenetic covariance matrix \mathbf{A} . We ran each MCMC sampling chain for 8000 warmup iterations and 2000 sampling iterations. We assessed model convergence as described above for the vital rate models.	1235
Vital rate mean-variance decomposition	1236
We performed a mean-variance decomposition to quantify the extent that mean and variance effects on stochastic population growth rates arise through different vital rates. Specifically, we repeated the calculation of λ_S as described in the main text for symbiotic populations as well as symbiont-free populations, as well as for four additional “treatments”. These treatments differentiate between mortality and growth related vital rates (adult survival, adult growth, seedling survival, and seedling growth) and reproductive vital rates (probability of flowering, inflorescence production, spikelet production, seed production, and recruitment). Each treatment set vital rate mean	1237

1243 and interannual variances according to the symbiont-free parameter values across vital
1244 rates while introducing (1) endophyte effects on the vital rate means for survival and
1245 growth vital rates only, (2) endophyte effects on the vital rate variances for survival and
1246 growth vital rates only, (3) endophyte effects on the vital rate means for reproductive
1247 vital rates only, and (4) endophyte effects on the vital rate variances for reproductive
1248 vital rates only.

1249 The combination of all six λ_S treatments allowed us to quantify to what extent the
1250 overall effect of symbiosis derives from changes in mean and variance of mortality and
1251 growth versus in reproductive vital rates. To explore how these contributions could
1252 be expected to change under increased variability relative to that observed during the
1253 study period, we repeated this decomposition under the scenarios of increased variance
1254 described in the main text, sampling transition matrices associated with the set of
1255 either six or two most extreme λ values experienced by symbiont-free populations.

1256 This analysis revealed that both mean and variance buffering effects are driven
1257 primarily by symbiont effects on survival and growth rather than on reproduction
1258 (Fig. S53) .

1259

1260

1261

1262

1263

1264

1265

1266

1267

1268

1269

1270

1271

1272

1273

1274

1275

1276

1277

1278

1279

1280

1281

1282

1283

1284

1285

1286

1287

1288

Supplemental Figures S1-S89

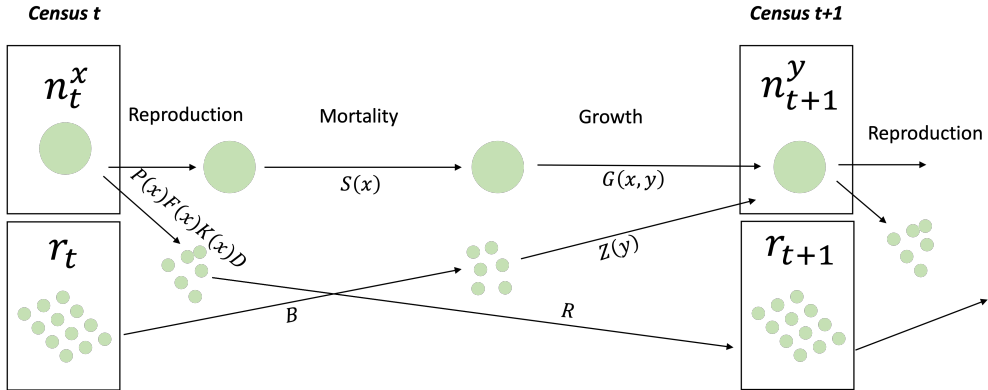
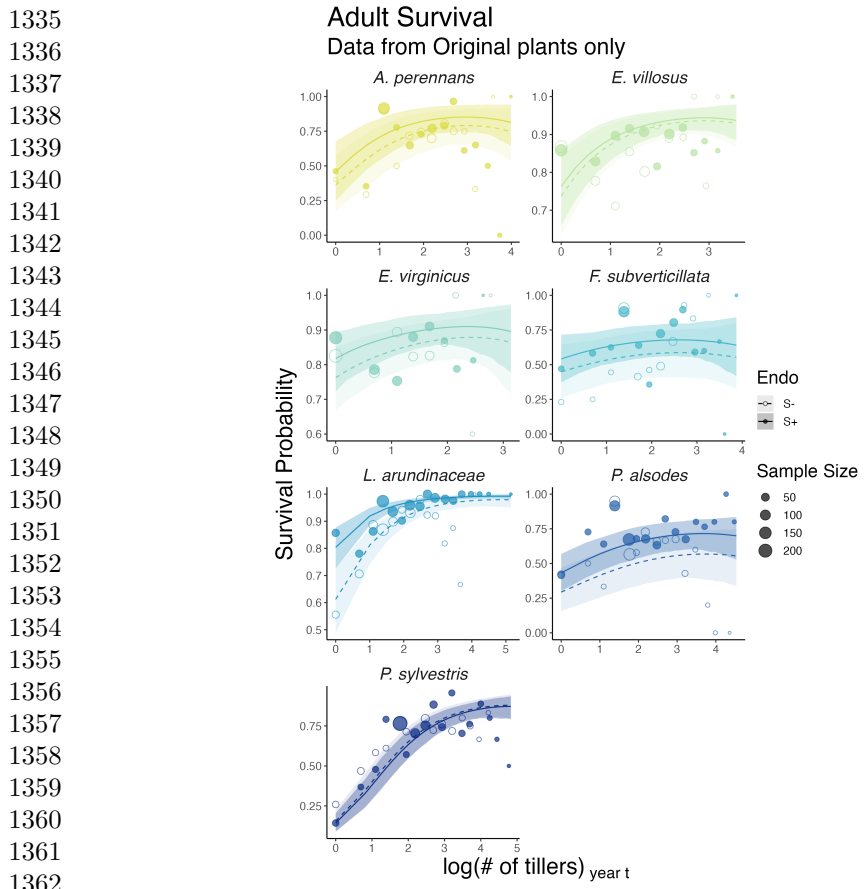


Figure S1: Life cycle diagram depicting the generalized structure of matrix population model. The population consists of different life stages at each census t or census $t+1$. Individuals transition from size x to size y . n is a vector of discrete sizes representing number of tillers, according to their likelihood of survival (S) and growth (G). Reproduction generates new recruits (small circles) through four steps, the probability of flowering (P), the number of flowering tillers produced (F), the number of spikelets per inflorescence produced (K), and the number of seeds per spikelet (D). The probability of successful recruitment (R) determines the success of these offspring, and any new recruits (r) are incorporated into the census. These non-reproductive, typically one-tiller recruits transition into the population of mature individuals with survival (B) and growth (Z) probability. Symbiotic and symbiont-free populations have the same model structure with species-specific and symbiont status-specific transition probabilities used to construct matrices.

1289
1290
1291
1292
1293
1294
1295
1296
1297
1298
1299
1300
1301
1302
1303
1304
1305
1306
1307
1308
1309
1310
1311
1312
1313
1314
1315
1316
1317
1318
1319
1320
1321
1322
1323
1324
1325
1326
1327
1328
1329
1330
1331
1332
1333
1334



1363 Figure S2: Effect of endophyte symbiosis on mean adult survival. Fitted curves repre-
1364 sent the size-specific mean survival probability for originally transplanted plants along
1365 with data binned by size and averaged over many individuals, years, and plots shown
1366 as open circles with a dashed line for symbiont-free (S-) plants, while the solid line
1367 and filled circles represent symbiotic (S+) plants. 80% credible intervals are shown
1368 with dark shading for S+, or light shading for S-.

1369
1370
1371
1372
1373
1374
1375
1376
1377
1378
1379
1380

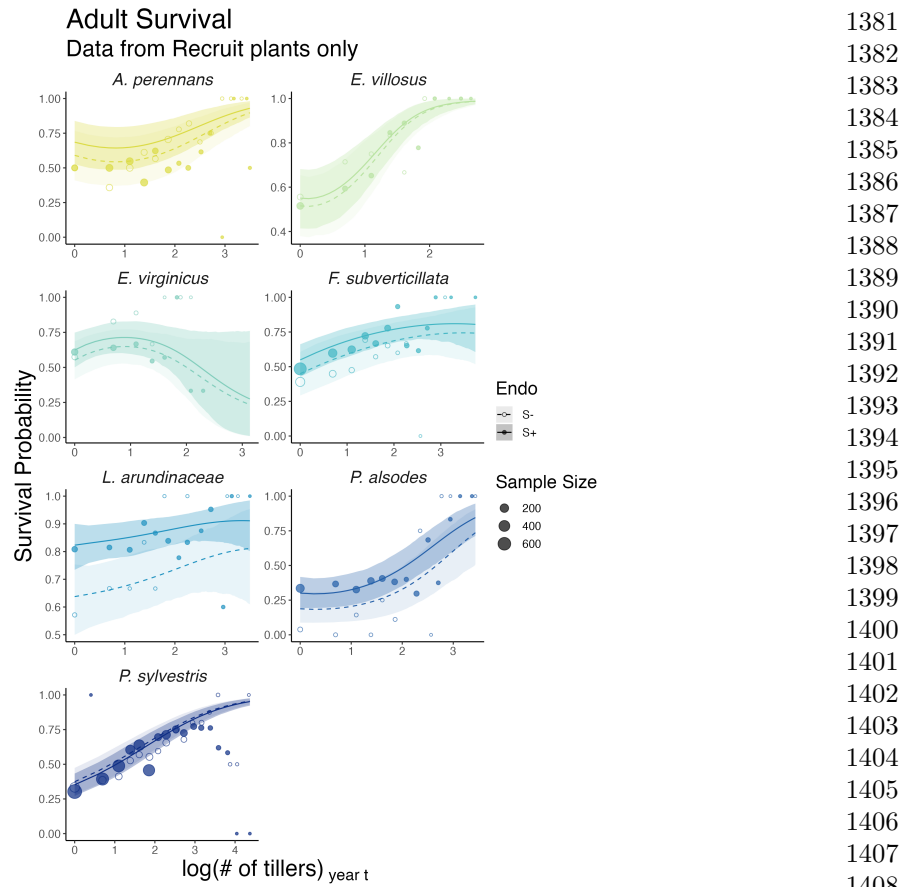
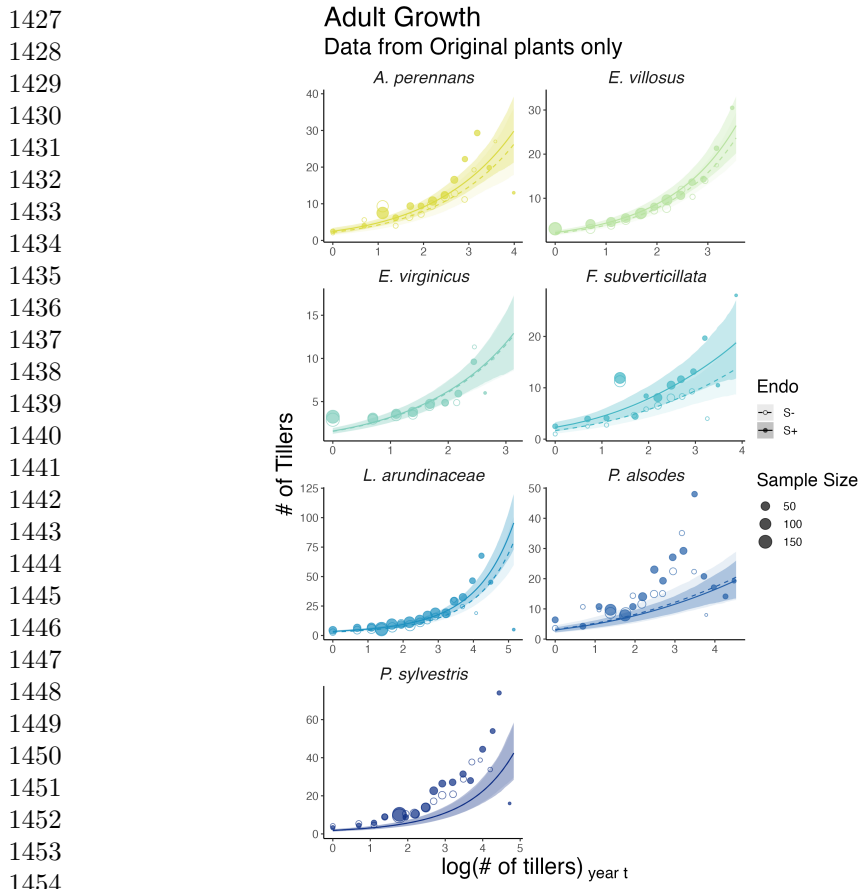


Figure S3: Effect of endophyte symbiosis on mean adult survival. Fitted curves represent the size-specific mean survival probability for recruited plants along with data binned by size and averaged over many individuals, years, and plots shown as open circles with a dashed line for symbiont-free (S-) plants, while the solid line and filled circles represent symbiotic (S+) plants. 80% credible intervals are shown with dark shading for S+, or light shading for S-.



1455 Figure S4: Effect of endophyte symbiosis on mean adult growth. Fitted curves represent
1456 the size-specific mean expected plant size for originally transplanted plants along with
1457 data binned by size and averaged over many individuals, years, and plots shown as
1458 open circles with a dashed line for symbiont-free (S-) plants, while the solid line and
1459 filled circles represent symbiotic (S+) plants. 80% credible intervals are shown with
1460 dark shading for S+, or light shading for S-.

1461
1462
1463
1464
1465
1466
1467
1468
1469
1470
1471
1472

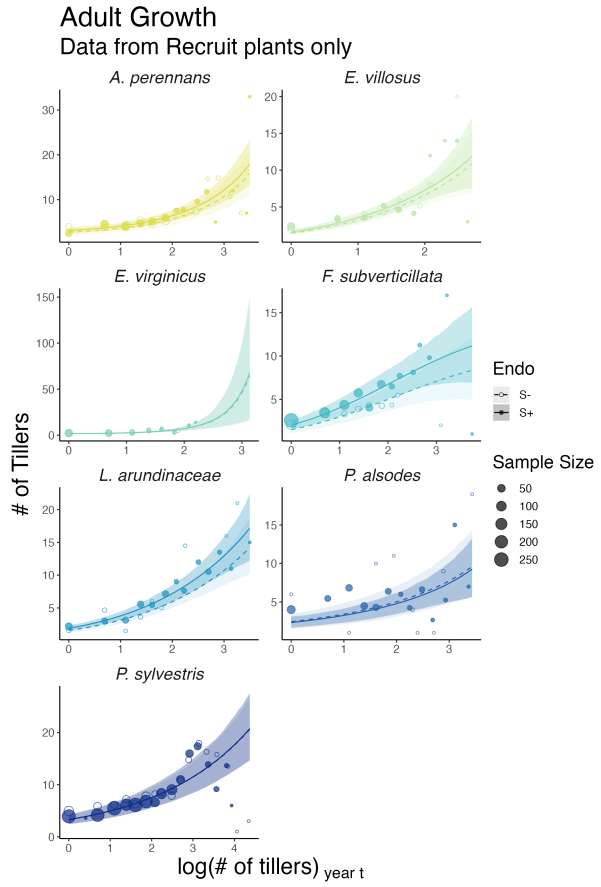
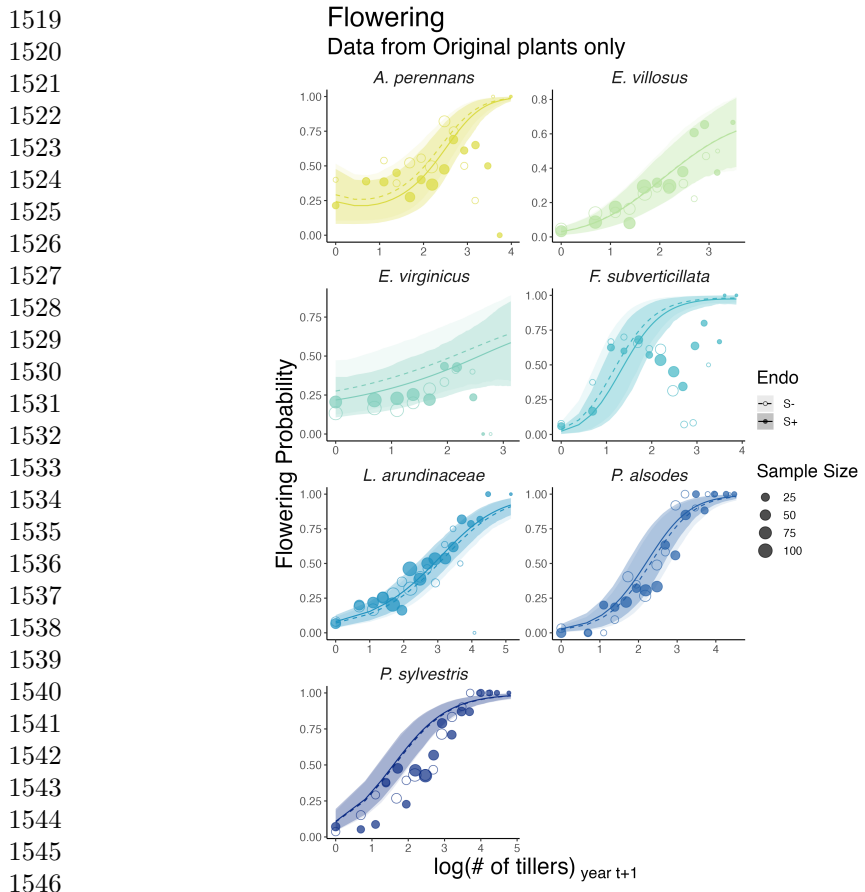


Figure S5: Effect of endophyte symbiosis on mean adult growth. Fitted curves represent the size-specific mean expected plant size for recruited plants along with data binned by size and averaged over many individuals, years, and plots shown as open circles with a dashed line for symbiont-free (S-) plants, while the solid line and filled circles represent symbiotic (S+) plants. 80% credible intervals are shown with dark shading for S+, or light shading for S-.

1473
1474
1475
1476
1477
1478
1479
1480
1481
1482
1483
1484
1485
1486
1487
1488
1489
1490
1491
1492
1493
1494
1495
1496
1497
1498
1499
1500
1501
1502
1503
1504
1505
1506
1507
1508
1509
1510
1511
1512
1513
1514
1515
1516
1517
1518



1547 Figure S6: Effect of endophyte symbiosis on mean flowering. Fitted curves represent
1548 the size-specific mean flowering probability for originally transplanted plants along
1549 with data binned by size and averaged over many individuals, years, and plots shown
1550 as open circles with a dashed line for symbiont-free (S-) plants, while the solid line
1551 and filled circles represent symbiotic (S+) plants. 80% credible intervals are shown
1552 with dark shading for S+, or light shading for S-.

1553
1554
1555
1556
1557
1558
1559
1560
1561
1562
1563
1564

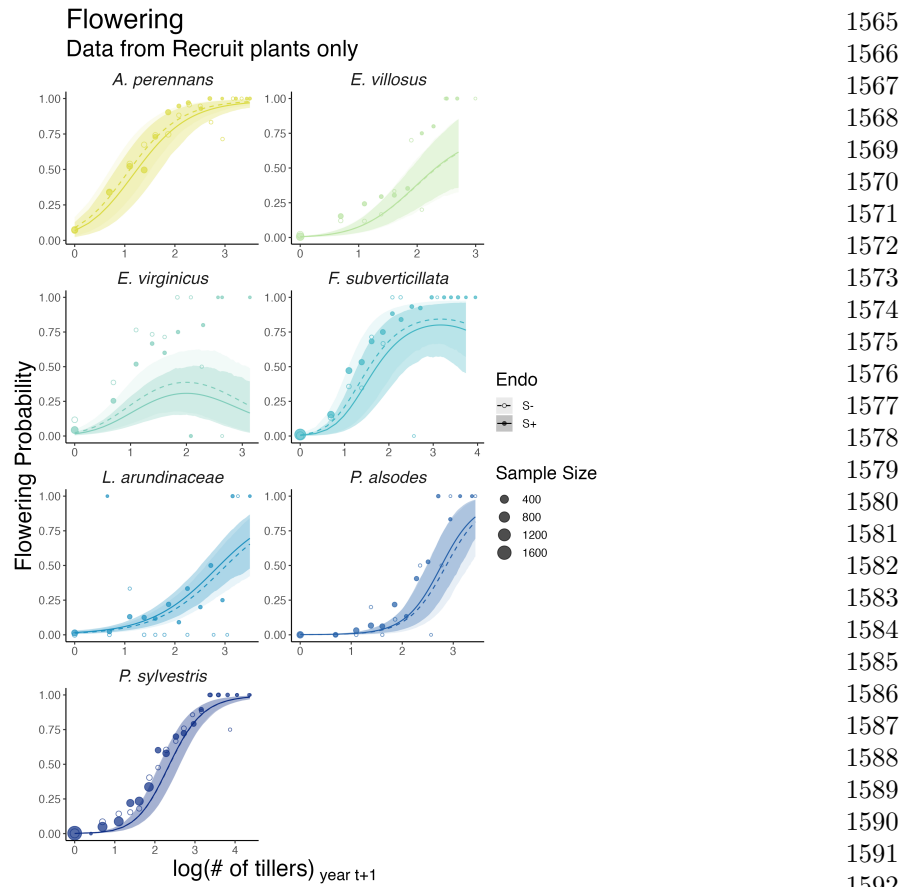
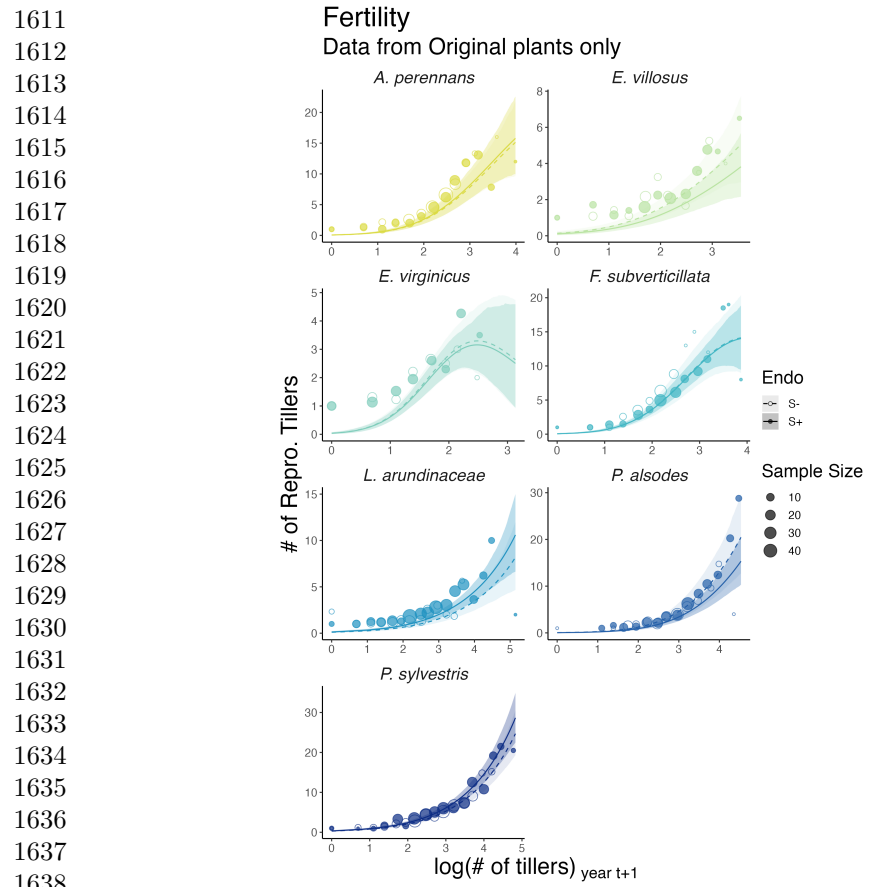


Figure S7: Effect of endophyte symbiosis on mean flowering. Fitted curves represent the size-specific mean flowering probability for recruited plants along with data binned by size and averaged over many individuals, years, and plots shown as open circles with a dashed line for symbiont-free (S-) plants, while the solid line and filled circles represent symbiotic (S+) plants. 80% credible intervals are shown with dark shading for S+, or light shading for S-.



1639 Figure S8: Effect of endophyte symbiosis on mean fertility. Fitted curves represent
 1640 the size-specific mean expected number of flowering tillers for originally transplanted
 1641 plants along with data binned by size and averaged over many individuals, years, and
 1642 plots shown as open circles with a dashed line for symbiont-free (S-) plants, while the
 1643 solid line and filled circles represent symbiotic (S+) plants. 80% credible intervals
 1644 are shown with dark shading for S+, or light shading for S-.

1645
 1646
 1647
 1648
 1649
 1650
 1651
 1652
 1653
 1654
 1655
 1656

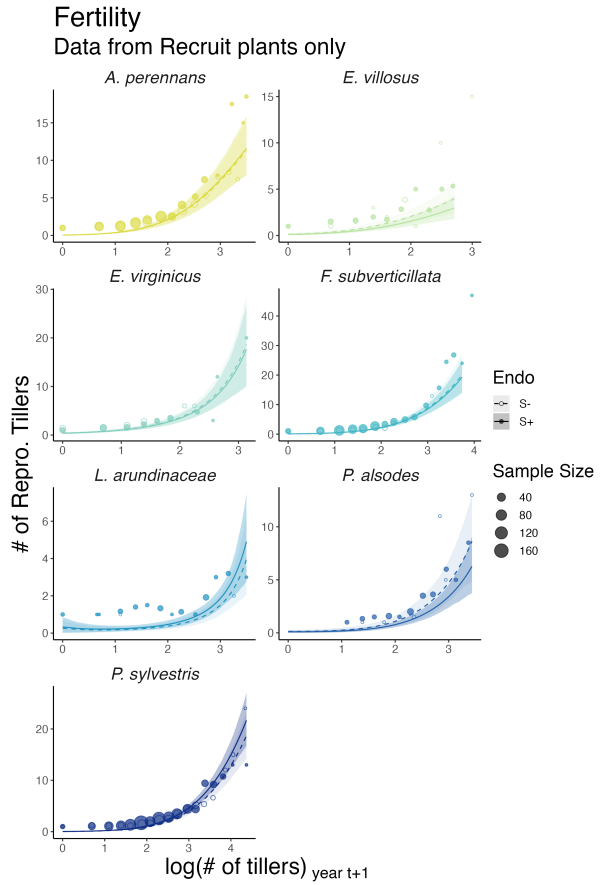
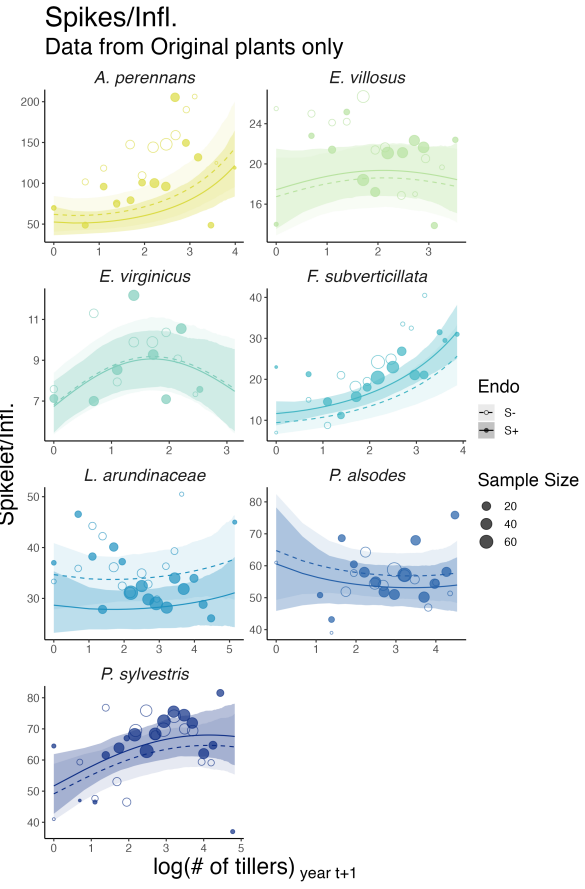


Figure S9: Effect of endophyte symbiosis on mean fertility. Fitted curves represent the size-specific mean expected number of flowering tillers for recruited plants along with data binned by size and averaged over many individuals, years, and plots shown as open circles with a dashed line for symbiont-free (S-) plants, while the solid line and filled circles represent symbiotic (S+) plants. 80% credible intervals are shown with dark shading for S+, or light shading for S-.

1657
1658
1659
1660
1661
1662
1663
1664
1665
1666
1667
1668
1669
1670
1671
1672
1673
1674
1675
1676
1677
1678
1679
1680
1681
1682
1683
1684
1685
1686
1687
1688
1689
1690
1691
1692
1693
1694
1695
1696
1697
1698
1699
1700
1701
1702

1703
1704
1705
1706
1707
1708
1709
1710
1711
1712
1713
1714
1715
1716
1717
1718
1719
1720
1721
1722
1723
1724
1725
1726
1727
1728
1729
1730



1731 Figure S10: Effect of endophyte symbiosis on mean spikelet production. Fitted curves
1732 represent the size-specific mean expected number of spikelets per inflorescence for
1733 originally transplanted plants along with data binned by size and averaged over many
1734 individuals, years, and plots shown as open circles with a dashed line for symbiont-
1735 free (S-) plants, while the solid line and filled circles represent symbiotic (S+) plants.
1736 80% credible intervals are shown with dark shading for S+, or light shading for S-.

1737
1738
1739
1740
1741
1742
1743
1744
1745
1746
1747
1748

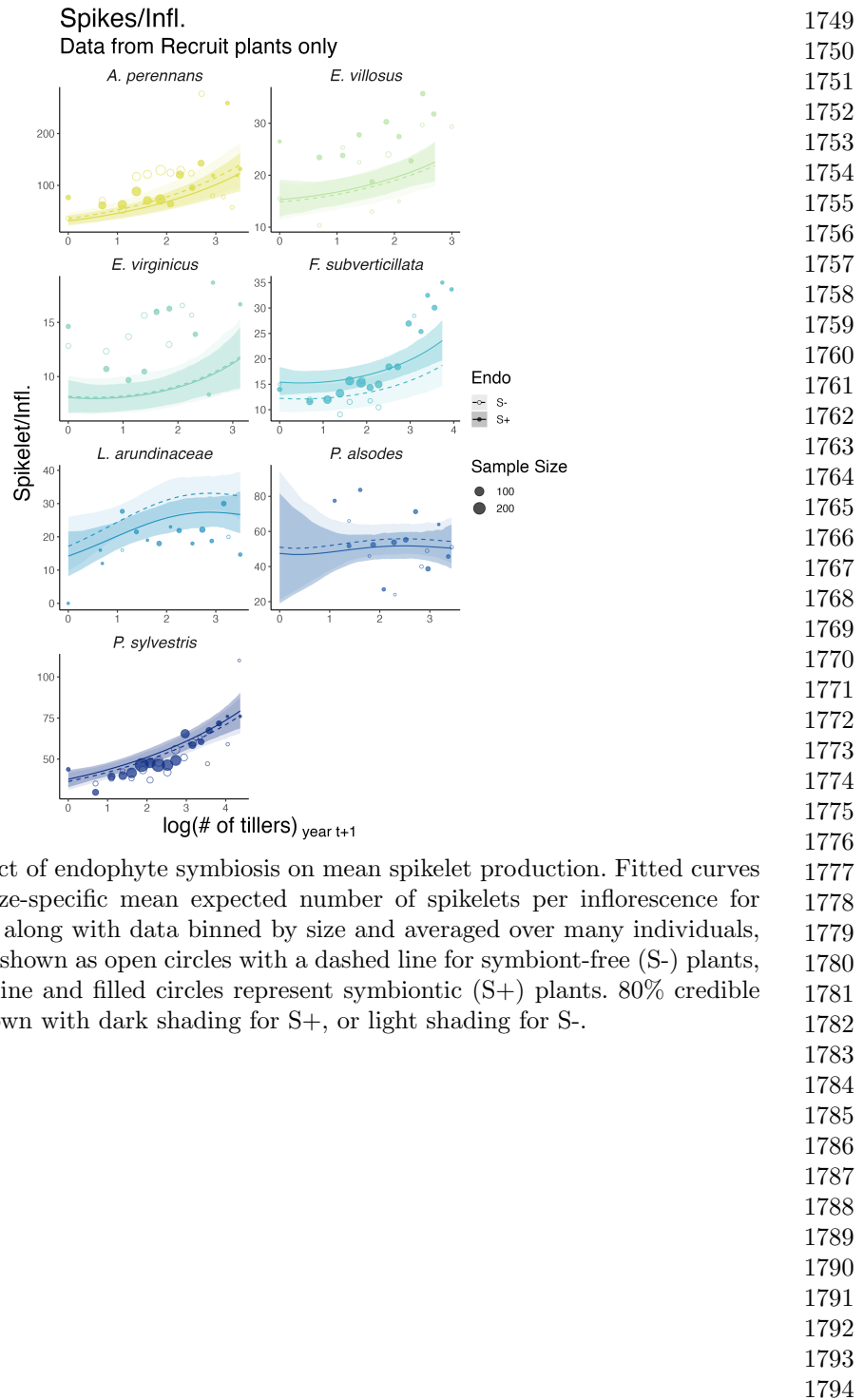
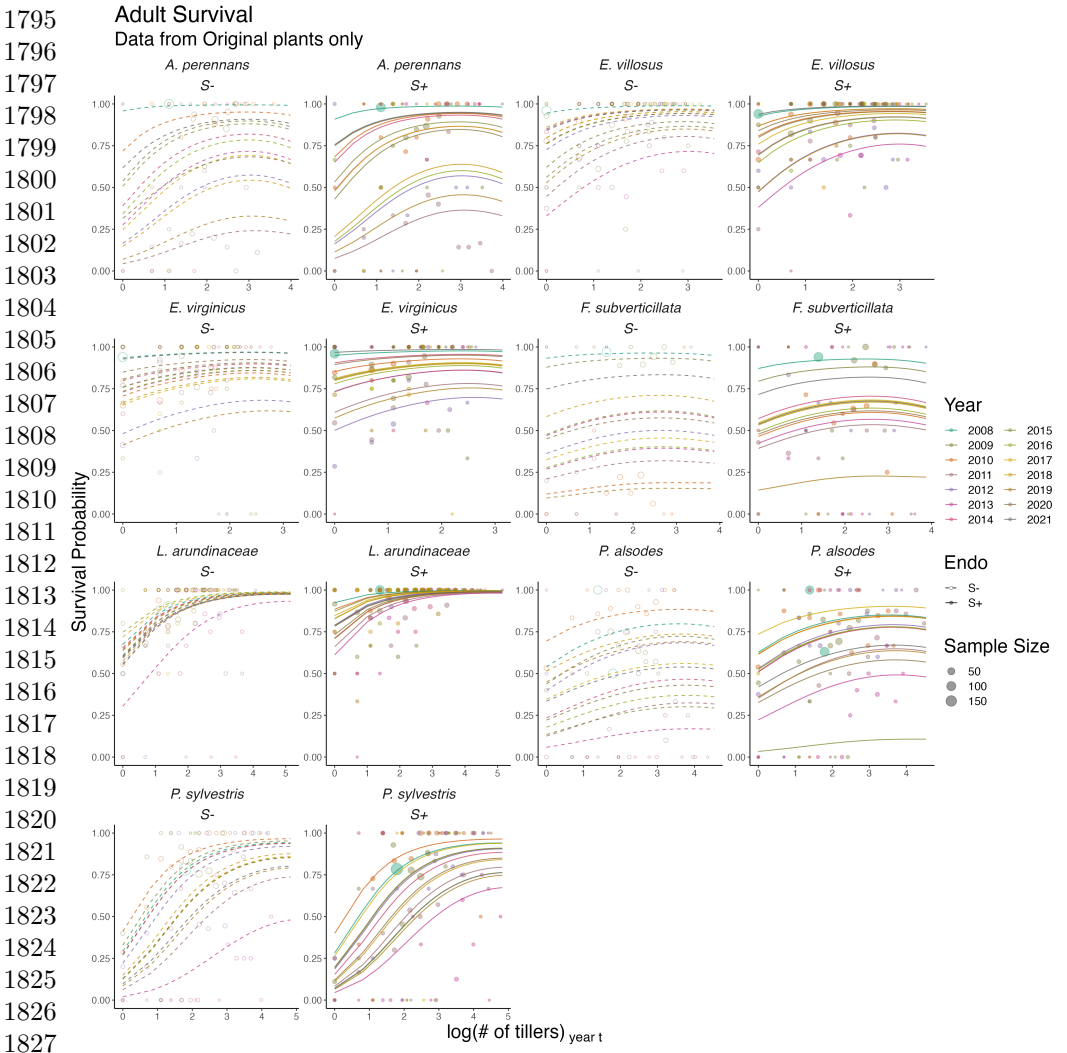


Figure S11: Effect of endophyte symbiosis on mean spikelet production. Fitted curves represent the size-specific mean expected number of spikelets per inflorescence for recruited plants along with data binned by size and averaged over many individuals, years, and plots shown as open circles with a dashed line for symbiont-free (S-) plants, while the solid line and filled circles represent symbiotic (S+) plants. 80% credible intervals are shown with dark shading for S+, or light shading for S-.



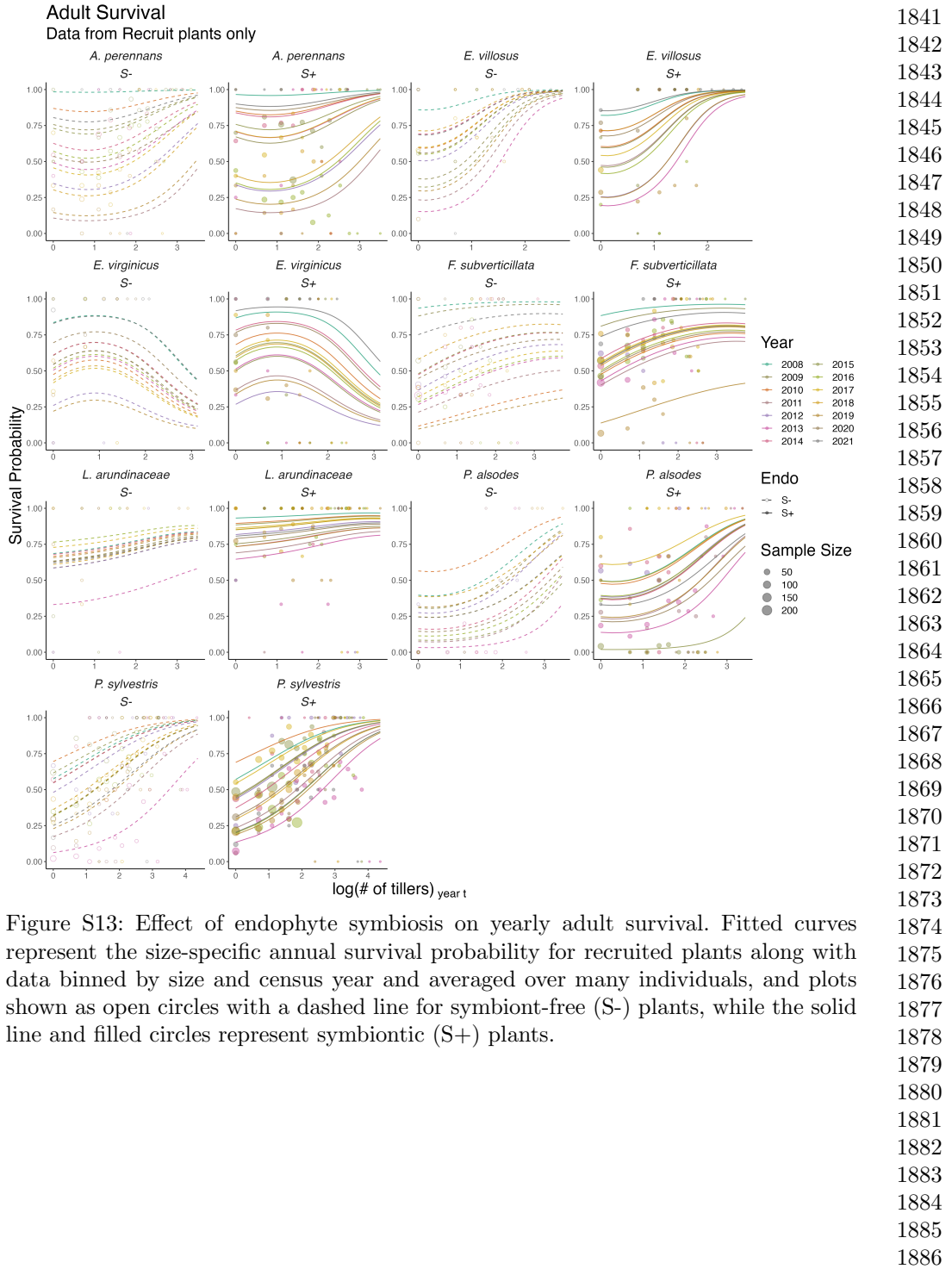
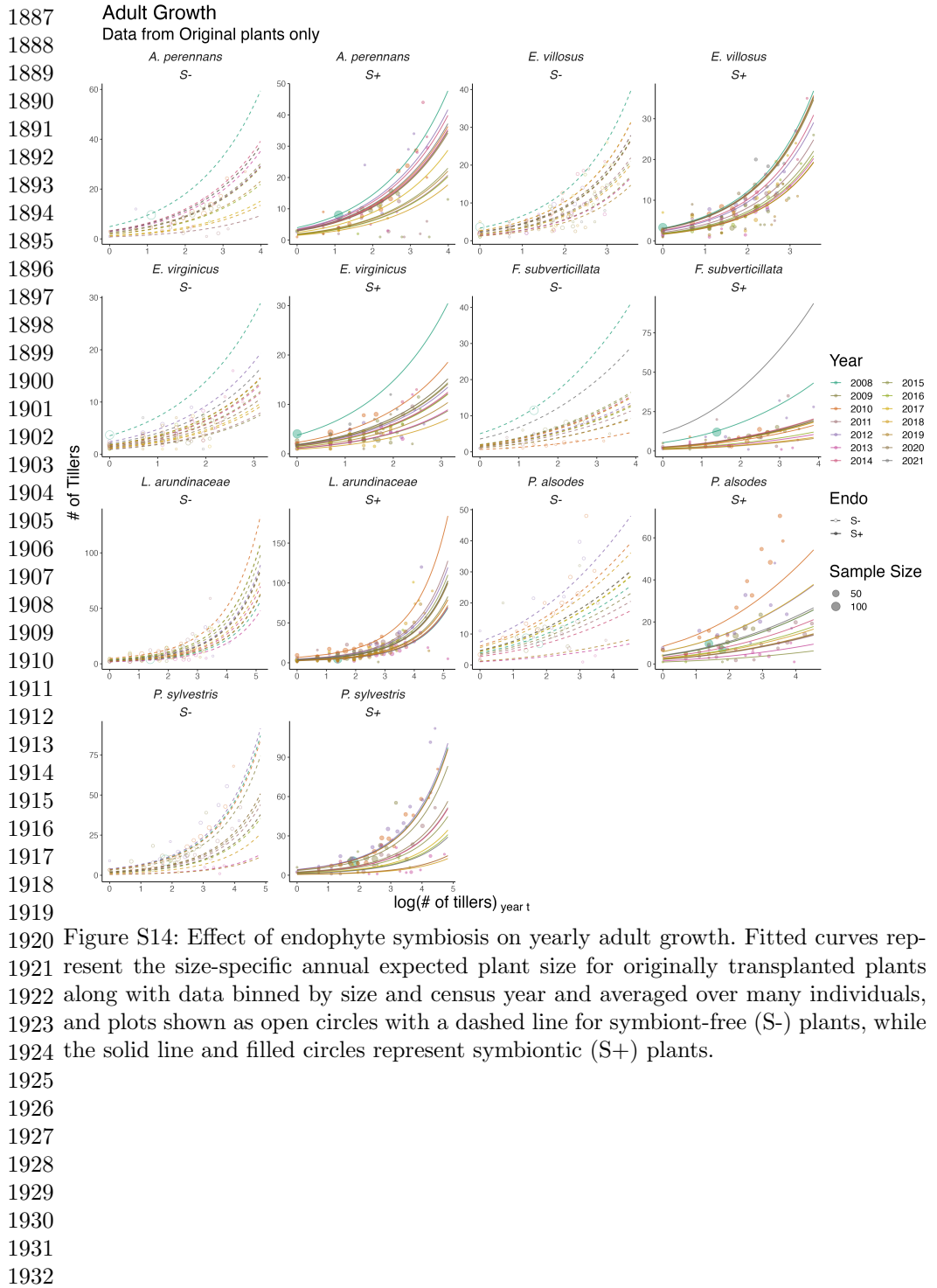


Figure S13: Effect of endophyte symbiosis on yearly adult survival. Fitted curves represent the size-specific annual survival probability for recruited plants along with data binned by size and census year and averaged over many individuals, and plots shown as open circles with a dashed line for symbiont-free (S-) plants, while the solid line and filled circles represent symbiotic (S+) plants.



1920 Figure S14: Effect of endophyte symbiosis on yearly adult growth. Fitted curves represent the size-specific annual expected plant size for originally transplanted plants 1921 along with data binned by size and census year and averaged over many individuals, 1922 and plots shown as open circles with a dashed line for symbiont-free (S-) plants, while 1923 the solid line and filled circles represent symbiotic (S+) plants.

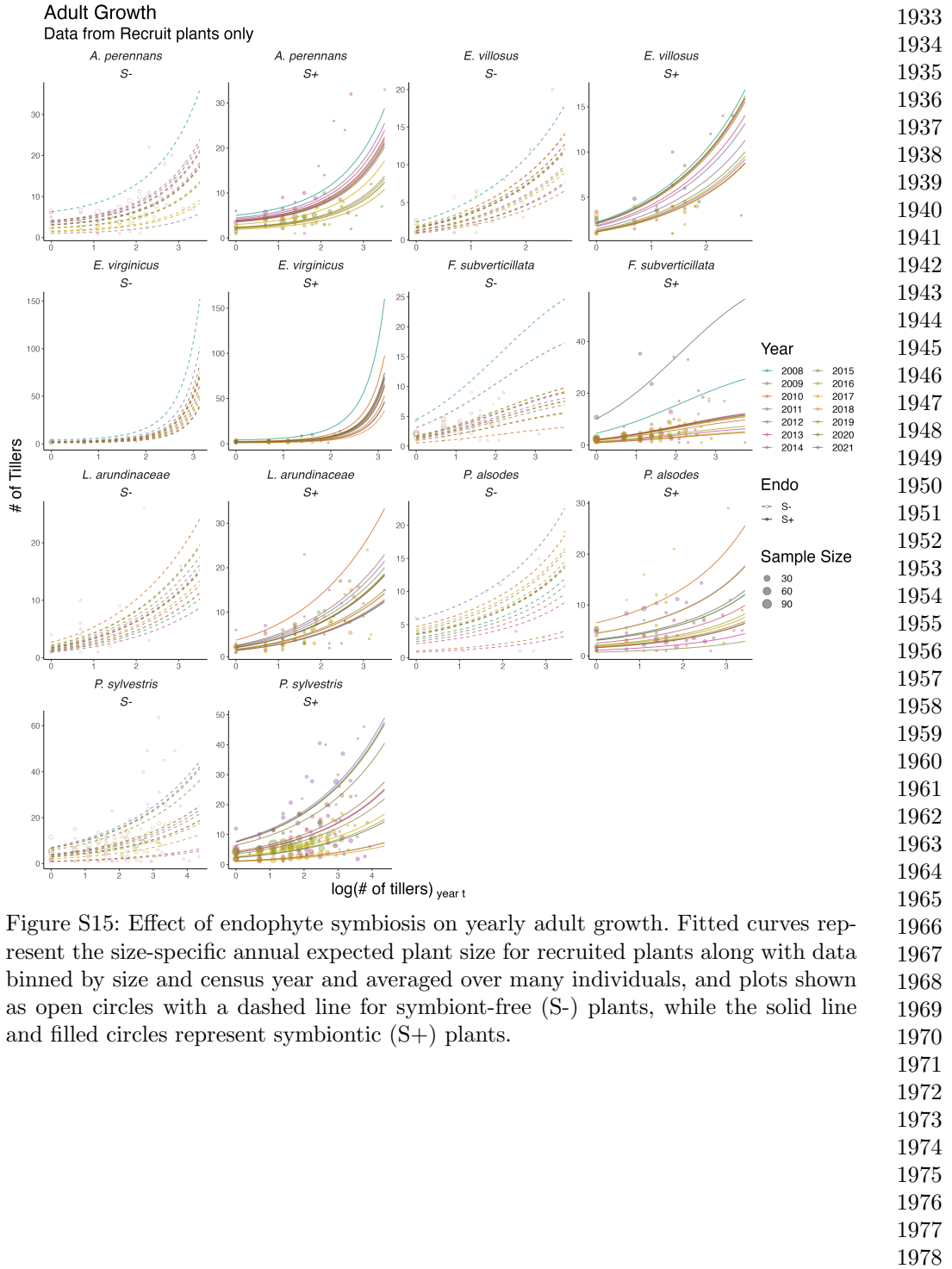
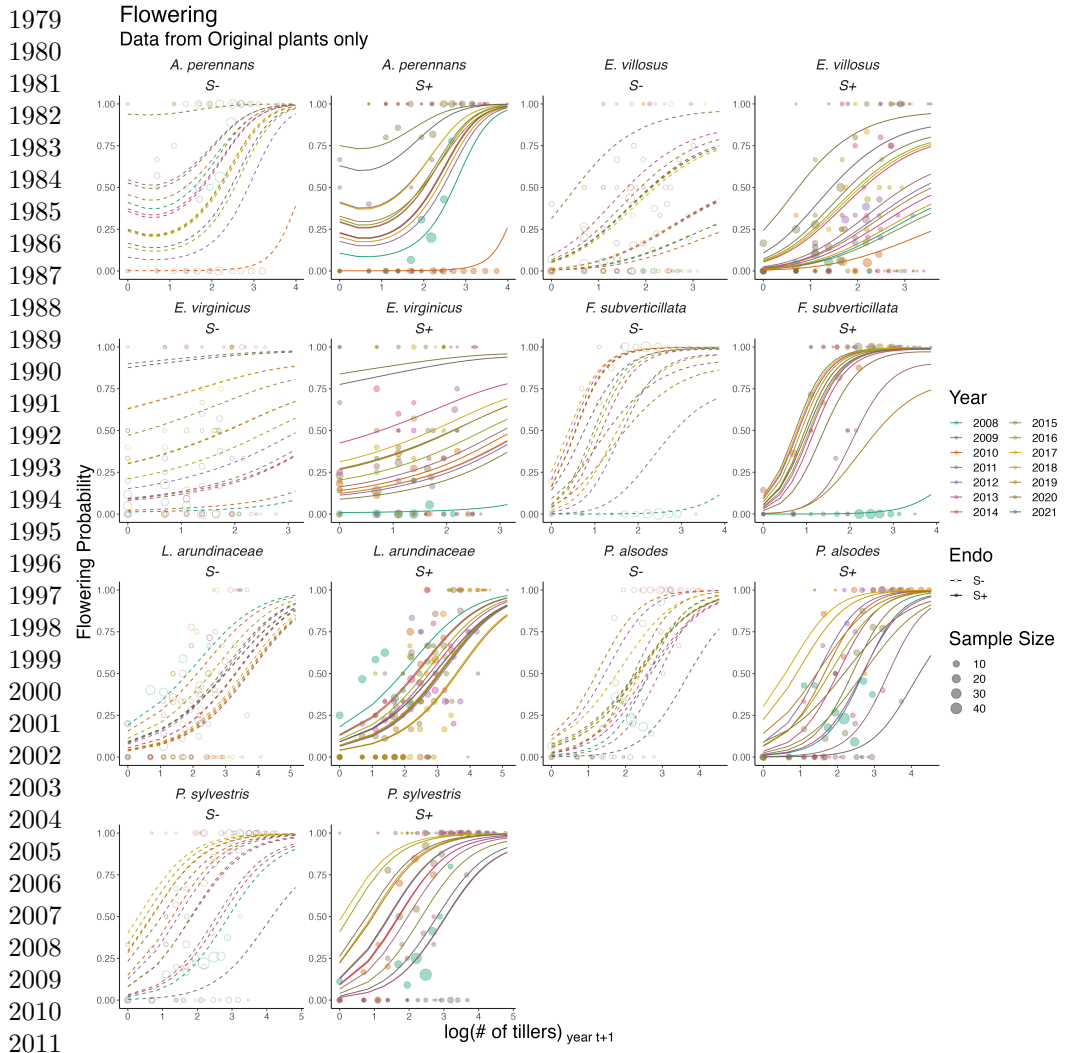


Figure S15: Effect of endophyte symbiosis on yearly adult growth. Fitted curves represent the size-specific annual expected plant size for recruited plants along with data binned by size and census year and averaged over many individuals, and plots shown as open circles with a dashed line for symbiont-free (S-) plants, while the solid line and filled circles represent symbiotic (S+) plants.



2012 Figure S16: Effect of endophyte symbiosis on yearly flowering. Fitted curves represent 2013 the size-specific annual flowering probability for originally transplanted plants along 2014 with data binned by size and census year and averaged over many individuals, and 2015 plots shown as open circles with a dashed line for symbiont-free (S-) plants, while the 2016 solid line and filled circles represent symbiotic (S+) plants.

2017
2018
2019
2020
2021
2022
2023
2024

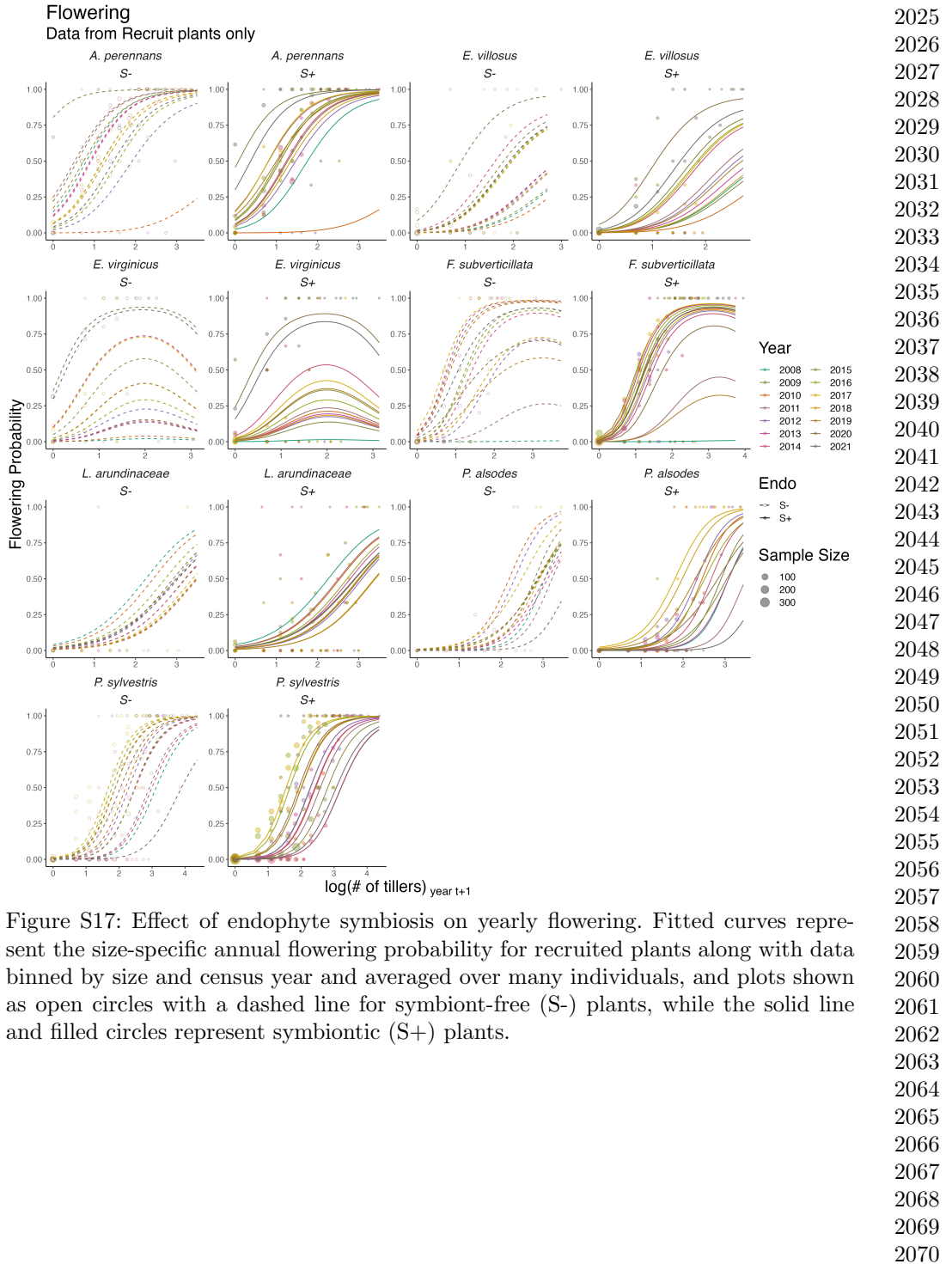
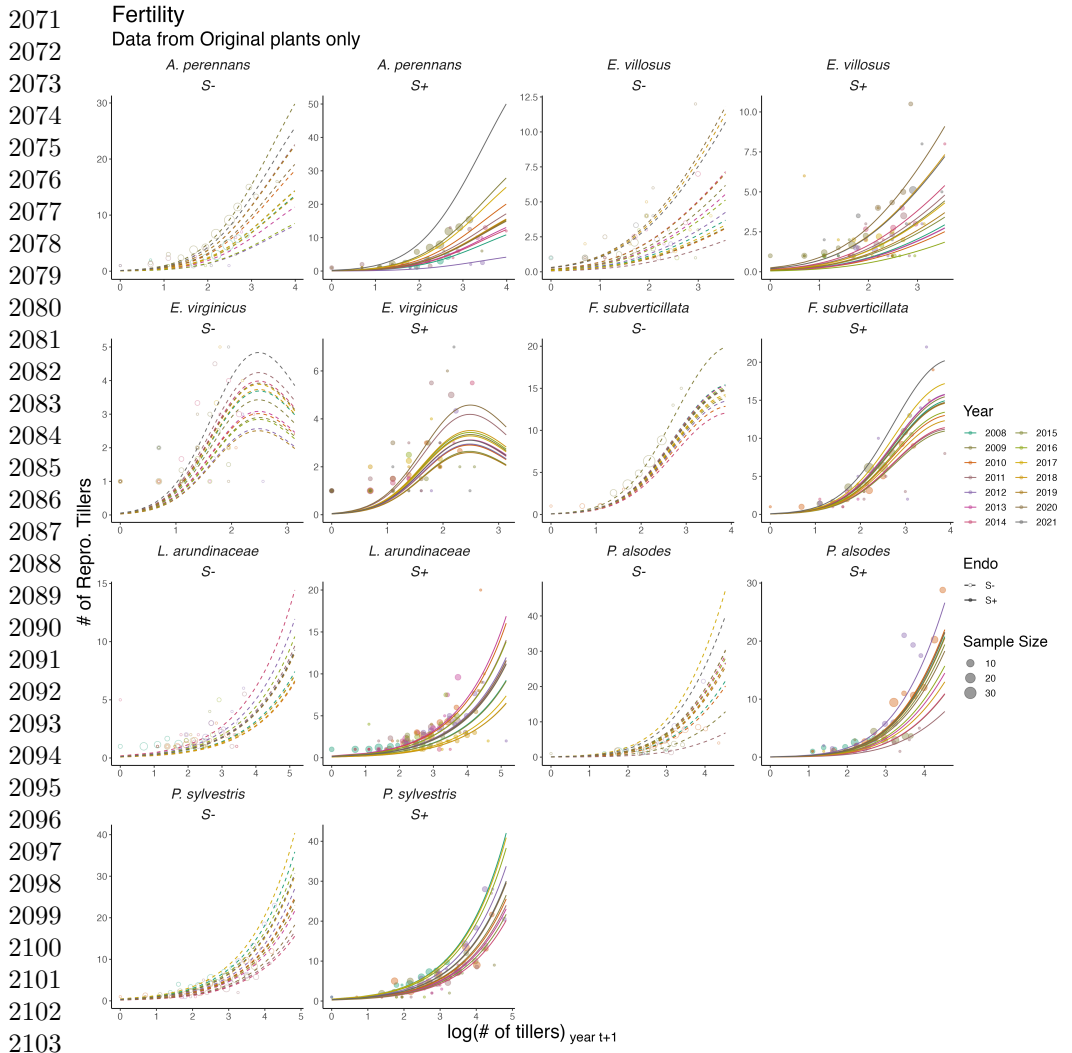


Figure S17: Effect of endophyte symbiosis on yearly flowering. Fitted curves represent the size-specific annual flowering probability for recruited plants along with data binned by size and census year and averaged over many individuals, and plots shown as open circles with a dashed line for symbiont-free (S-) plants, while the solid line and filled circles represent symbiotic (S+) plants.



2104 Figure S18: Effect of endophyte symbiosis on yearly fertility. Fitted curves represent
2105 the size-specific annual expected number of flowering tillers for originally transplanted
2106 plants along with data binned by size and census year and averaged over many individ-
2107 uals, and plots shown as open circles with a dashed line for symbiont-free (S-) plants,
2108 while the solid line and filled circles represent symbiotic (S+) plants.

2109
2110
2111
2112
2113
2114
2115
2116

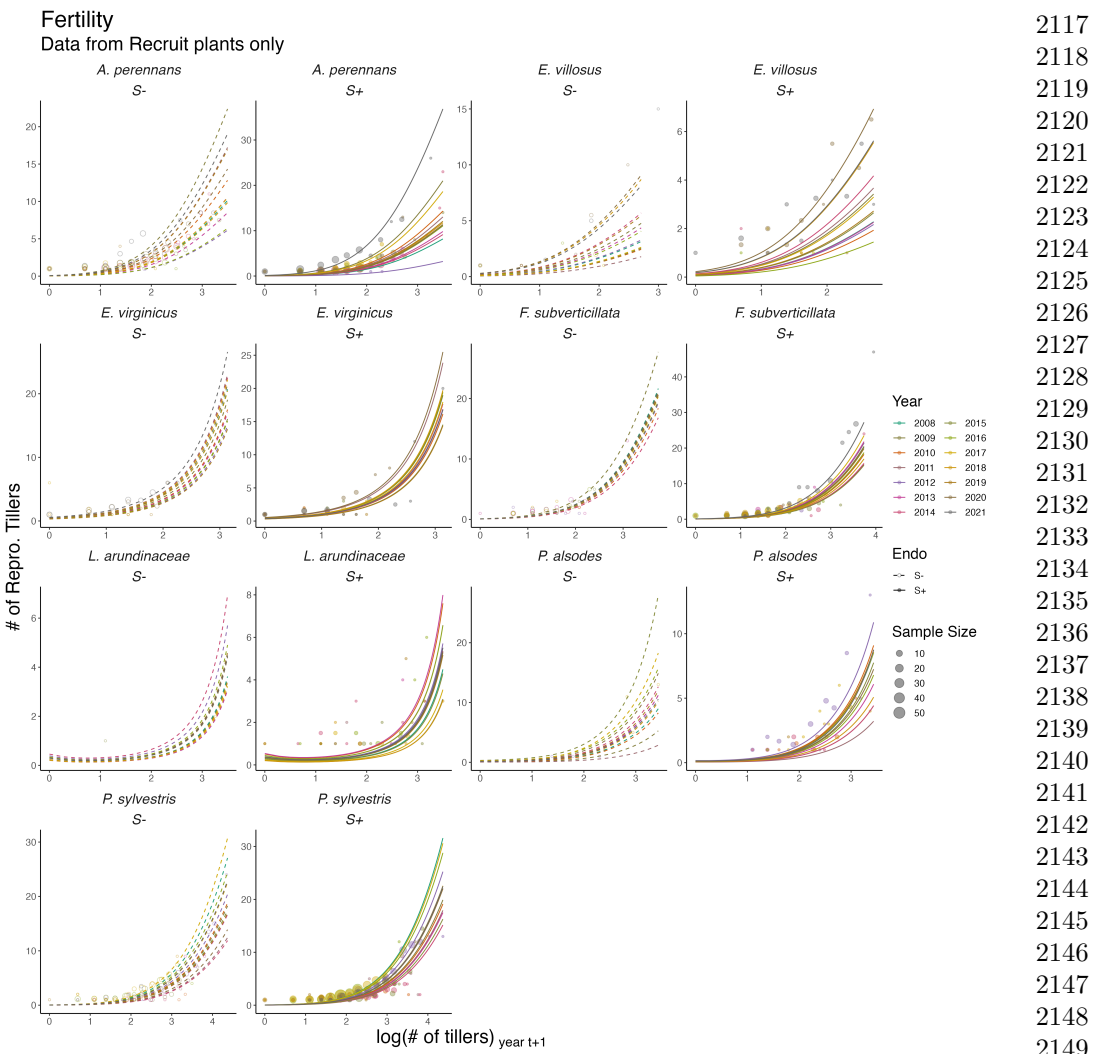
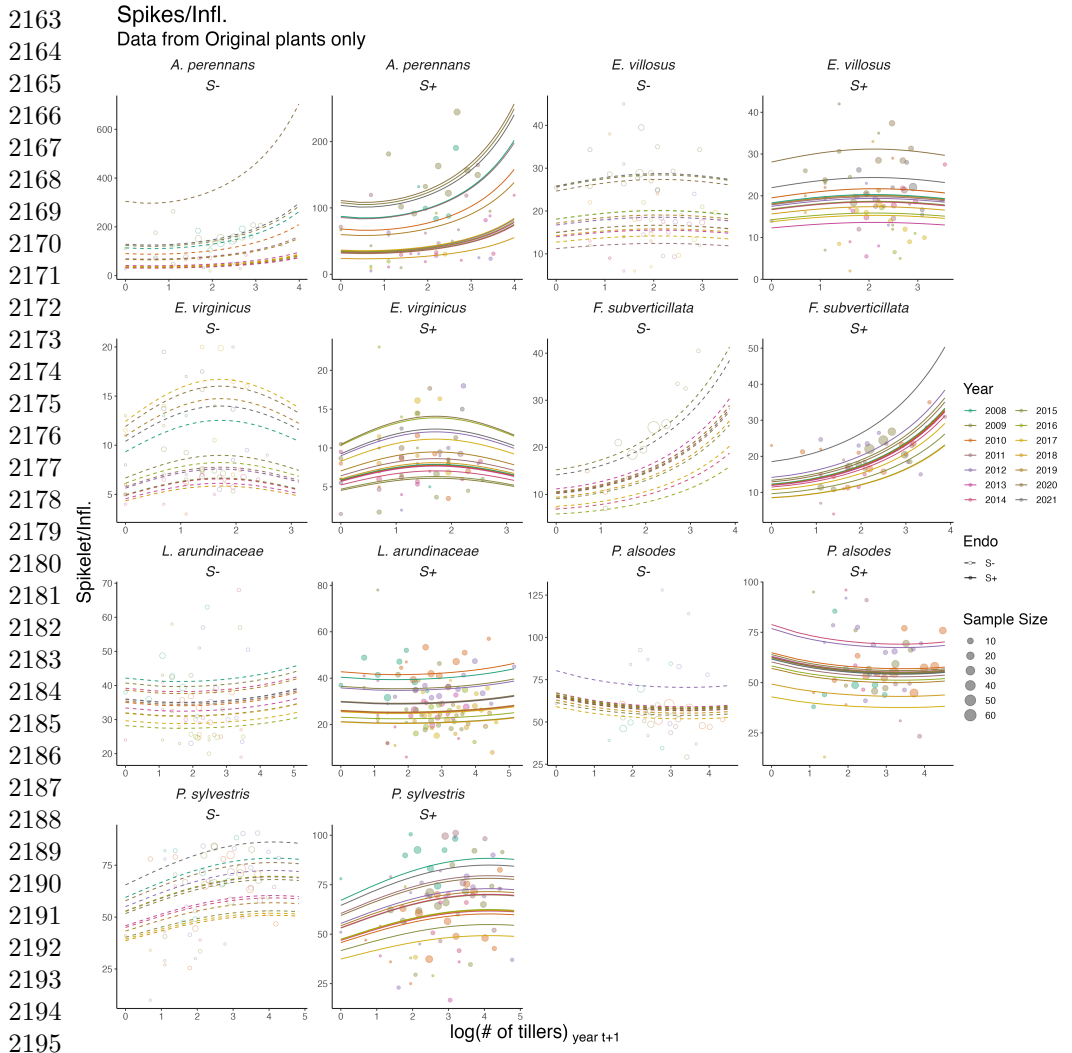


Figure S19: Effect of endophyte symbiosis on yearly fertility. Fitted curves represent the size-specific annual expected number of flowering tillers for recruited plants along with data binned by size and census year and averaged over many individuals, and plots shown as open circles with a dashed line for symbiont-free (S-) plants, while the solid line and filled circles represent symbiotic (S+) plants.



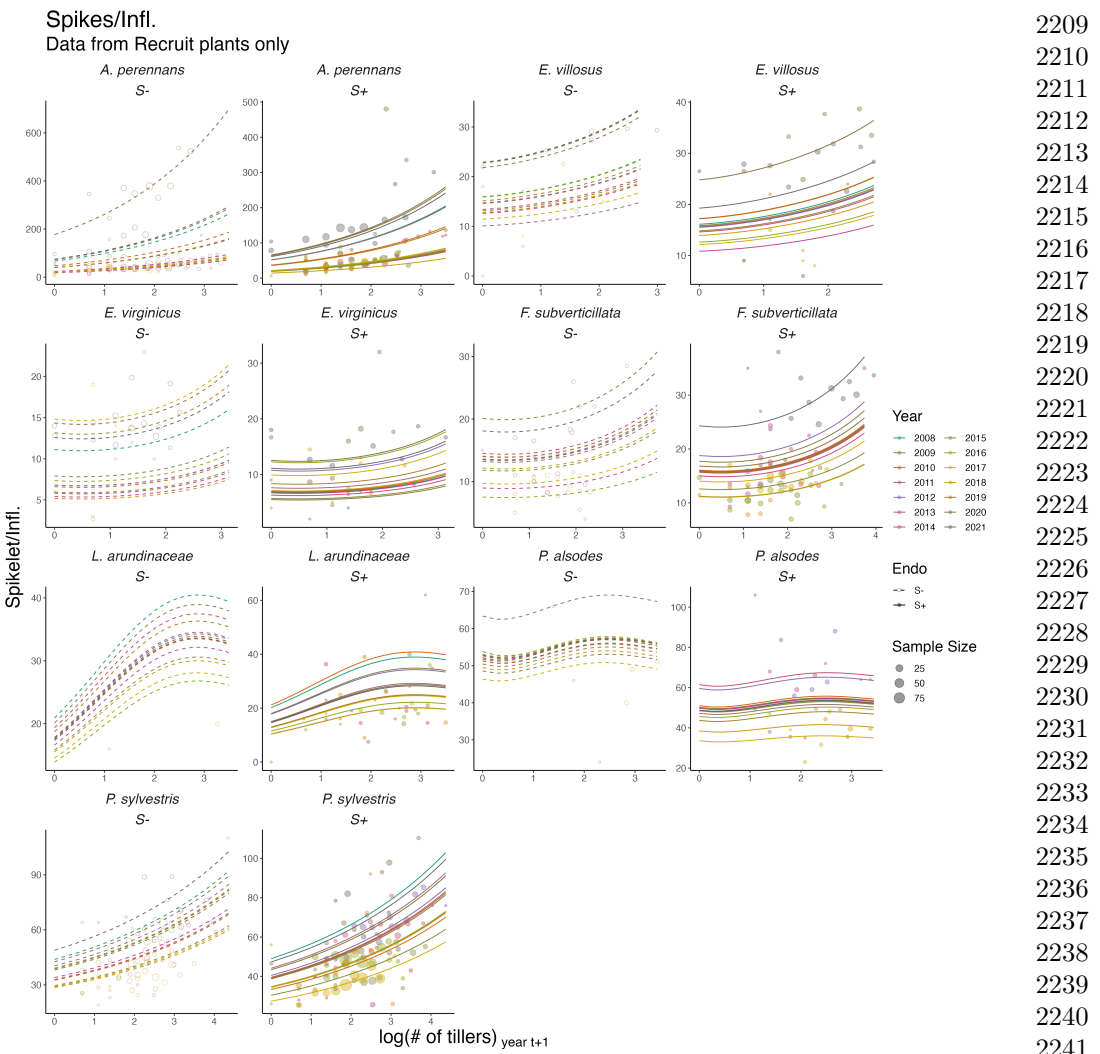
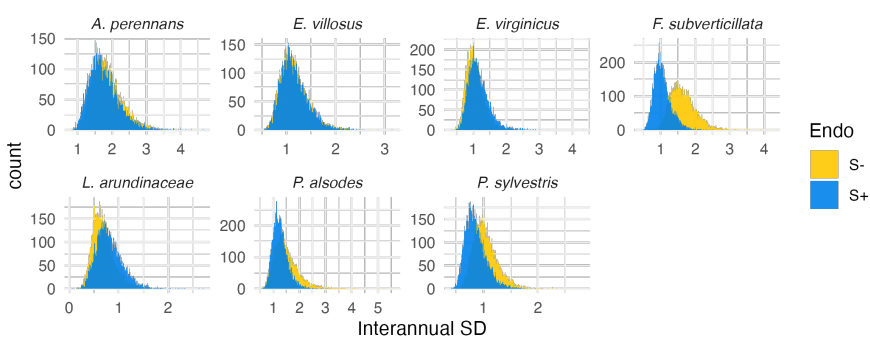


Figure S21: Effect of endophyte symbiosis on yearly spikelet production. Fitted curves represent the size-specific annual expected number of spikelets per inflorescence for recruited plants along with data binned by size and census year and averaged over many individuals, and plots shown as open circles with a dashed line for symbiont-free (S-) plants, while the solid line and filled circles represent symbiotic (S+) plants.

2255

Survival

2256



2257

2258

2259

2260

2261

2262

2263

2264

2265

2266

2267

2267 Figure S22: Posterior distributions of the standard deviations of inter-annual year
2268 effects for survival. Histograms include 7500 post-warmup MCMC samples for
2269 symbiotic (S+; blue) and symbiont-free (S-; tan) plants from fitted vital rate model.

2270

2271

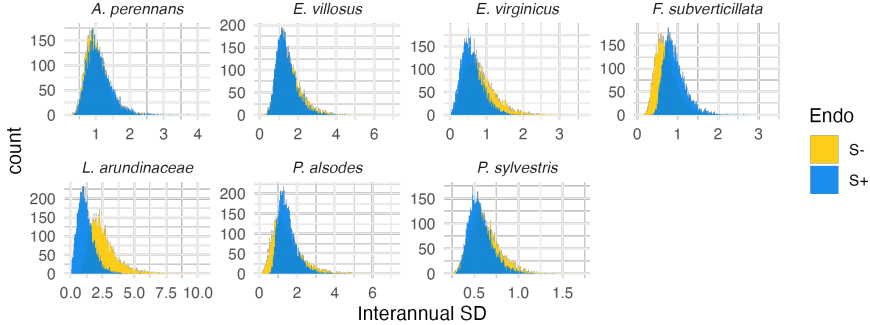
2272

2273

2274

Seedling Survival

2275



2276

2277

2278

2279

2280

2281

2282

2283

2284

2285

2285 Figure S23: Posterior distributions of the standard deviations of inter-annual year
2286 effects for seedling survival. Histograms include 7500 post-warmup MCMC samples for
2287 symbiotic (S+; blue) and symbiont-free (S-; tan) plants from fitted vital rate model.

2289

2290

2291

2292

2293

2294

2295

2296

2297

2298

2299

2300

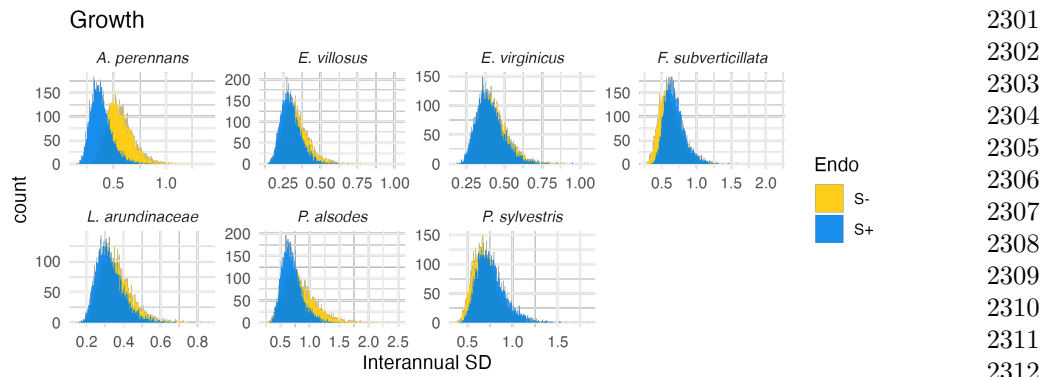


Figure S24: Posterior distributions of the standard deviations of inter-annual year effects for growth. Histograms include 7500 post-warmup MCMC samples for symbiotic (S+; blue) and symbiont-free (S-; tan) plants from fitted vital rate model.

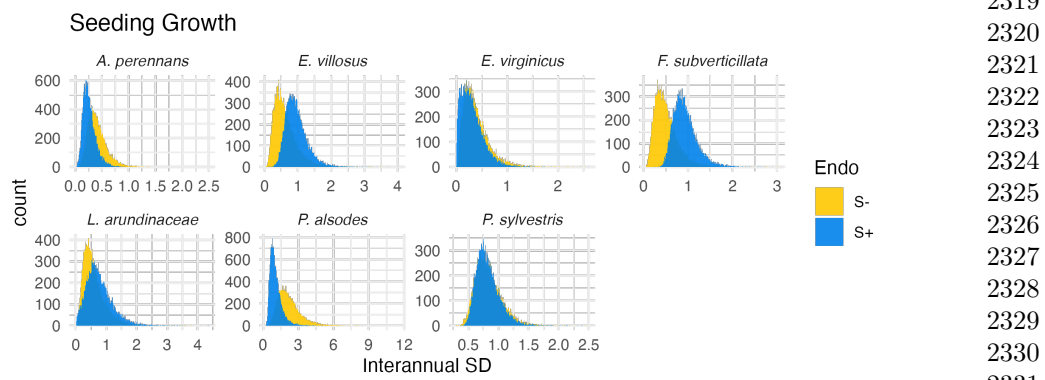
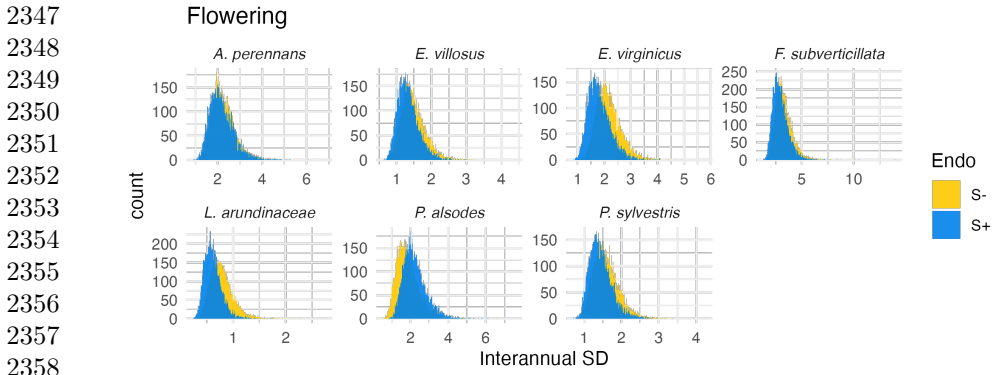
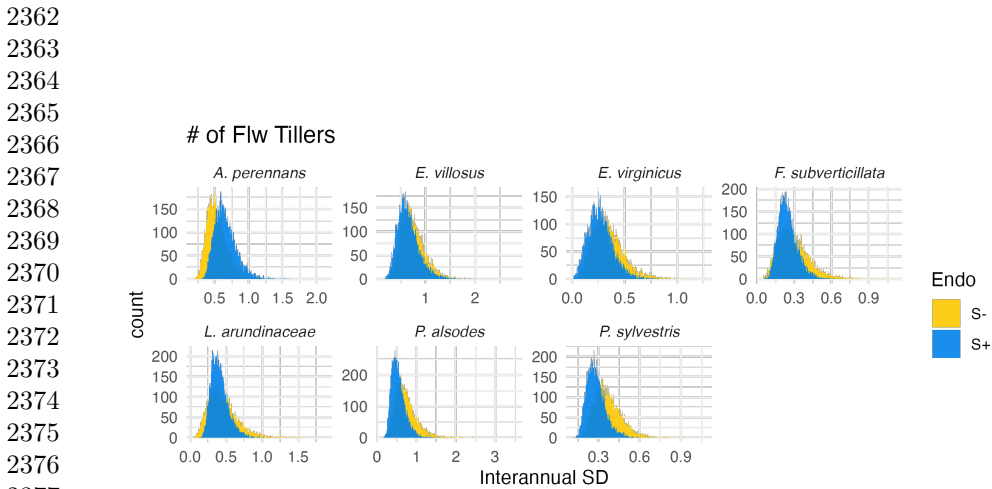


Figure S25: Posterior distributions of the standard deviations of inter-annual year effects for seedling growth. Histograms include 7500 post-warmup MCMC samples for symbiotic (S+; blue) and symbiont-free (S-; tan) plants from fitted vital rate model.



2359 Figure S26: Posterior distributions of the standard deviations of inter-annual year
2360 effects for flowering probability. Histograms include 7500 post-warmup MCMC samples
2361 for symbiotic (S+; blue) and symbiont-free (S-; tan) plants from fitted vital rate model.



2378 Figure S27: Posterior distributions of the standard deviations of inter-annual year
2379 effects for fertility (no. of flowering tillers). Histograms include 7500 post-warmup
2380 MCMC samples for symbiotic (S+; blue) and symbiont-free (S-; tan) plants from fitted
2381 vital rate model.

2382

2383

2384

2385

2386

2387

2388

2389

2390

2391

2392

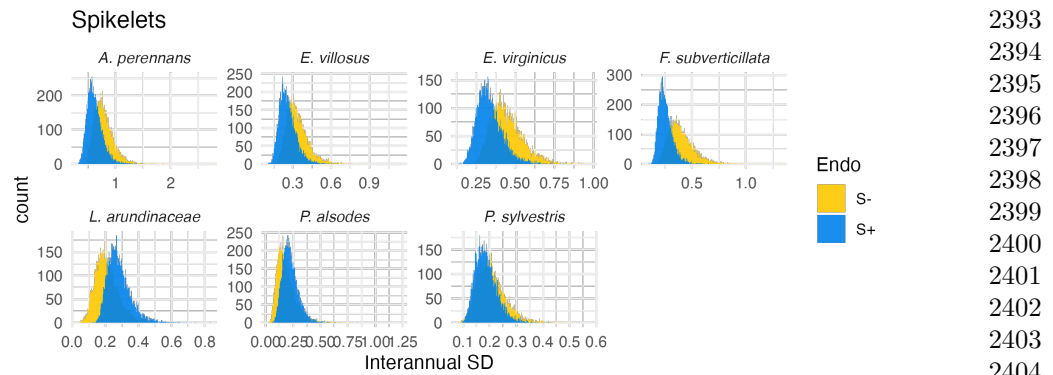


Figure S28: Posterior distributions of the standard deviations of inter-annual year effects for spikelets per inflorescence. Histograms include 7500 post-warmup MCMC samples for symbiotic (S+; blue) and symbiont-free (S-; tan) plants from fitted vital rate model.

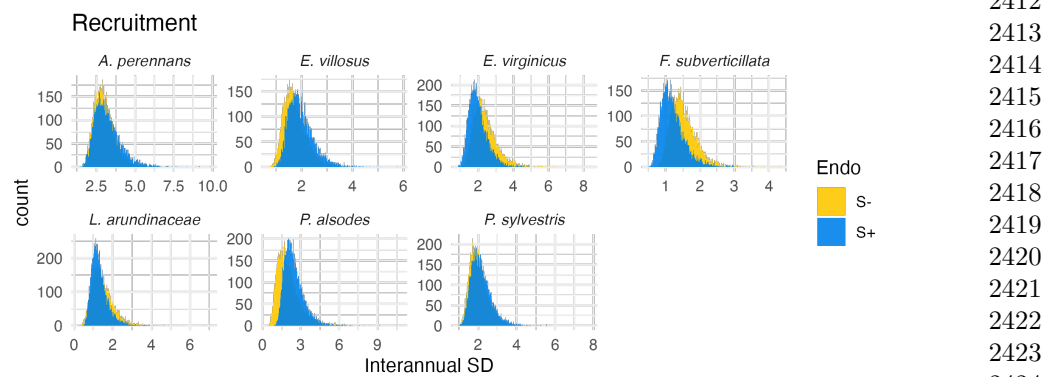


Figure S29: Posterior distributions of the standard deviations of inter-annual year effects for recruitment. Histograms include 7500 post-warmup MCMC samples for symbiotic (S+; blue) and symbiont-free (S-; tan) plants from fitted vital rate model.

2439
2440
2441
2442
2443
2444
2445
2446
2447
2448
2449
2450
2451
2452
2453
2454
2461
2462
2463
2464
2465
2466
2467
2468
2469
2470
2471
2472
2473
2474
2475
2476
2477
2478
2479
2480
2481
2482
2483
2484

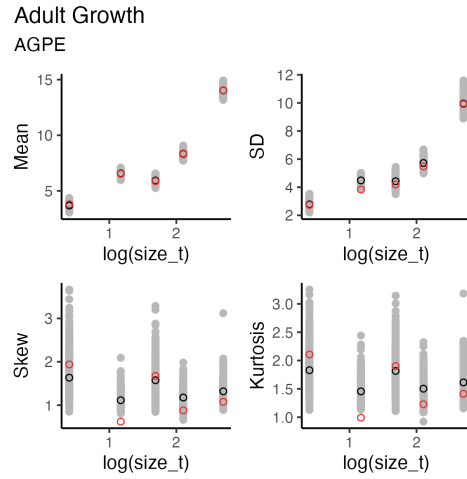


Figure S30: Graphical posterior predictive check for mean and higher moments of *A. perennans* growth model across size. Consistency between real data and fitted values across sizes indicates that the vital rate models are accurately capturing size dependence. Points show the value of statistical moments binned across size for the observed data (red circles) compared to the simulated datasets (grey circles) and the median of the simulated values (black circles) generated from 500 posterior draws from the fitted model.

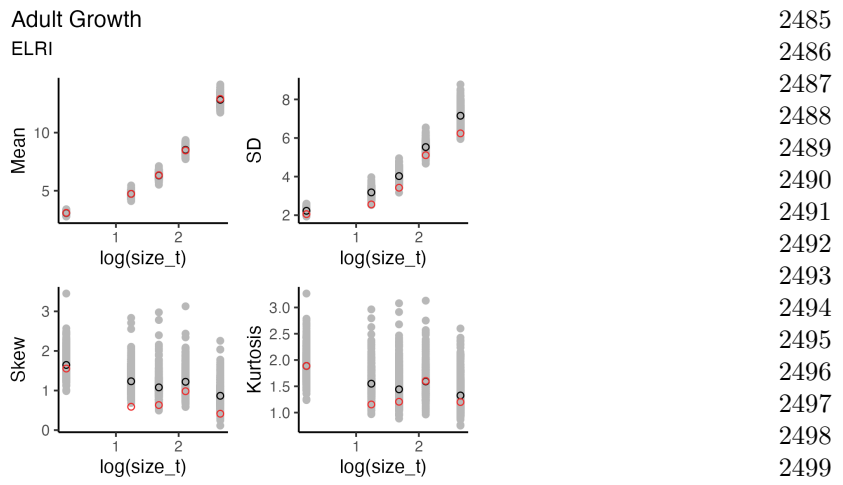
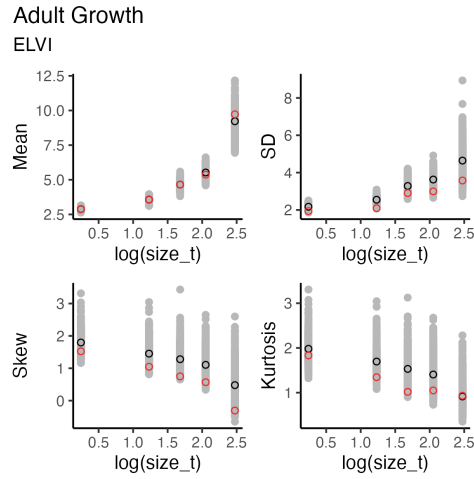


Figure S31: Graphical posterior predictive check for mean and higher moments of *E. villosus* growth model across size. Consistency between real data and fitted values across sizes indicates that the vital rate models are accurately capturing size dependence. Points show the value of statistical moments binned across size for the observed data (red circles) compared to the simulated datasets (grey circles) and the median of the simulated values (black circles) generated from 500 posterior draws from the fitted model.

2531
2532
2533
2534
2535
2536
2537
2538
2539
2540
2541
2542
2543
2544
2545
2546
2553
2554
2555
2556
2557
2558
2559
2560
2561
2562
2563
2564
2565
2566
2567
2568
2569
2570
2571
2572
2573
2574
2575
2576



2546 Figure S32: Graphical posterior predictive check for mean and higher moments of *E.*
2547 *virginicus* growth model across size. Consistency between real data and fitted values
2548 across sizes indicates that the vital rate models are accurately capturing size depen-
2549 dence. Points show the value of statistical moments binned across size for the observed
2550 data (red circles) compared to the simulated datasets (grey circles) and the median
2551 of the simulated values (black circles) generated from 500 posterior draws from the
2552 fitted model.

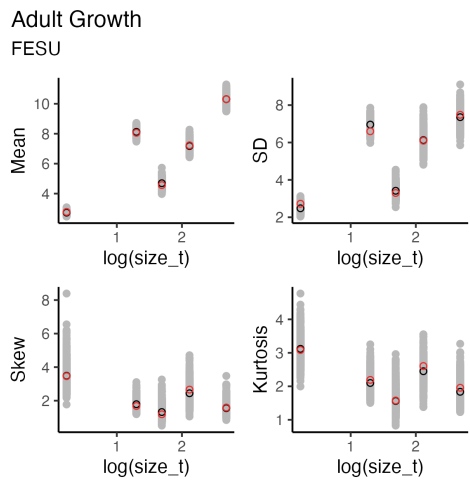


Figure S33: Graphical posterior predictive check for mean and higher moments of *F. subverticillata* growth model across size. Consistency between real data and fitted values across sizes indicates that the vital rate models are accurately capturing size dependence. Points show the value of statistical moments binned across size for the observed data (red circles) compared to the simulated datasets (grey circles) and the median of the simulated values (black circles) generated from 500 posterior draws from the fitted model.

2577
2578
2579
2580
2581
2582
2583
2584
2585
2586
2587
2588
2589
2590
2591
2592
2593
2594
2595
2596
2597
2598
2599
2600
2601
2602
2603
2604
2605
2606
2607
2608
2609
2610
2611
2612
2613
2614
2615
2616
2617
2618
2619
2620
2621
2622

2623
2624
2625
2626
2627
2628
2629
2630
2631
2632
2633
2634
2635
2636
2637
2638
2639
2640
2641
2642
2643
2644
2645
2646
2647
2648
2649
2650
2651
2652
2653
2654
2655
2656
2657
2658
2659
2660
2661
2662
2663
2664
2665
2666
2667
2668

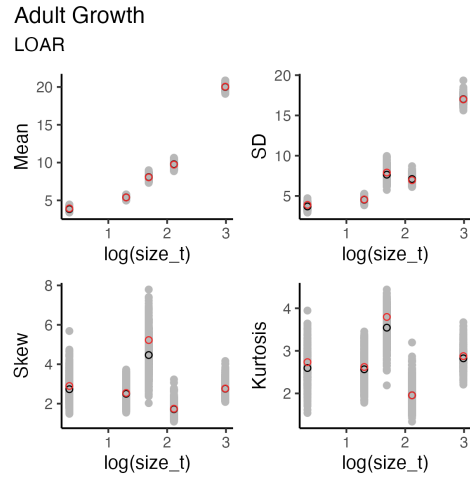


Figure S34: Graphical posterior predictive check for mean and higher moments of *L. arundinacea* growth model across size. Consistency between real data and fitted values across sizes indicates that the vital rate models are accurately capturing size dependence. Points show the value of statistical moments binned across size for the observed data (red circles) compared to the simulated datasets (grey circles) and the median of the simulated values (black circles) generated from 500 posterior draws from the fitted model.

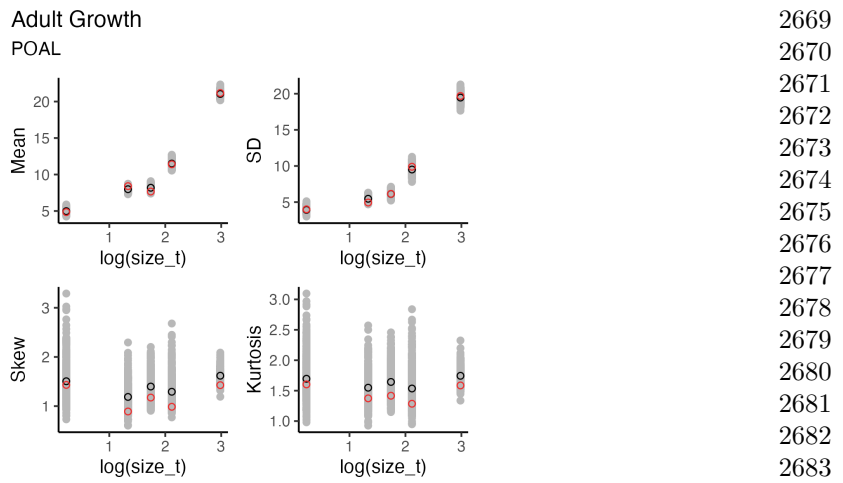


Figure S35: Graphical posterior predictive check for mean and higher moments of *P. alsodes* growth model across size. Consistency between real data and fitted values across sizes indicates that the vital rate models are accurately capturing size dependence. Points show the value of statistical moments binned across size for the observed data (red circles) compared to the simulated datasets (grey circles) and the median of the simulated values (black circles) generated from 500 posterior draws from the fitted model.

2669
2670
2671
2672
2673
2674
2675
2676
2677
2678
2679
2680
2681
2682
2683
2684
2685
2686
2687
2688
2689
2690
2691
2692
2693
2694
2695
2696
2697
2698
2699
2700
2701
2702
2703
2704
2705
2706
2707
2708
2709
2710
2711
2712
2713
2714

2715

2716

2717

2718

2719

2720

2721

2722

2723

2724

2725

2726

2727

2728

2729

2730

2731

2732

2733

2734

2735

2736

2737

2738

2739

2740

2741

2742

2743

2744

2745

2746

2747

2748

2749

2750

2751

2752

2753

2754

2755

2756

2757

2758

2759

2760

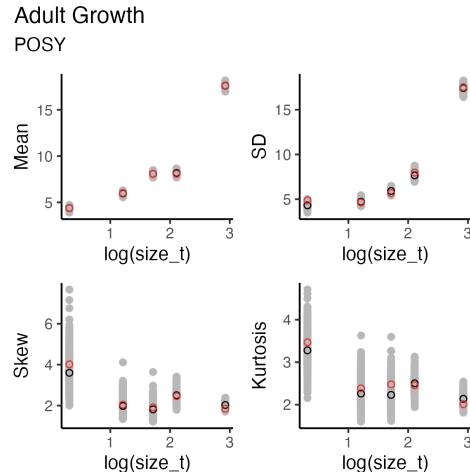


Figure S36: Graphical posterior predictive check for mean and higher moments of *P. sylvestris* growth model across size. Consistency between real data and fitted values across sizes indicates that the vital rate models are accurately capturing size dependence. Points show the value of statistical moments binned across size for the observed data (red circles) compared to the simulated datasets (grey circles) and the median of the simulated values (black circles) generated from 500 posterior draws from the fitted model.

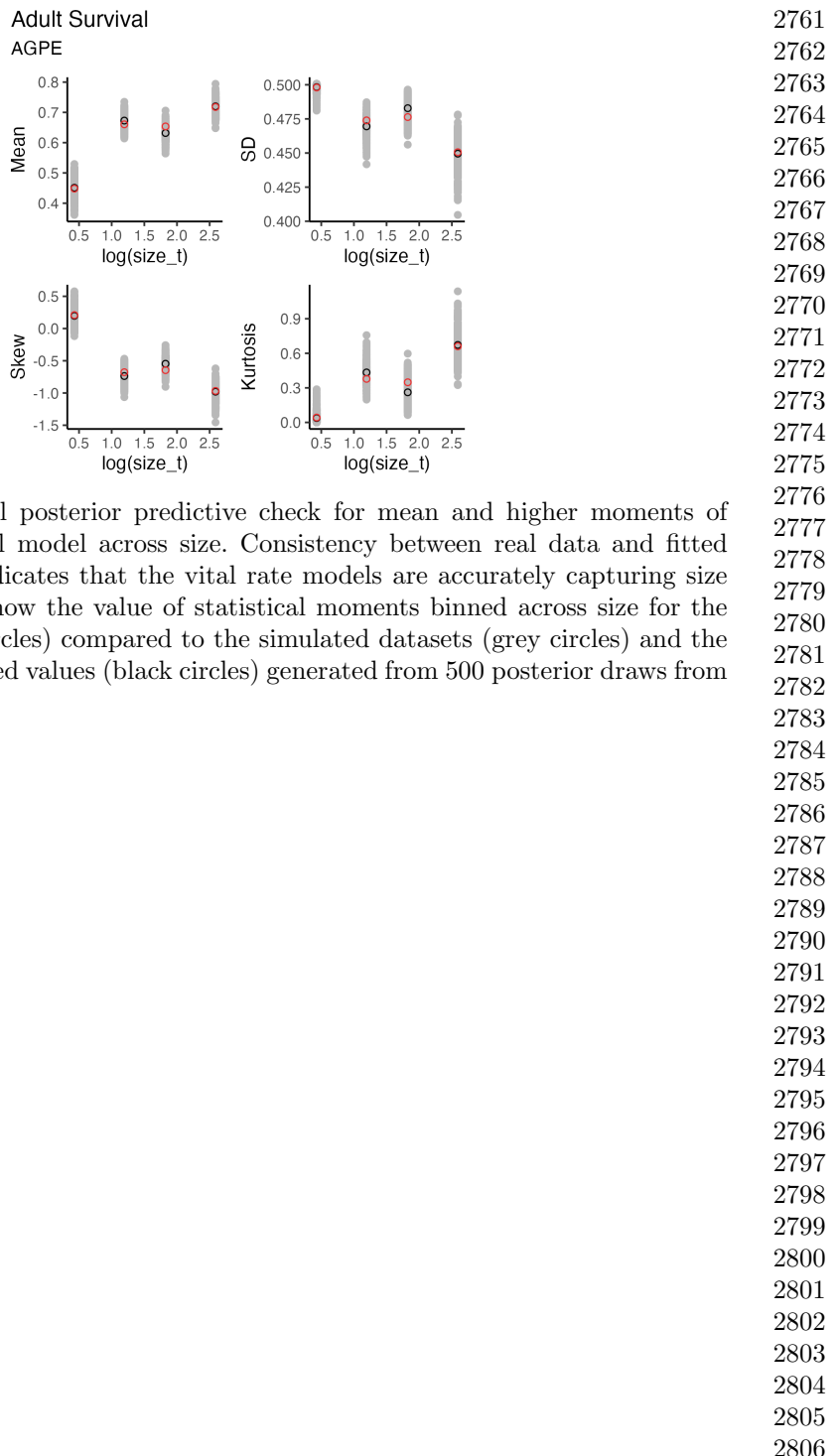


Figure S37: Graphical posterior predictive check for mean and higher moments of *A. perennans* survival model across size. Consistency between real data and fitted values across sizes indicates that the vital rate models are accurately capturing size dependence. Points show the value of statistical moments binned across size for the observed data (red circles) compared to the simulated datasets (grey circles) and the median of the simulated values (black circles) generated from 500 posterior draws from the fitted model.

2807

2808

2809

2810

2811

2812

2813

2814

2815

2816

2817

2818

2819

2820

2821

2822

Figure S38: Graphical posterior predictive check for mean and higher moments of *E. villosus* survival model across size. Consistency between real data and fitted values across sizes indicates that the vital rate models are accurately capturing size dependence. Points show the value of statistical moments binned across size for the observed data (red circles) compared to the simulated datasets (grey circles) and the median of the simulated values (black circles) generated from 500 posterior draws from the fitted model.

2829

2830

2831

2832

2833

2834

2835

2836

2837

2838

2839

2840

2841

2842

2843

2844

2845

2846

2847

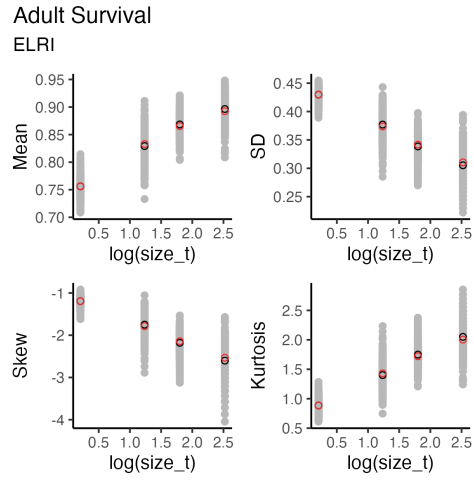
2848

2849

2850

2851

2852



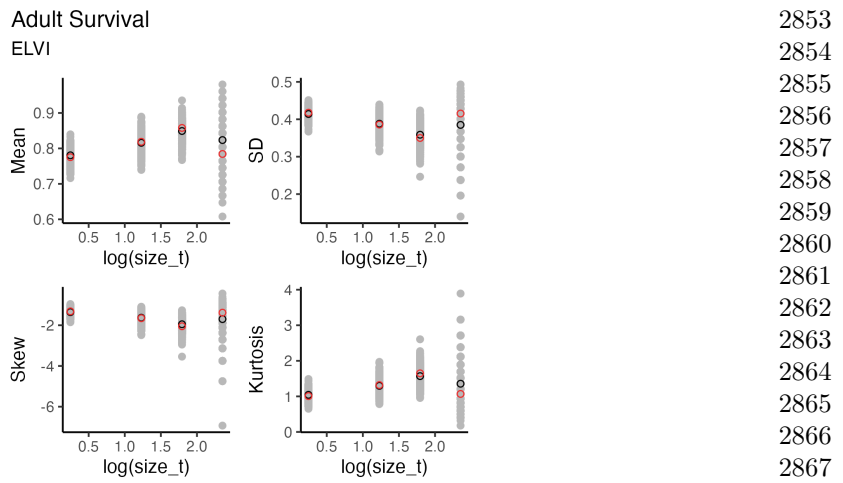


Figure S39: Graphical posterior predictive check for mean and higher moments of *E. virginicus* survival model across size. Consistency between real data and fitted values across sizes indicates that the vital rate models are accurately capturing size dependence. Points show the value of statistical moments binned across size for the observed data (red circles) compared to the simulated datasets (grey circles) and the median of the simulated values (black circles) generated from 500 posterior draws from the fitted model.

2853
2854
2855
2856
2857
2858
2859
2860
2861
2862
2863
2864
2865
2866
2867
2868
2869
2870
2871
2872
2873
2874
2875
2876
2877
2878
2879
2880
2881
2882
2883
2884
2885
2886
2887
2888
2889
2890
2891
2892
2893
2894
2895
2896
2897
2898

2899

2900

2901

2902

2903

2904

2905

2906

2907

2908

2909

2910

2911

2912

2913

2914

Figure S40: Graphical posterior predictive check for mean and higher moments of *F. subverticillata* survival model across size. Consistency between real data and fitted values across sizes indicates that the vital rate models are accurately capturing size dependence. Points show the value of statistical moments binned across size for the observed data (red circles) compared to the simulated datasets (grey circles) and the median of the simulated values (black circles) generated from 500 posterior draws from the fitted model.

2921

2922

2923

2924

2925

2926

2927

2928

2929

2930

2931

2932

2933

2934

2935

2936

2937

2938

2939

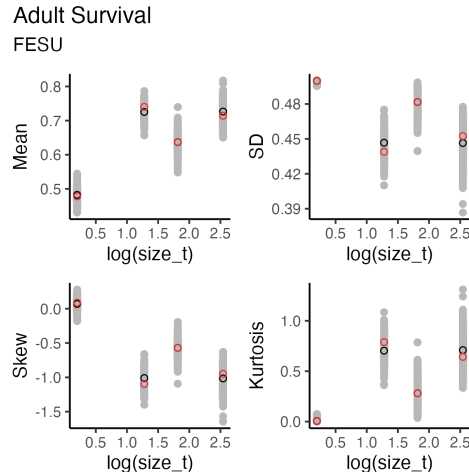
2940

2941

2942

2943

2944



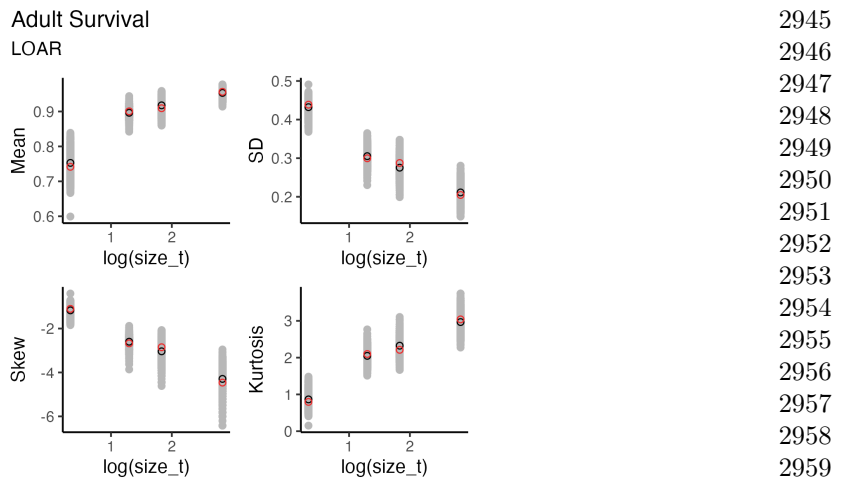


Figure S41: Graphical posterior predictive check for mean and higher moments of *L. arundinacea* survival model across size. Consistency between real data and fitted values across sizes indicates that the vital rate models are accurately capturing size dependence. Points show the value of statistical moments binned across size for the observed data (red circles) compared to the simulated datasets (grey circles) and the median of the simulated values (black circles) generated from 500 posterior draws from the fitted model.

2945
2946
2947
2948
2949
2950
2951
2952
2953
2954
2955
2956
2957
2958
2959
2960
2961
2962
2963
2964
2965
2966
2967
2968
2969
2970
2971
2972
2973
2974
2975
2976
2977
2978
2979
2980
2981
2982
2983
2984
2985
2986
2987
2988
2989
2990

2991
2992
2993
2994
2995
2996
2997
2998
2999
3000
3001
3002
3003
3004
3005
3006
3007
3008
3009
3010
3011
3012
3013
3014
3015
3016
3017
3018
3019
3020
3021
3022
3023
3024
3025
3026
3027
3028
3029
3030
3031
3032
3033
3034
3035
3036

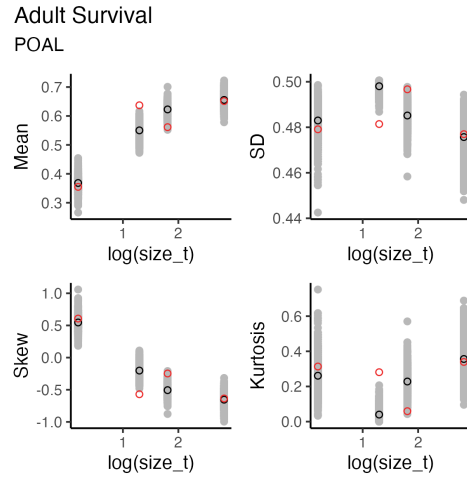
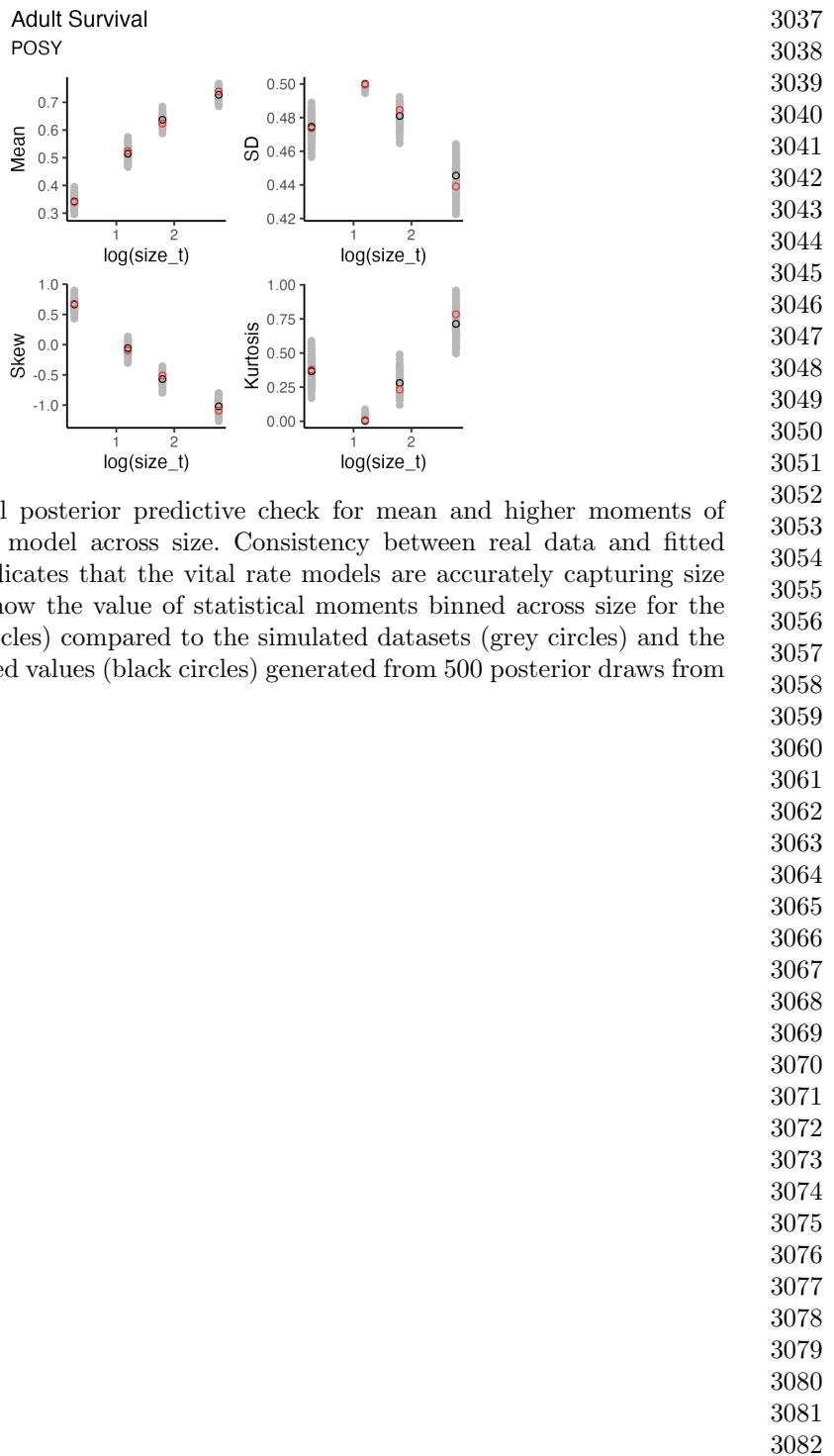


Figure S42: Graphical posterior predictive check for mean and higher moments of *P. alsodes* survival model across size. Consistency between real data and fitted values across sizes indicates that the vital rate models are accurately capturing size dependence. Points show the value of statistical moments binned across size for the observed data (red circles) compared to the simulated datasets (grey circles) and the median of the simulated values (black circles) generated from 500 posterior draws from the fitted model.



3083
3084
3085
3086
3087
3088
3089
3090
3091
3092
3093
3094
3095
3096
3097
3098
3105
3106
3107
3108
3109
3110
3111
3112
3113
3114
3115
3116
3117
3118
3119
3120
3121
3122
3123
3124
3125
3126
3127
3128

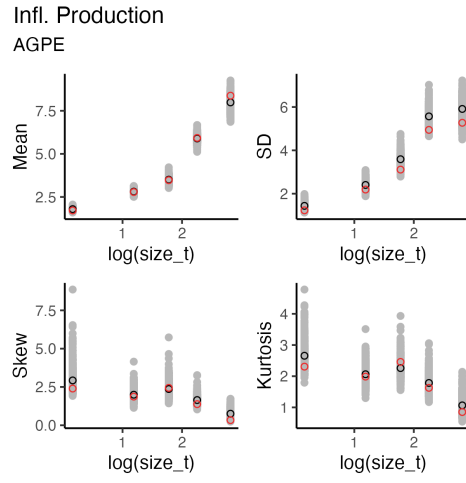


Figure S44: Graphical posterior predictive check for mean and higher moments of *A. perennans* inflorescence production model across size. Consistency between real data and fitted values across sizes indicates that the vital rate models are accurately capturing size dependence. Points show the value of statistical moments binned across size for the observed data (red circles) compared to the simulated datasets (grey circles) and the median of the simulated values (black circles) generated from 500 posterior draws from the fitted model.

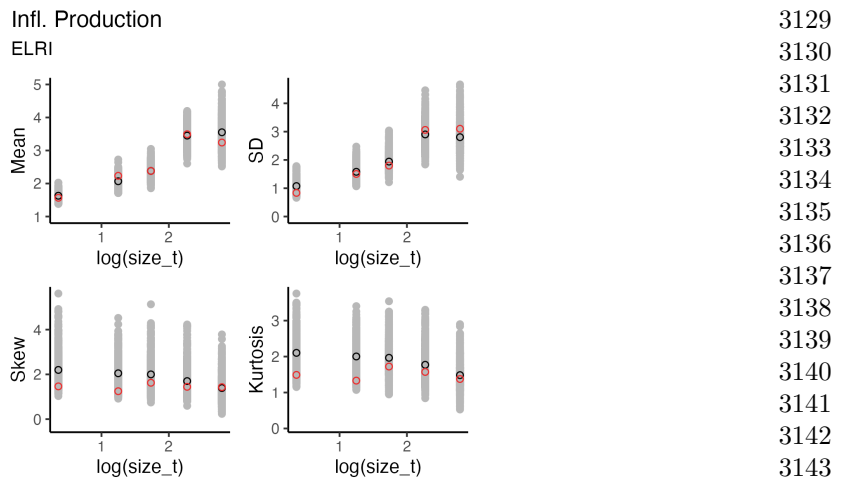


Figure S45: Graphical posterior predictive check for mean and higher moments of *E. villosus* inflorescence production model across size. Consistency between real data and fitted values across sizes indicates that the vital rate models are accurately capturing size dependence. Points show the value of statistical moments binned across size for the observed data (red circles) compared to the simulated datasets (grey circles) and the median of the simulated values (black circles) generated from 500 posterior draws from the fitted model.

3129
3130
3131
3132
3133
3134
3135
3136
3137
3138
3139
3140
3141
3142
3143
3144
3145
3146
3147
3148
3149
3150
3151
3152
3153
3154
3155
3156
3157
3158
3159
3160
3161
3162
3163
3164
3165
3166
3167
3168
3169
3170
3171
3172
3173
3174

3175
3176
3177
3178
3179
3180
3181
3182
3183
3184
3185
3186
3187
3188
3189
3190
3191
3192
3193
3194
3195
3196
3197
3198
3199
3200
3201
3202
3203
3204
3205
3206
3207
3208
3209
3210
3211
3212
3213
3214
3215
3216
3217
3218
3219
3220

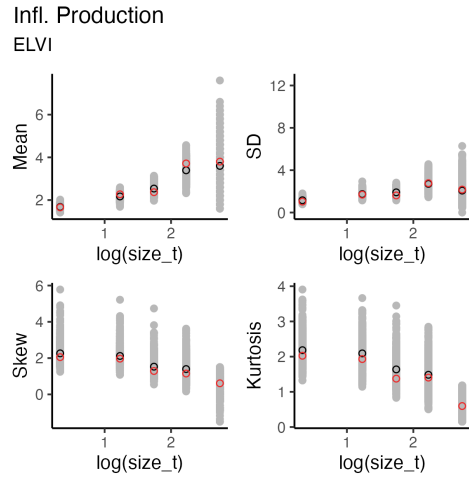


Figure S46: Graphical posterior predictive check for mean and higher moments of *E. virginicus* inflorescence production model across size. Consistency between real data and fitted values across sizes indicates that the vital rate models are accurately capturing size dependence. Points show the value of statistical moments binned across size for the observed data (red circles) compared to the simulated datasets (grey circles) and the median of the simulated values (black circles) generated from 500 posterior draws from the fitted model.

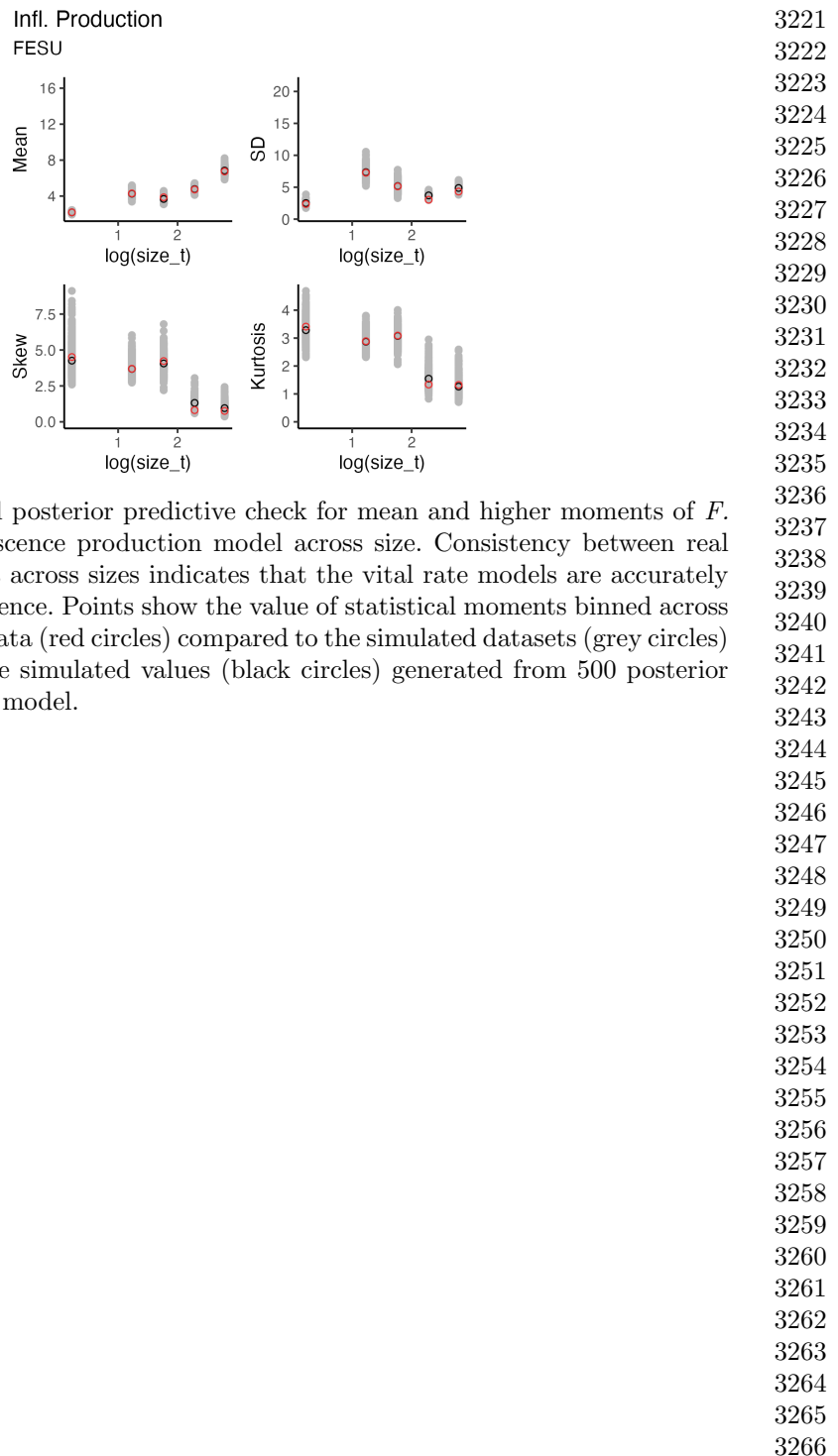


Figure S47: Graphical posterior predictive check for mean and higher moments of *F. subverticillata* inflorescence production model across size. Consistency between real data and fitted values across sizes indicates that the vital rate models are accurately capturing size dependence. Points show the value of statistical moments binned across size for the observed data (red circles) compared to the simulated datasets (grey circles) and the median of the simulated values (black circles) generated from 500 posterior draws from the fitted model.

3267
3268
3269
3270
3271
3272
3273
3274
3275
3276
3277
3278
3279
3280
3281
3282
3283
3284
3285
3286
3287
3288
3289
3290
3291
3292
3293
3294
3295
3296
3297
3298
3299
3300
3301
3302
3303
3304
3305
3306
3307
3308
3309
3310
3311
3312

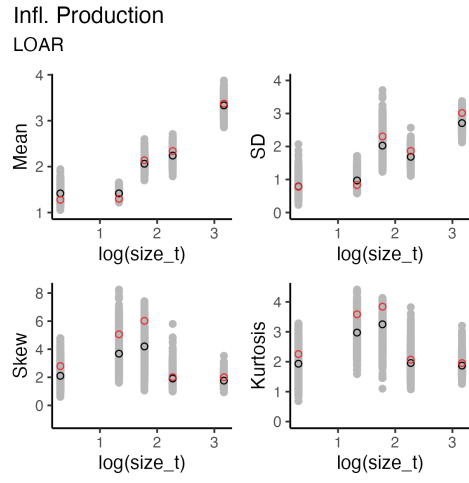


Figure S48: Graphical posterior predictive check for mean and higher moments of *L. arundinacea* inflorescence production model across size. Consistency between real data and fitted values across sizes indicates that the vital rate models are accurately capturing size dependence. Points show the value of statistical moments binned across size for the observed data (red circles) compared to the simulated datasets (grey circles) and the median of the simulated values (black circles) generated from 500 posterior draws from the fitted model.

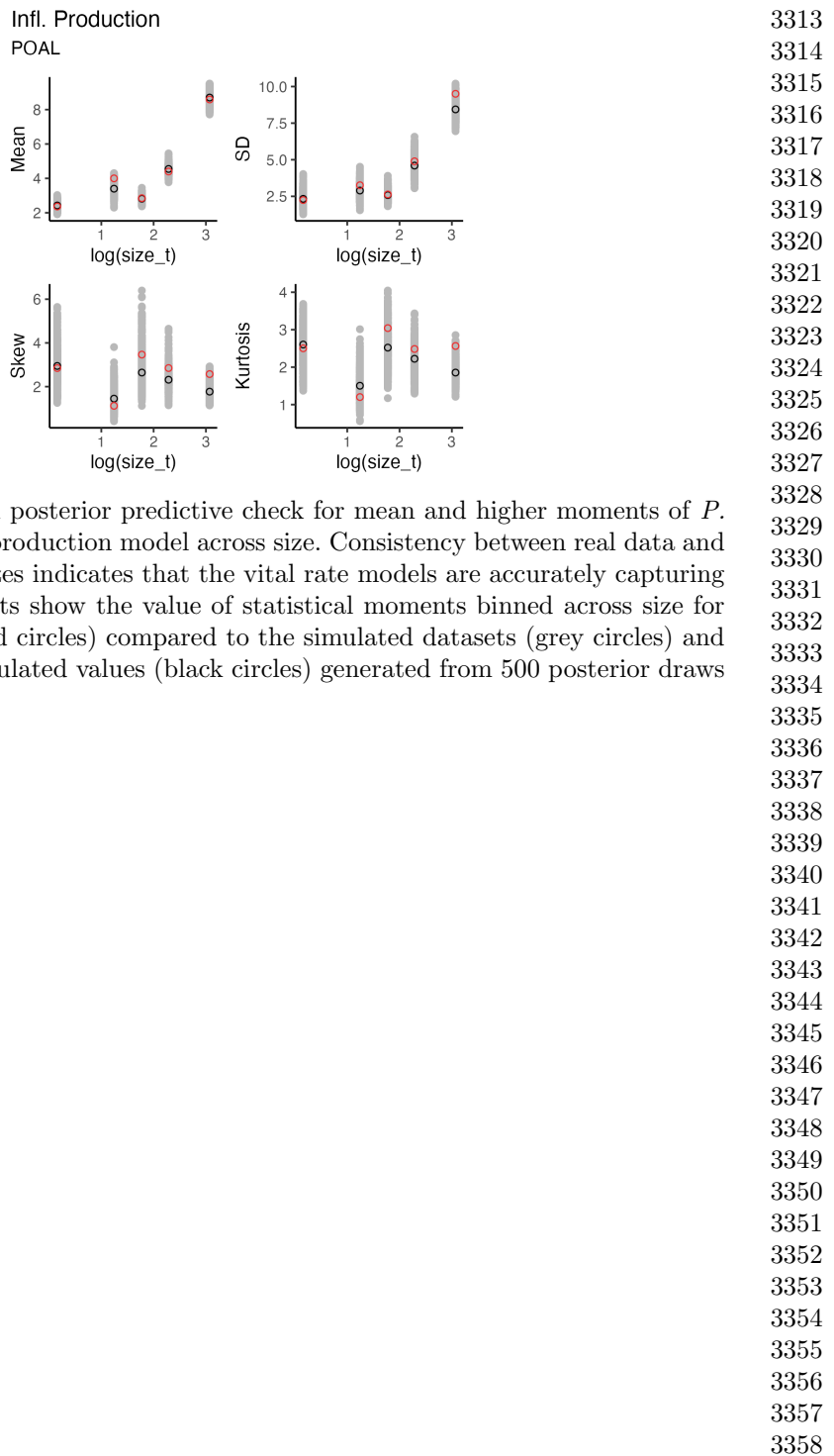


Figure S49: Graphical posterior predictive check for mean and higher moments of *P. alsodes* inflorescence production model across size. Consistency between real data and fitted values across sizes indicates that the vital rate models are accurately capturing size dependence. Points show the value of statistical moments binned across size for the observed data (red circles) compared to the simulated datasets (grey circles) and the median of the simulated values (black circles) generated from 500 posterior draws from the fitted model.

3359
3360
3361
3362
3363
3364
3365
3366
3367
3368
3369
3370
3371
3372
3373
3374
3382
3383
3384
3385
3386
3387
3388
3389
3390
3391
3392
3393
3394
3395
3396
3397
3398
3399
3400
3401
3402
3403
3404

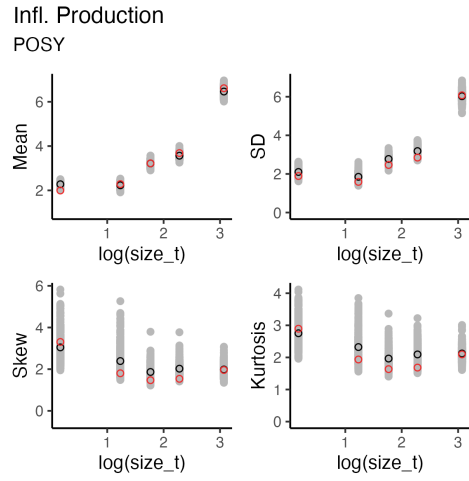
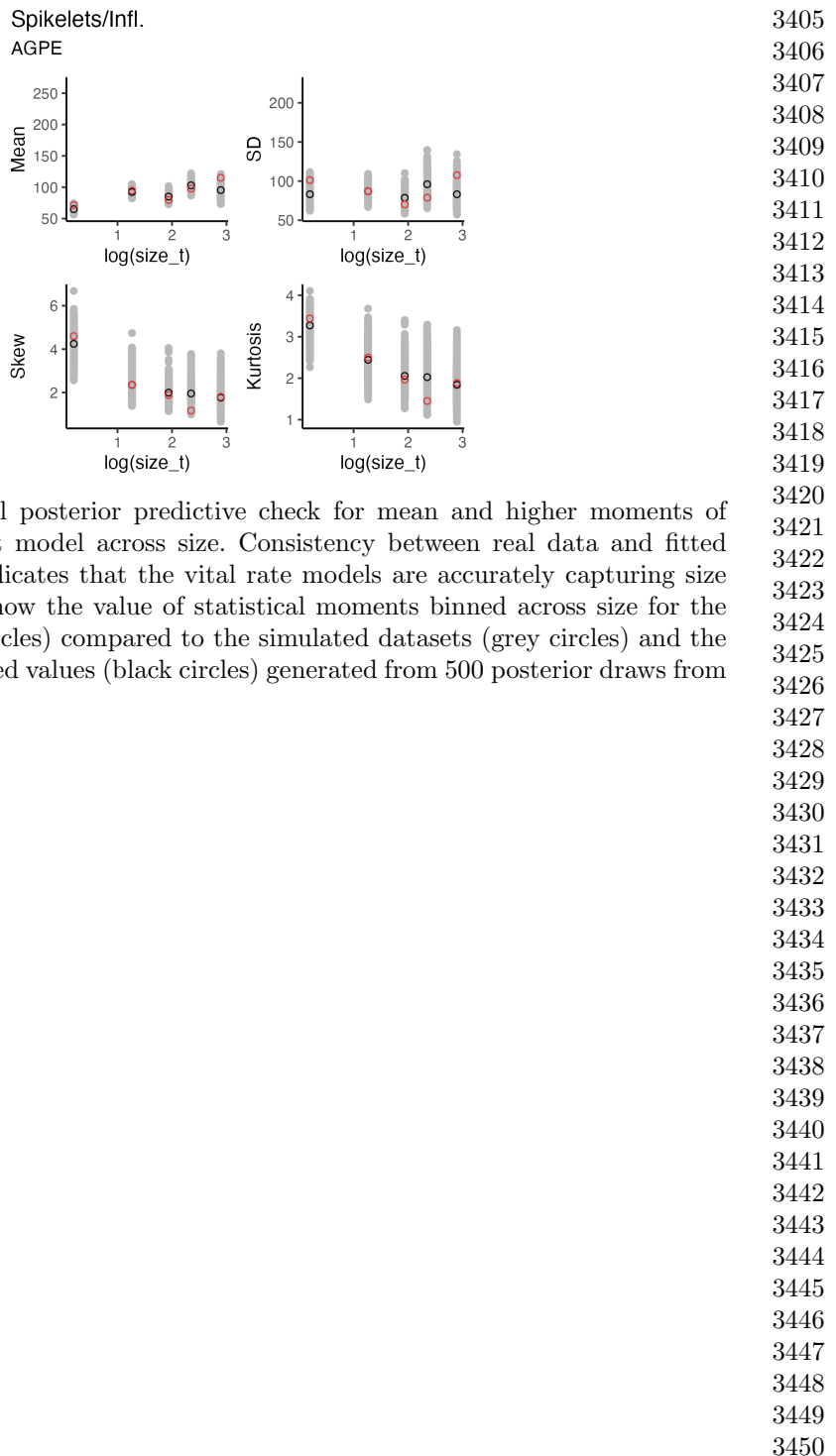


Figure S50: Graphical posterior predictive check for mean and higher moments of *P. sylvestris* inflorescence production model across size. Consistency between real data and fitted values across sizes indicates that the vital rate models are accurately capturing size dependence. Points show the value of statistical moments binned across size for the observed data (red circles) compared to the simulated datasets (grey circles) and the median of the simulated values (black circles) generated from 500 posterior draws from the fitted model.



3451
3452
3453
3454
3455
3456
3457
3458
3459
3460
3461
3462
3463
3464
3465
3466
3467
3468
3469
3470
3471
3472
3473
3474
3475
3476
3477
3478
3479
3480
3481
3482
3483
3484
3485
3486
3487
3488
3489
3490
3491
3492
3493
3494
3495
3496

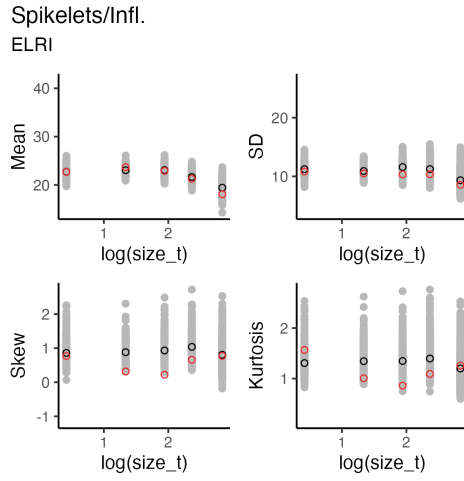
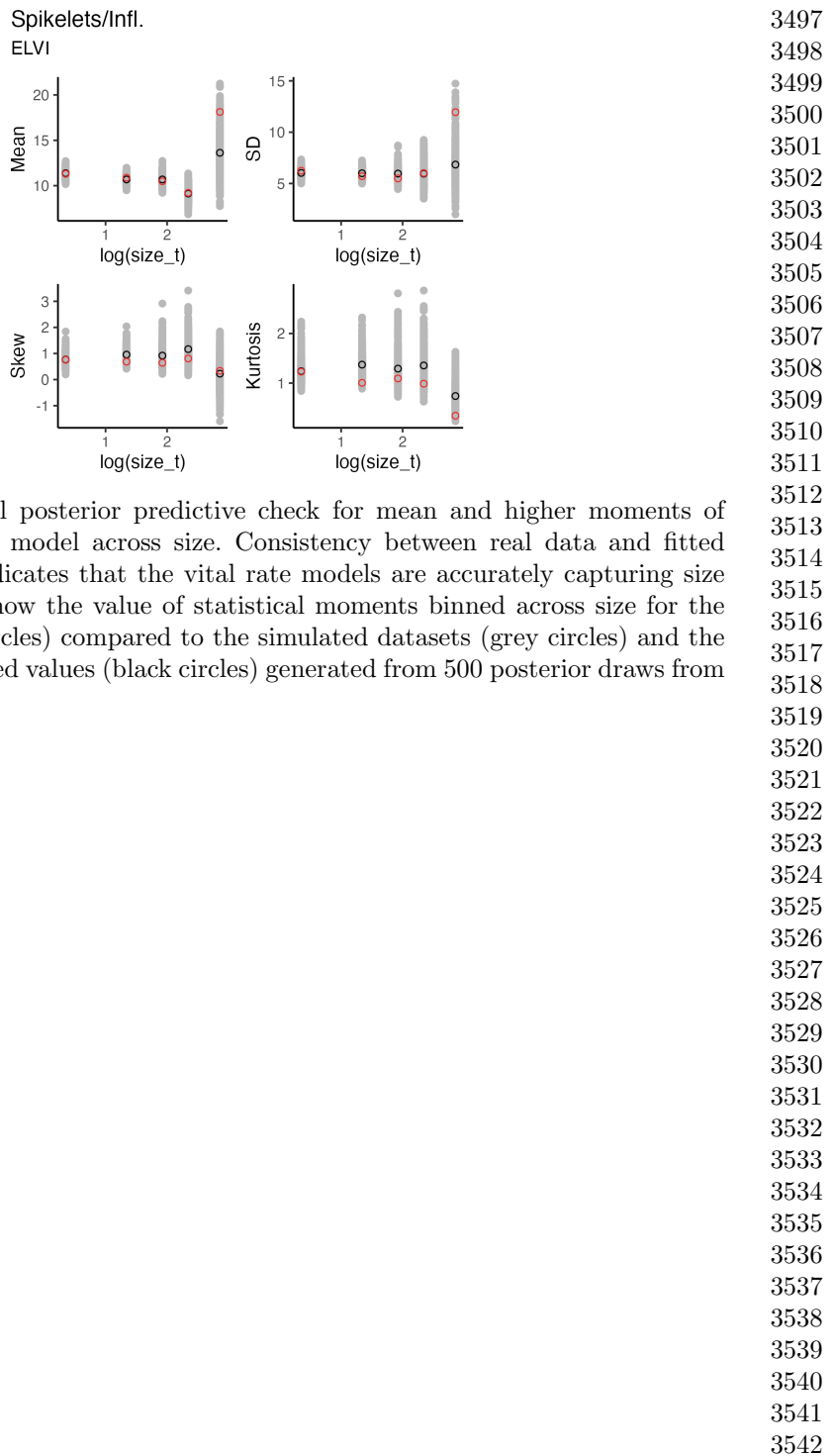


Figure S52: Graphical posterior predictive check for mean and higher moments of *E. villosus* spikelet model across size. Consistency between real data and fitted values across sizes indicates that the vital rate models are accurately capturing size dependence. Points show the value of statistical moments binned across size for the observed data (red circles) compared to the simulated datasets (grey circles) and the median of the simulated values (black circles) generated from 500 posterior draws from the fitted model.



3543
3544
3545
3546
3547
3548
3549
3550
3551
3552
3553
3554
3555
3556
3557
3558
3559
3560
3561
3562
3563
3564
3565
3566
3567
3568
3569
3570
3571
3572
3573
3574
3575
3576
3577
3578
3579
3580
3581
3582
3583
3584
3585
3586
3587
3588

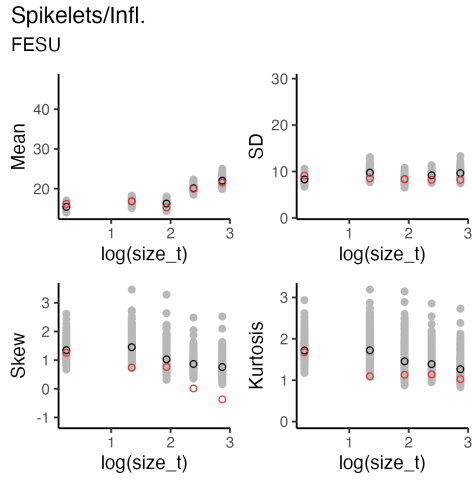


Figure S54: Graphical posterior predictive check for mean and higher moments of *F. subverticillata* spikelet model across size. Consistency between real data and fitted values across sizes indicates that the vital rate models are accurately capturing size dependence. Points show the value of statistical moments binned across size for the observed data (red circles) compared to the simulated datasets (grey circles) and the median of the simulated values (black circles) generated from 500 posterior draws from the fitted model.

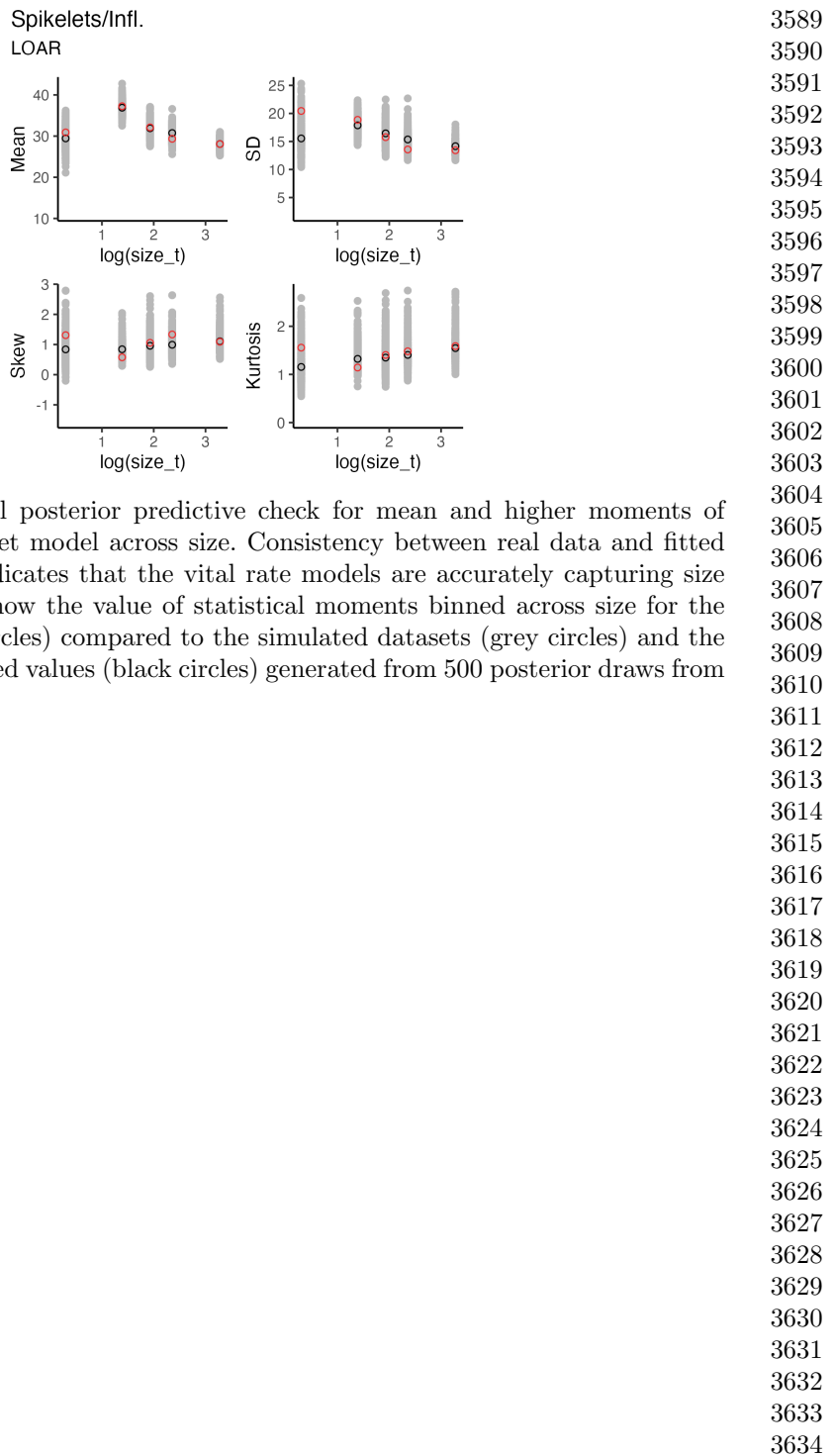


Figure S55: Graphical posterior predictive check for mean and higher moments of *L. arundinacea* spikelet model across size. Consistency between real data and fitted values across sizes indicates that the vital rate models are accurately capturing size dependence. Points show the value of statistical moments binned across size for the observed data (red circles) compared to the simulated datasets (grey circles) and the median of the simulated values (black circles) generated from 500 posterior draws from the fitted model.

3635
3636
3637
3638
3639
3640
3641
3642
3643
3644
3645
3646
3647
3648
3649
3650
3651
3652
3653
3654
3655
3656
3657
3658
3659
3660
3661
3662
3663
3664
3665
3666
3667
3668
3669
3670
3671
3672
3673
3674
3675
3676
3677
3678
3679
3680

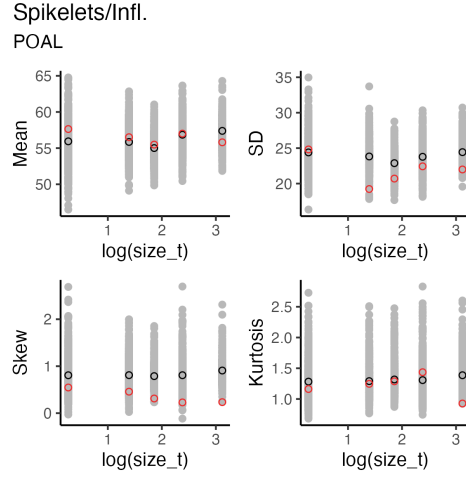


Figure S56: Graphical posterior predictive check for mean and higher moments of $P. alsodes$ spikelet model across size. Consistency between real data and fitted values across sizes indicates that the vital rate models are accurately capturing size dependence. Points show the value of statistical moments binned across size for the observed data (red circles) compared to the simulated datasets (grey circles) and the median of the simulated values (black circles) generated from 500 posterior draws from the fitted model.

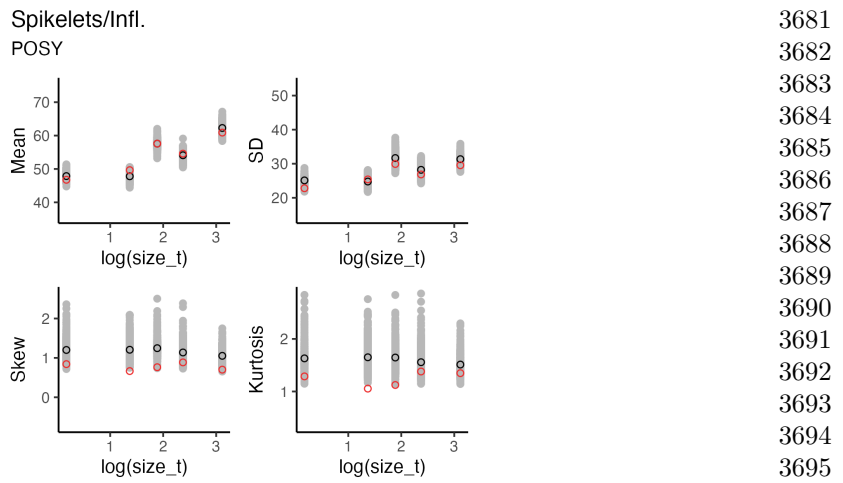
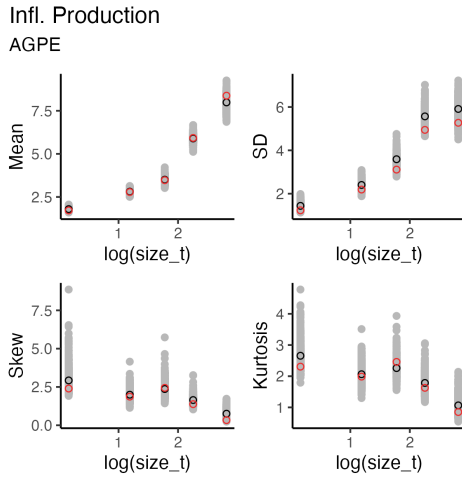


Figure S57: Graphical posterior predictive check for mean and higher moments of *P. sylvestris* spikelet model across size. Consistency between real data and fitted values across sizes indicates that the vital rate models are accurately capturing size dependence. Points show the value of statistical moments binned across size for the observed data (red circles) compared to the simulated datasets (grey circles) and the median of the simulated values (black circles) generated from 500 posterior draws from the fitted model.

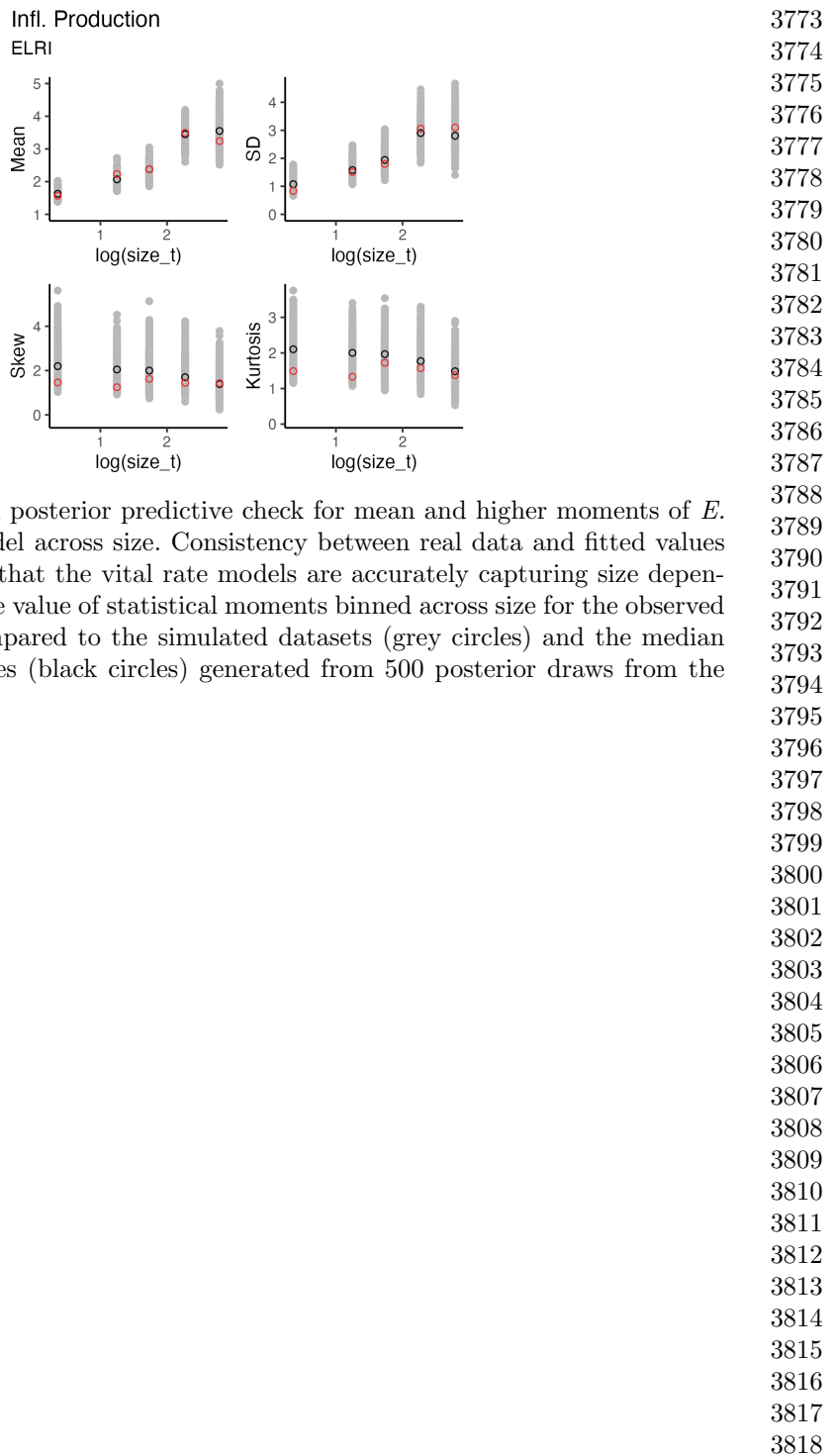
3727
3728



3729
3730
3731
3732
3733
3734
3735
3736
3737
3738
3739
3740
3741

3742 Figure S58: Graphical posterior predictive check for mean and higher moments of
3743 *A. perennans* flowering model across size. Consistency between real data and fitted
3744 values across sizes indicates that the vital rate models are accurately capturing size
3745 dependence. Points show the value of statistical moments binned across size for the
3746 observed data (red circles) compared to the simulated datasets (grey circles) and the
3747 median of the simulated values (black circles) generated from 500 posterior draws from
3748 the fitted model.

3749
3750
3751
3752
3753
3754
3755
3756
3757
3758
3759
3760
3761
3762
3763
3764
3765
3766
3767
3768
3769
3770
3771
3772



3819
3820
3821
3822
3823
3824
3825
3826
3827
3828
3829
3830
3831
3832
3833
3834
3841
3842
3843
3844
3845
3846
3847
3848
3849
3850
3851
3852
3853
3854
3855
3856
3857
3858
3859
3860
3861
3862
3863
3864

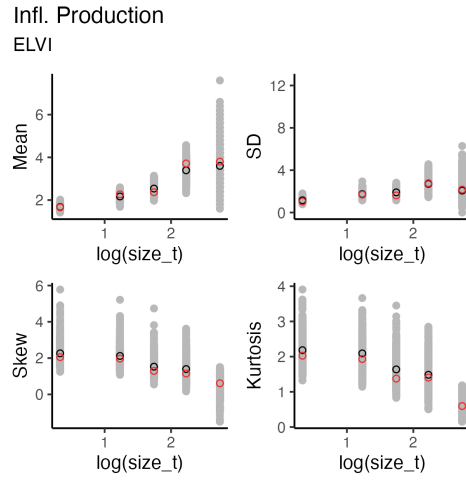


Figure S60: Graphical posterior predictive check for mean and higher moments of *E. virginicus* flowering model across size. Consistency between real data and fitted values across sizes indicates that the vital rate models are accurately capturing size dependence. Points show the value of statistical moments binned across size for the observed data (red circles) compared to the simulated datasets (grey circles) and the median of the simulated values (black circles) generated from 500 posterior draws from the fitted model.

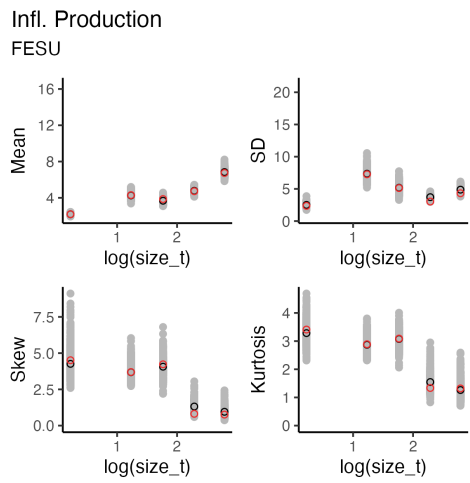


Figure S61: Graphical posterior predictive check for mean and higher moments of *F. subverticillata* flowering model across size. Consistency between real data and fitted values across sizes indicates that the vital rate models are accurately capturing size dependence. Points show the value of statistical moments binned across size for the observed data (red circles) compared to the simulated datasets (grey circles) and the median of the simulated values (black circles) generated from 500 posterior draws from the fitted model.

```

3865
3866
3867
3868
3869
3870
3871
3872
3873
3874
3875
3876
3877
3878
3879
3880
3881
3882
3883
3884
3885
3886
3887
3888
3889
3890
3891
3892
3893
3894
3895
3896
3897
3898
3899
3900
3901
3902
3903
3904
3905
3906
3907
3908
3909
3910

```

3911
3912
3913
3914
3915
3916
3917
3918
3919
3920
3921
3922
3923
3924
3925
3926
3927
3928
3929
3930
3931
3932
3933
3934
3935
3936
3937
3938
3939
3940
3941
3942
3943
3944
3945
3946
3947
3948
3949
3950
3951
3952
3953
3954
3955
3956

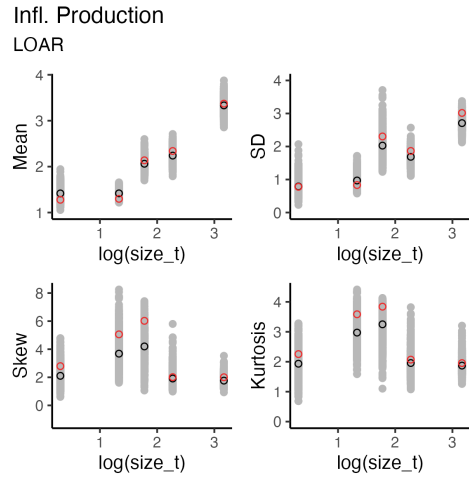


Figure S62: Graphical posterior predictive check for mean and higher moments of *L. arundinacea* flowering model across size. Consistency between real data and fitted values across sizes indicates that the vital rate models are accurately capturing size dependence. Points show the value of statistical moments binned across size for the observed data (red circles) compared to the simulated datasets (grey circles) and the median of the simulated values (black circles) generated from 500 posterior draws from the fitted model.

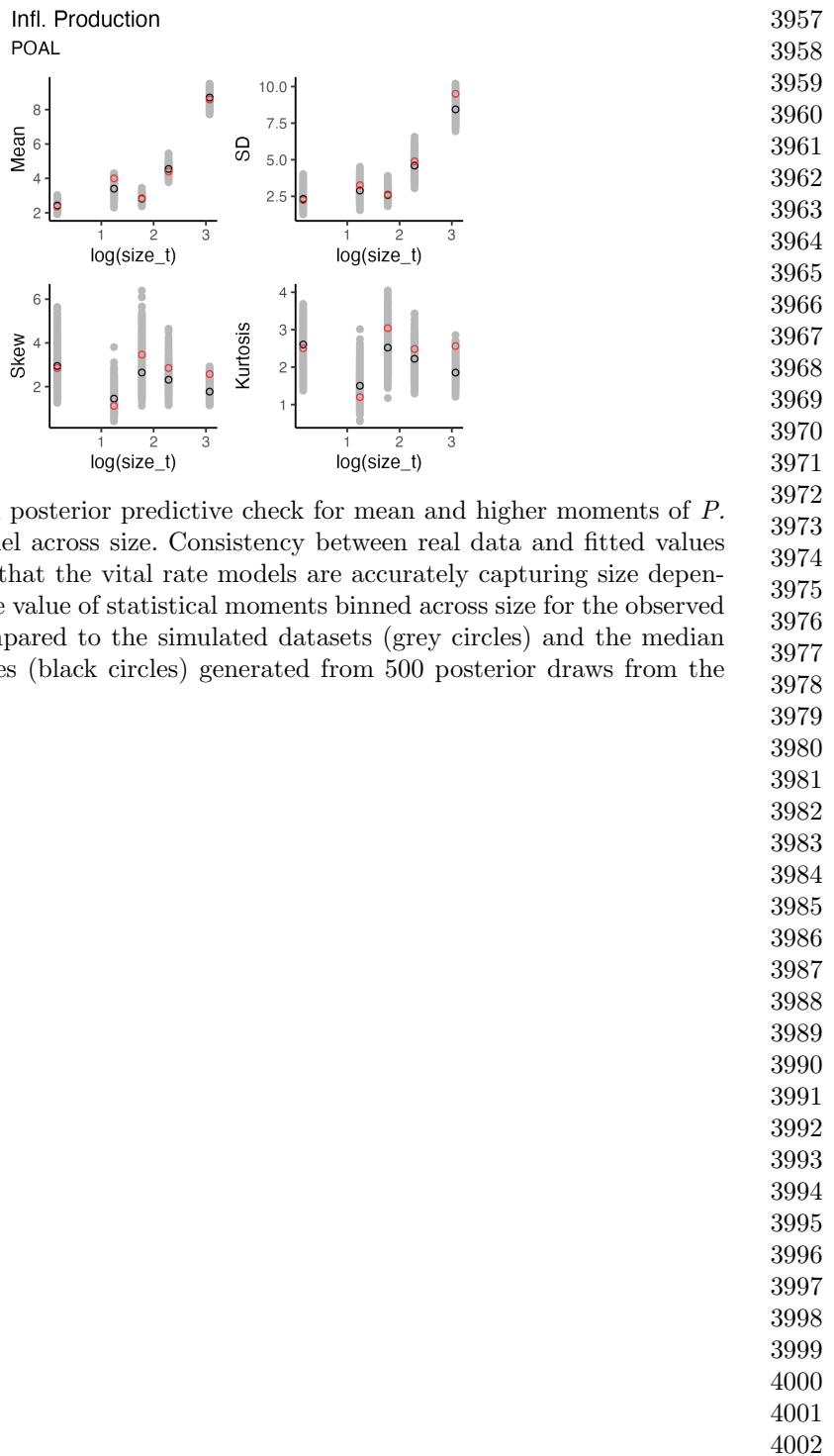


Figure S63: Graphical posterior predictive check for mean and higher moments of *P. alsodes* flowering model across size. Consistency between real data and fitted values across sizes indicates that the vital rate models are accurately capturing size dependence. Points show the value of statistical moments binned across size for the observed data (red circles) compared to the simulated datasets (grey circles) and the median of the simulated values (black circles) generated from 500 posterior draws from the fitted model.

4003
4004
4005
4006
4007
4008
4009
4010
4011
4012
4013
4014
4015
4016
4017
4018
4019
4020
4021
4022
4023
4024
4025
4026
4027
4028
4029
4030
4031
4032
4033
4034
4035
4036
4037
4038
4039
4040
4041
4042
4043
4044
4045
4046
4047
4048

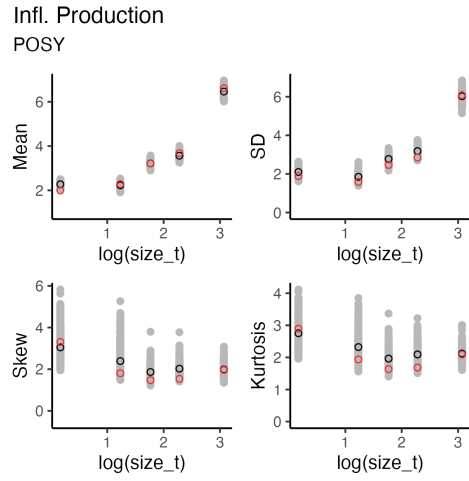


Figure S64: Graphical posterior predictive check for mean and higher moments of *P. sylvestris* flowering model across size. Consistency between real data and fitted values across sizes indicates that the vital rate models are accurately capturing size dependence. Points show the value of statistical moments binned across size for the observed data (red circles) compared to the simulated datasets (grey circles) and the median of the simulated values (black circles) generated from 500 posterior draws from the fitted model.

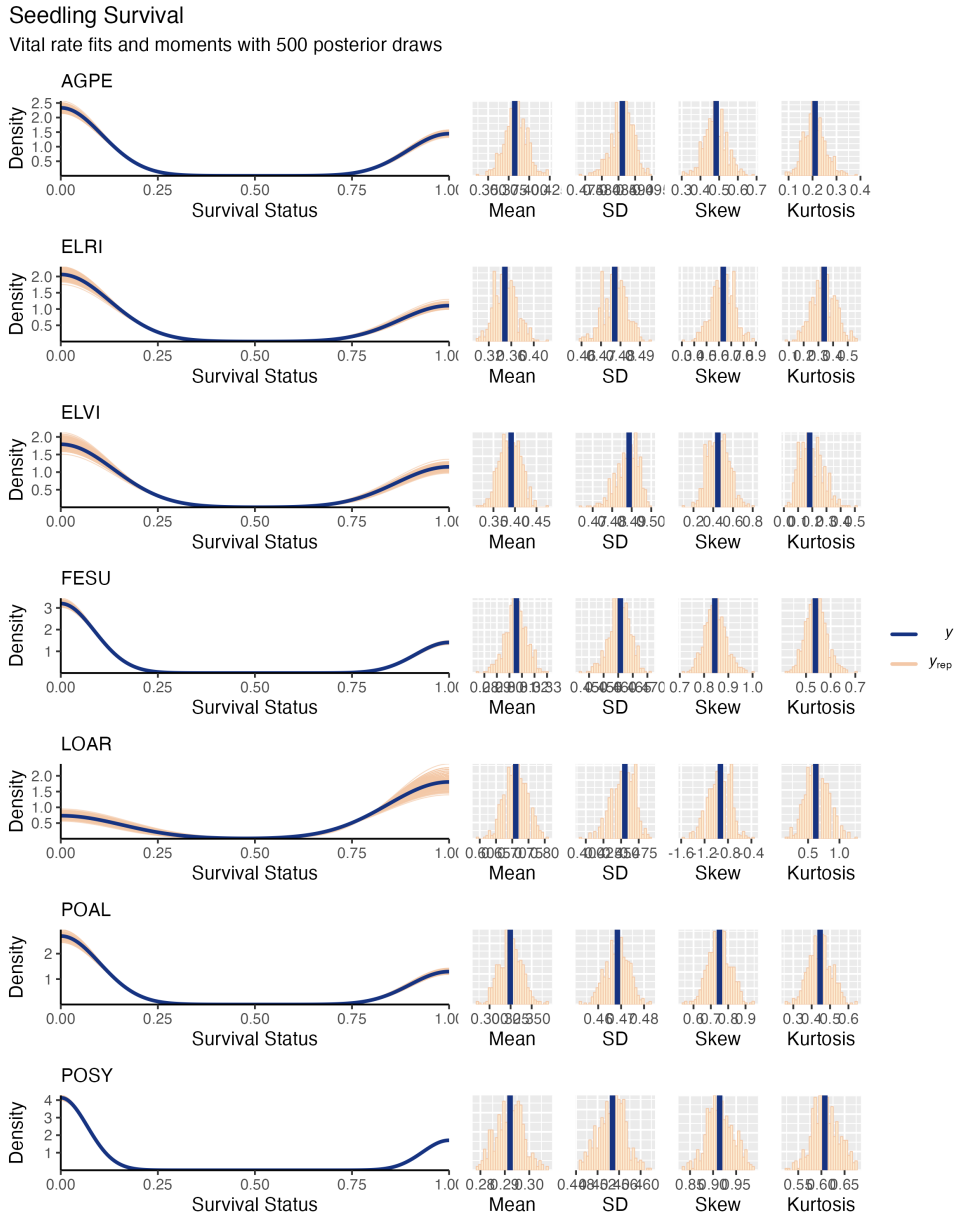
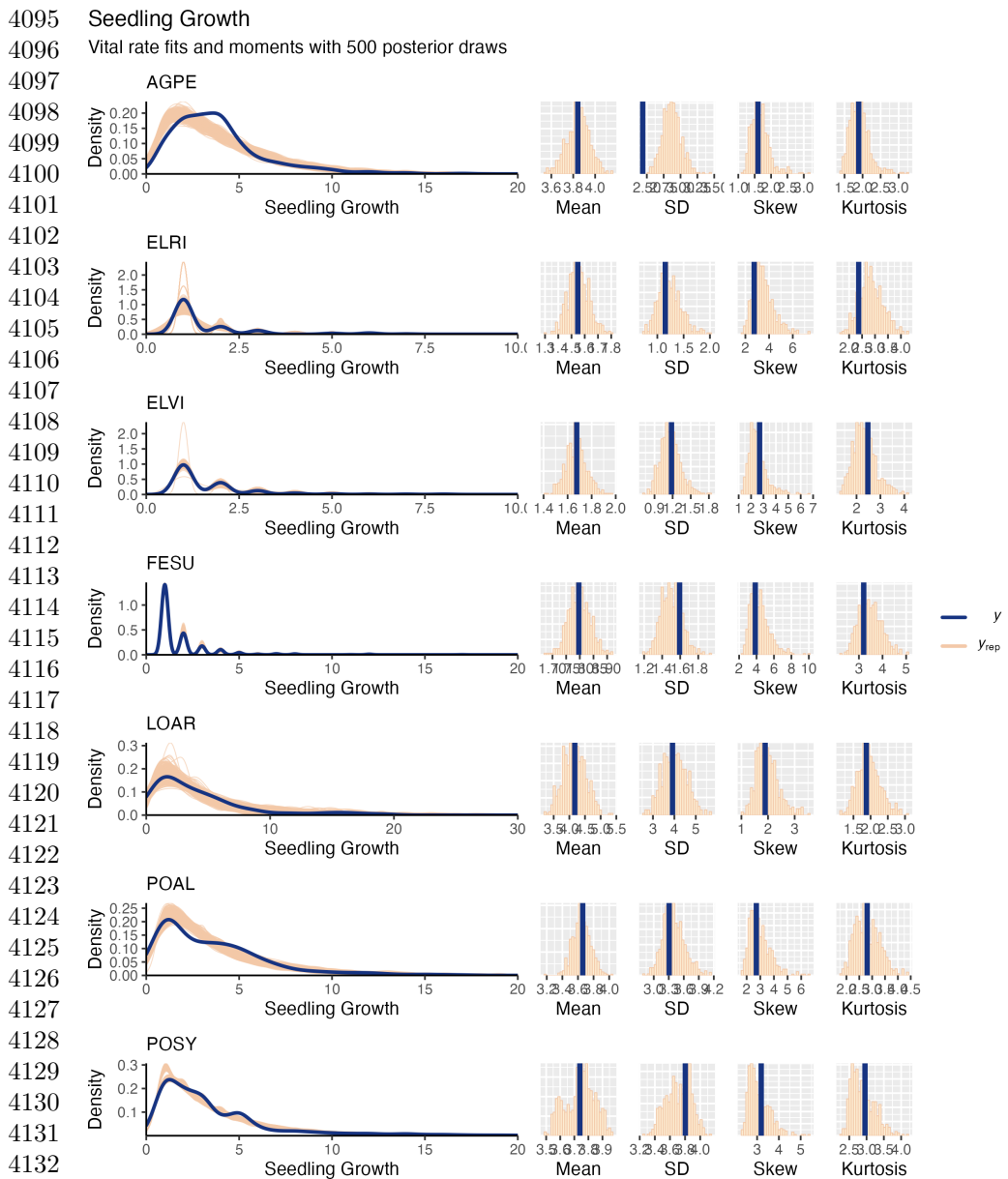


Figure S65: Posterior predictive check for statistical model of Seedling Survival. Consistency between real data and simulated values indicates that fitted models describe the data well. Lines show density distributions of observed data (blue line) compared to data simulated from fitted models (tan lines) generated from 500 draws from posterior distributions of model parameters along with the distribution's moments.

4049
4050
4051
4052
4053
4054
4055
4056
4057
4058
4059
4060
4061
4062
4063
4064
4065
4066
4067
4068
4069
4070
4071
4072
4073
4074
4075
4076
4077
4078
4079
4080
4081
4082
4083
4084
4085
4086
4087
4088
4089
4090
4091
4092
4093
4094



4133
 4134 Figure S66: Posterior predictive check for statistical model of Seedling Growth. Consis-
 4135 tency between real data and simulated values indicates that fitted models describe the
 4136 data well. Lines show density distributions of observed data (blue line) compared to
 4137 data simulated from fitted models (tan lines) generated from 500 draws from posterior
 4138 distributions of model parameters along with the distribution's moments.

4139
 4140

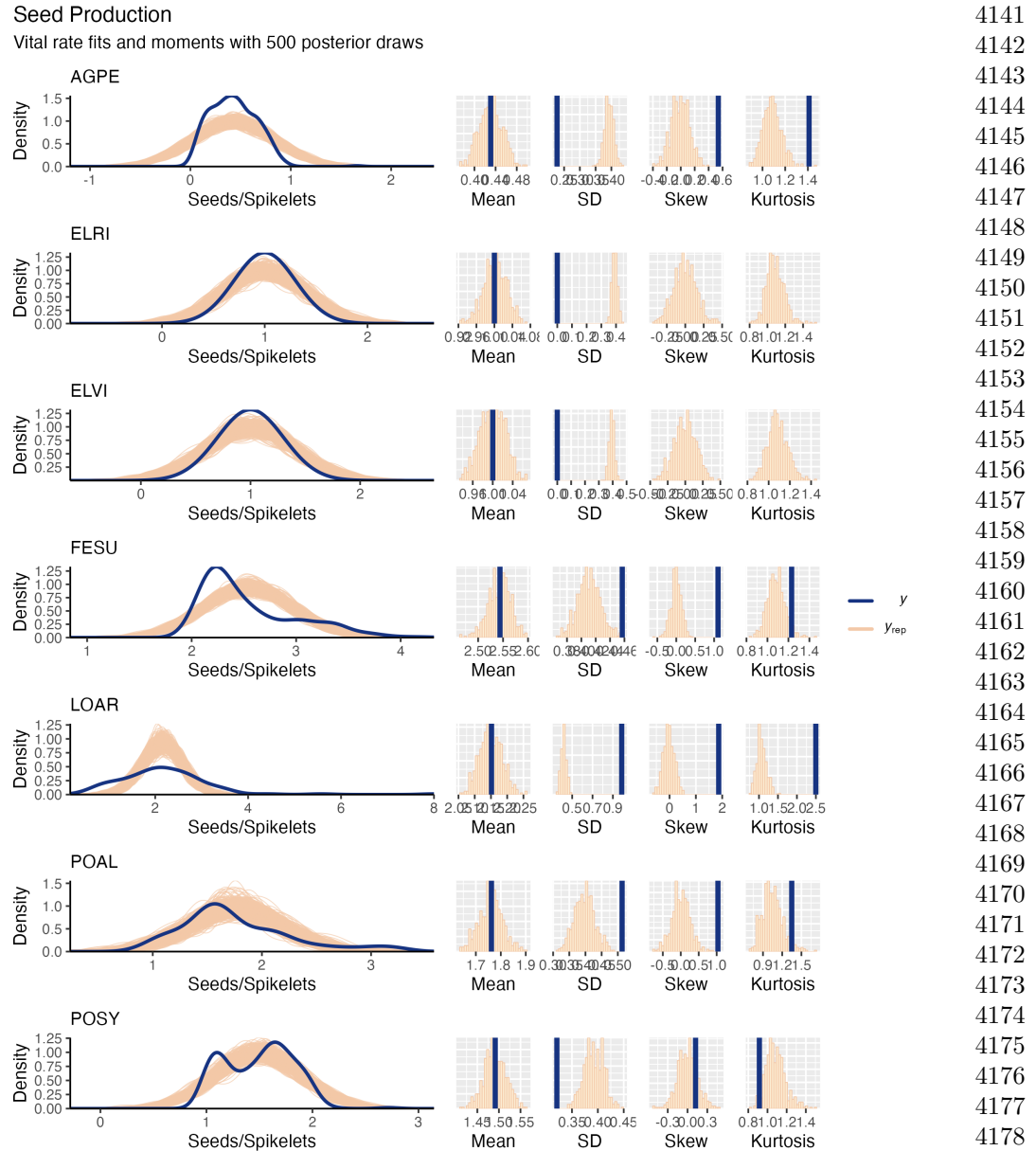
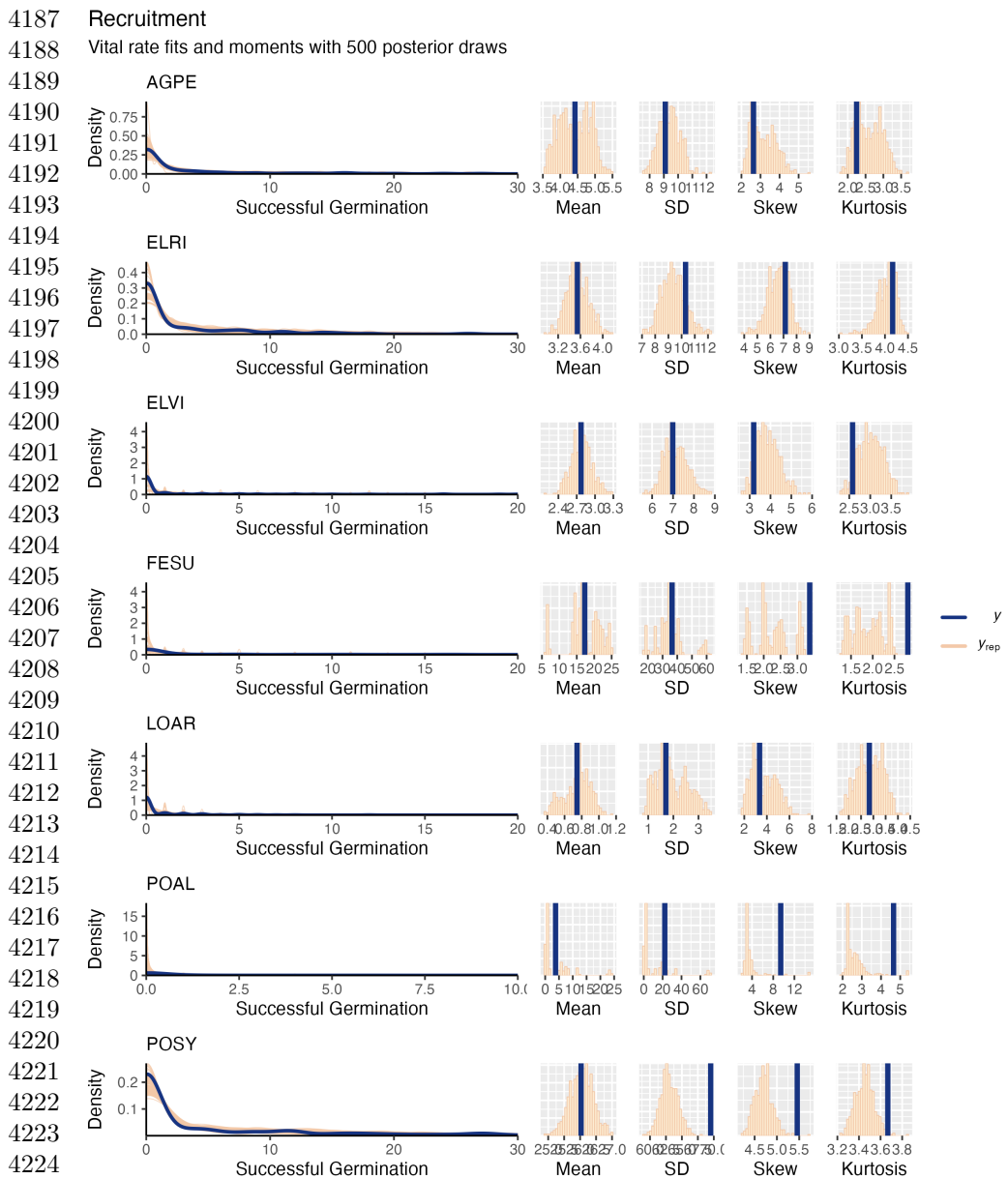


Figure S67: Posterior predictive check for statistical model of Mean Seeds/Spikelet. Consistency between real data and simulated values indicates that fitted models describe the data well. Lines show density distributions of observed data (blue line) compared to data simulated from fitted models (tan lines) generated from 500 draws from posterior distributions of model parameters along with the distribution's moments.



4226 Figure S68: Posterior predictive check for statistical model of Recruitment. Consis-
 4227 tency between real data and simulated values indicates that fitted models describe the
 4228 data well. Lines show density distributions of observed data (blue line) compared to
 4229 data simulated from fitted models (tan lines) generated from 500 draws from posterior
 4230 distributions of model parameters along with the distribution's moments.

4231
4232

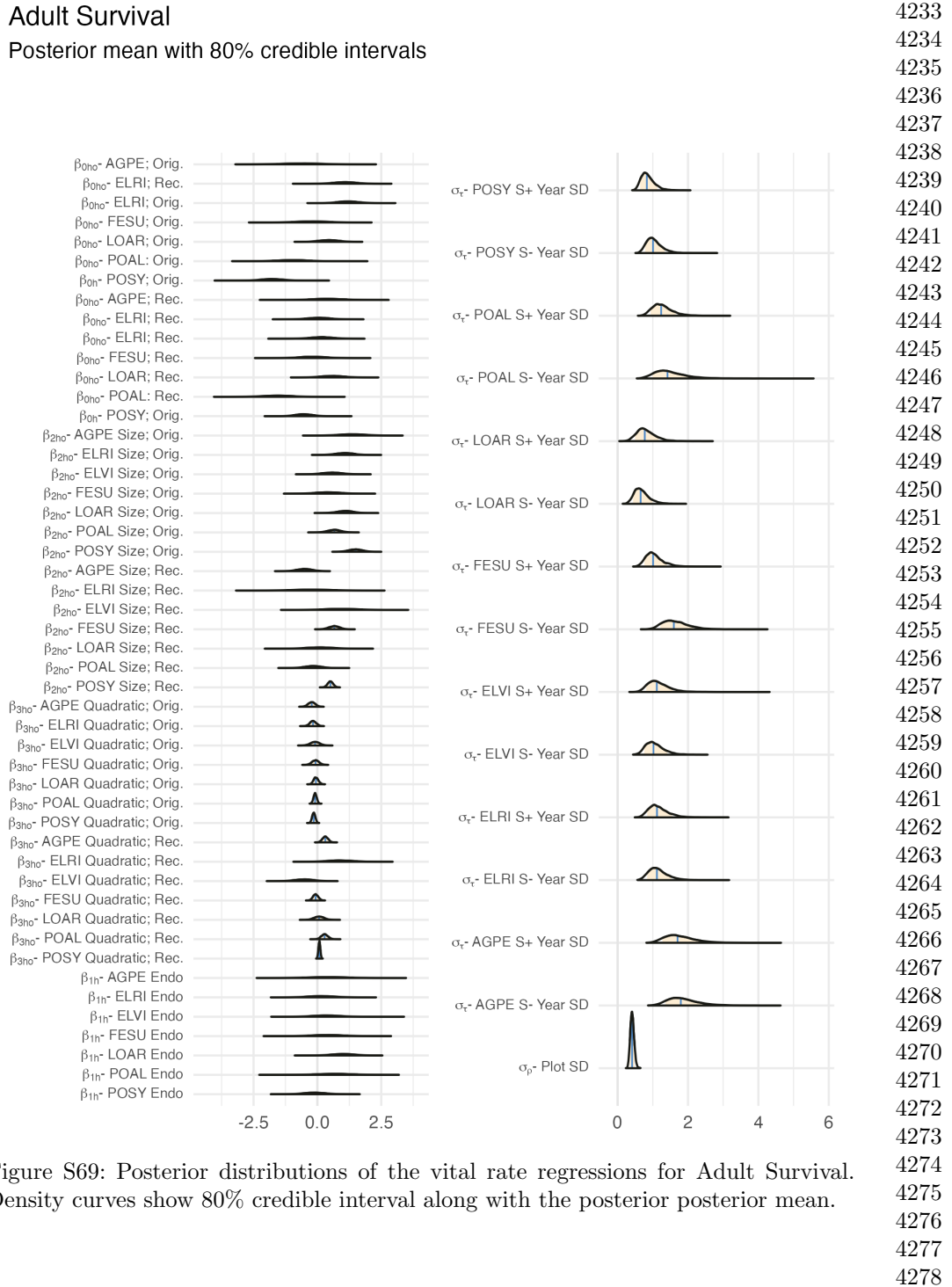
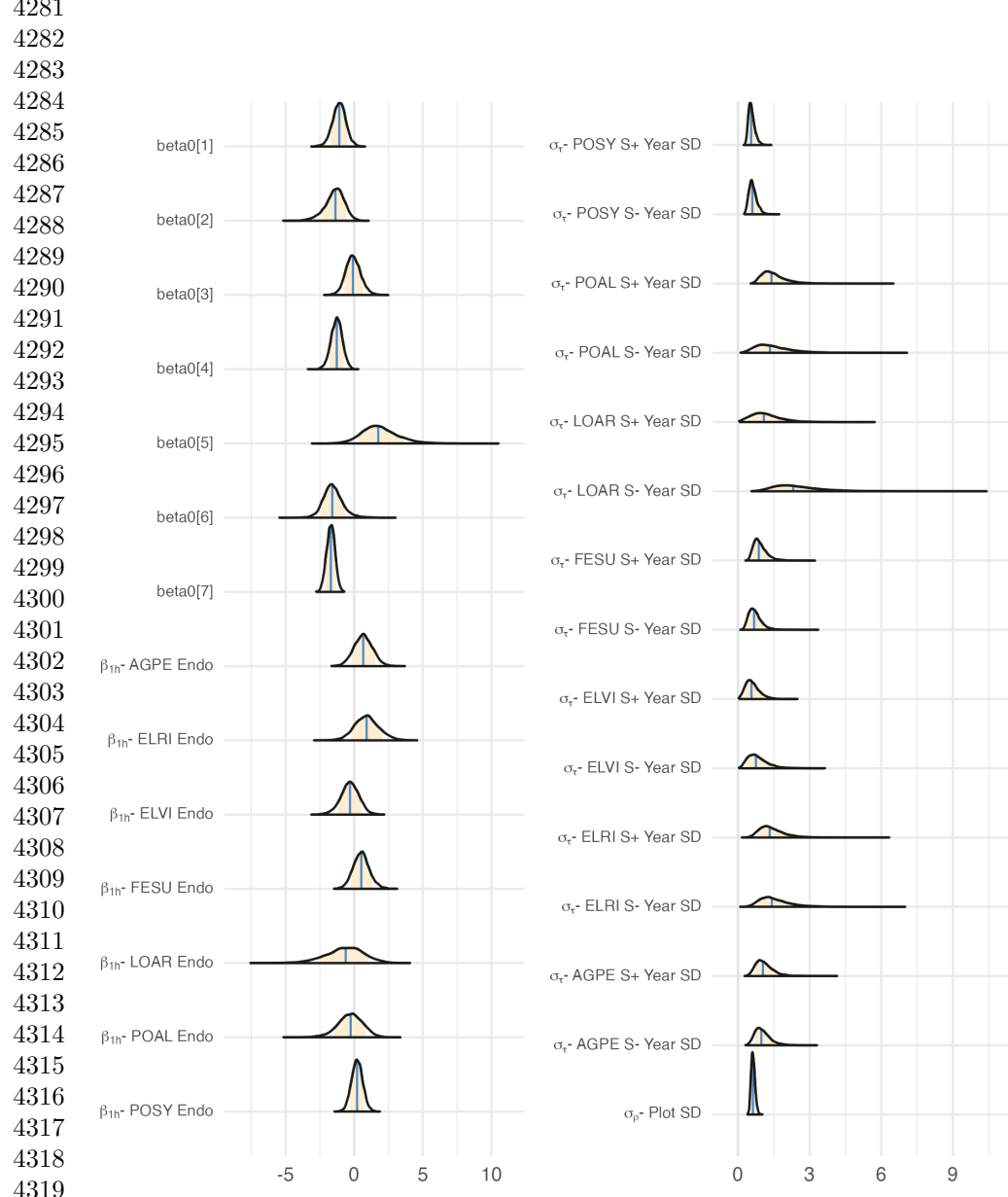


Figure S69: Posterior distributions of the vital rate regressions for Adult Survival. Density curves show 80% credible interval along with the posterior posterior mean.

4279 Seedling Survival
4280 Posterior mean with 80% credible intervals



4320 Figure S70: Posterior distributions of the vital rate regressions for Seedling Survival.
4321 Density curves show 80% credible interval along with the posterior posterior mean.
4322
4323
4324

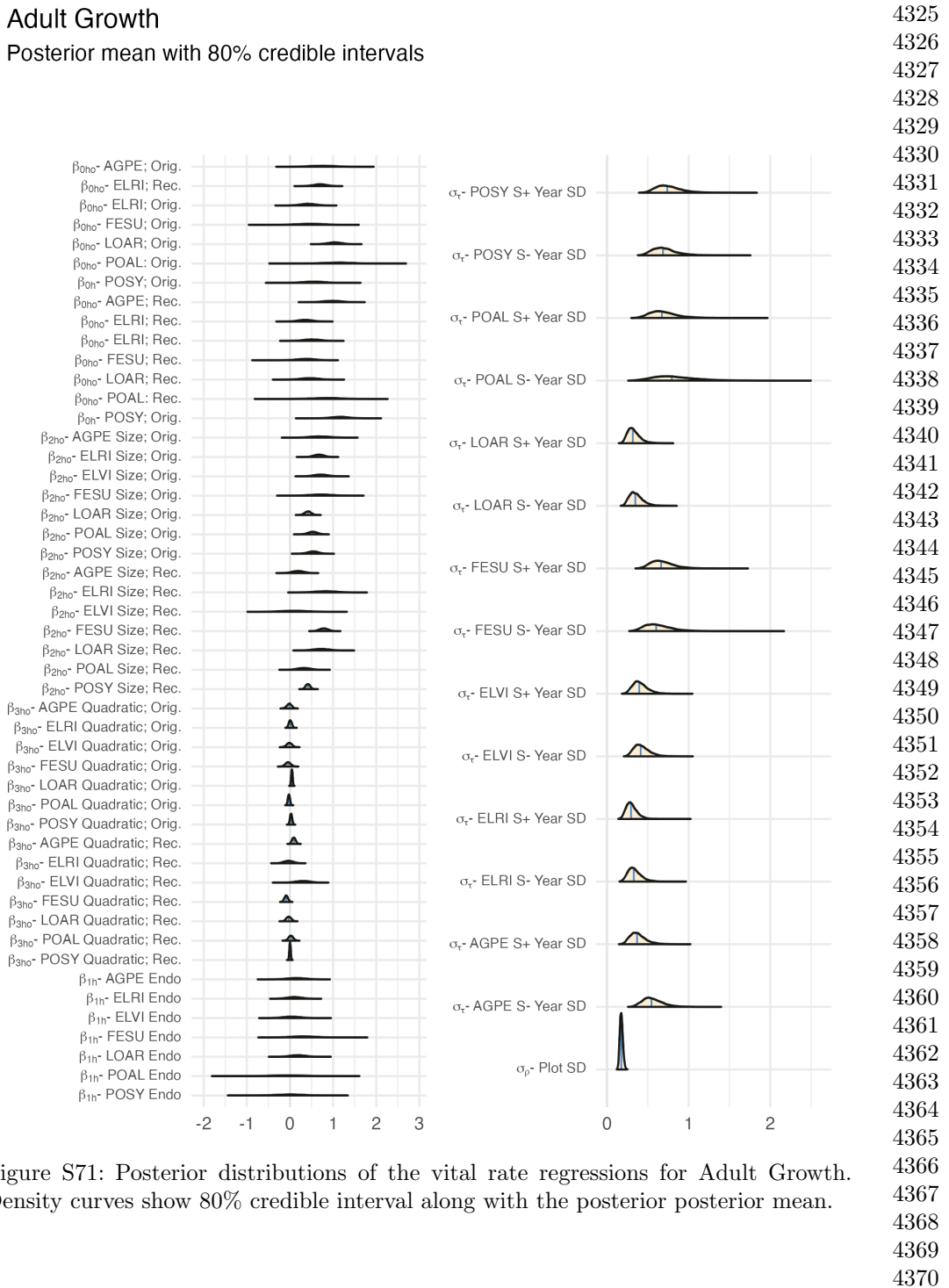
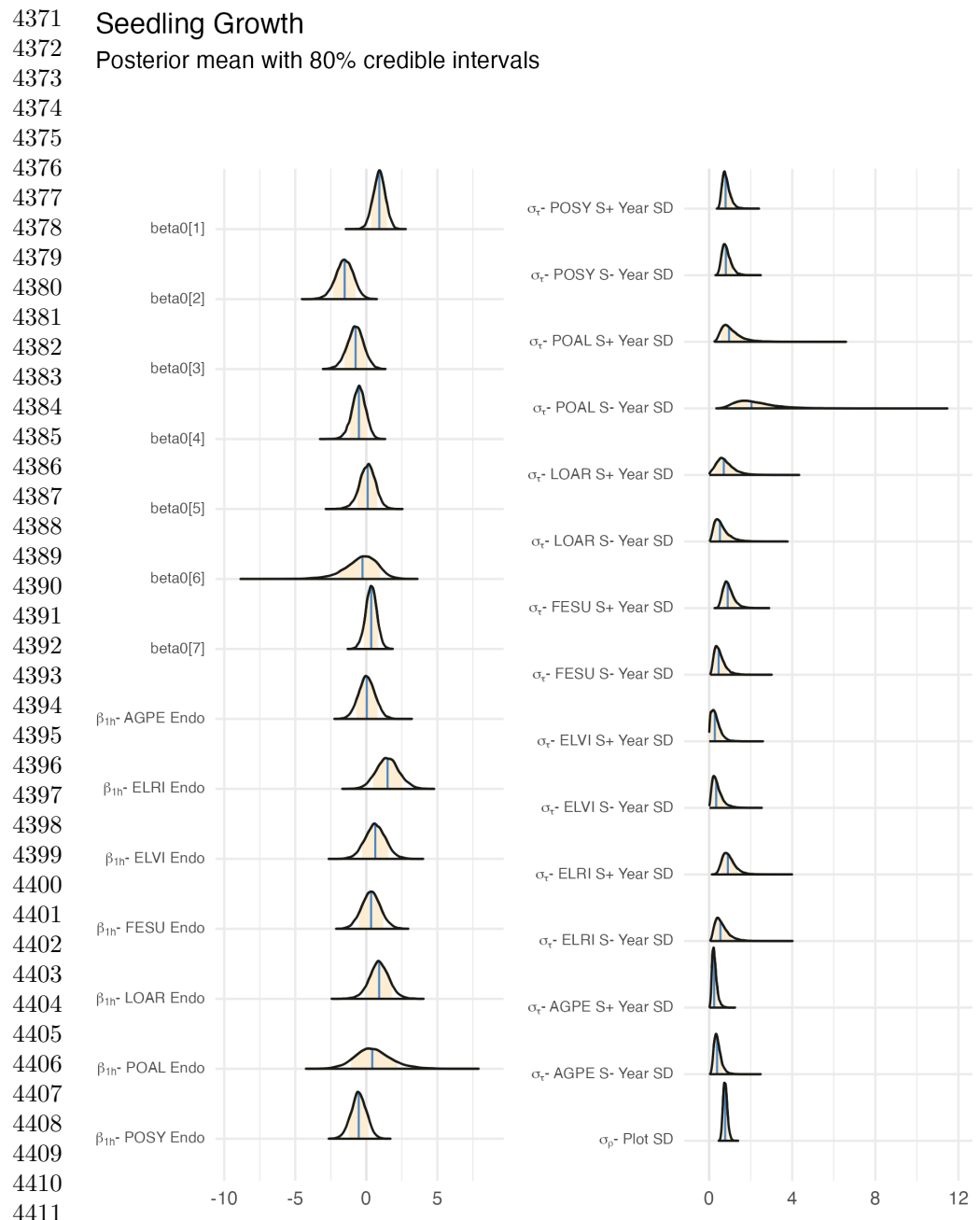


Figure S71: Posterior distributions of the vital rate regressions for Adult Growth. Density curves show 80% credible interval along with the posterior posterior mean.



4412 Figure S72: Posterior distributions of the vital rate regressions for Seedling Growth.
 4413 Density curves show 80% credible interval along with the posterior posterior mean.
 4414
 4415
 4416

Flowering Probability

Posterior mean with 80% credible intervals

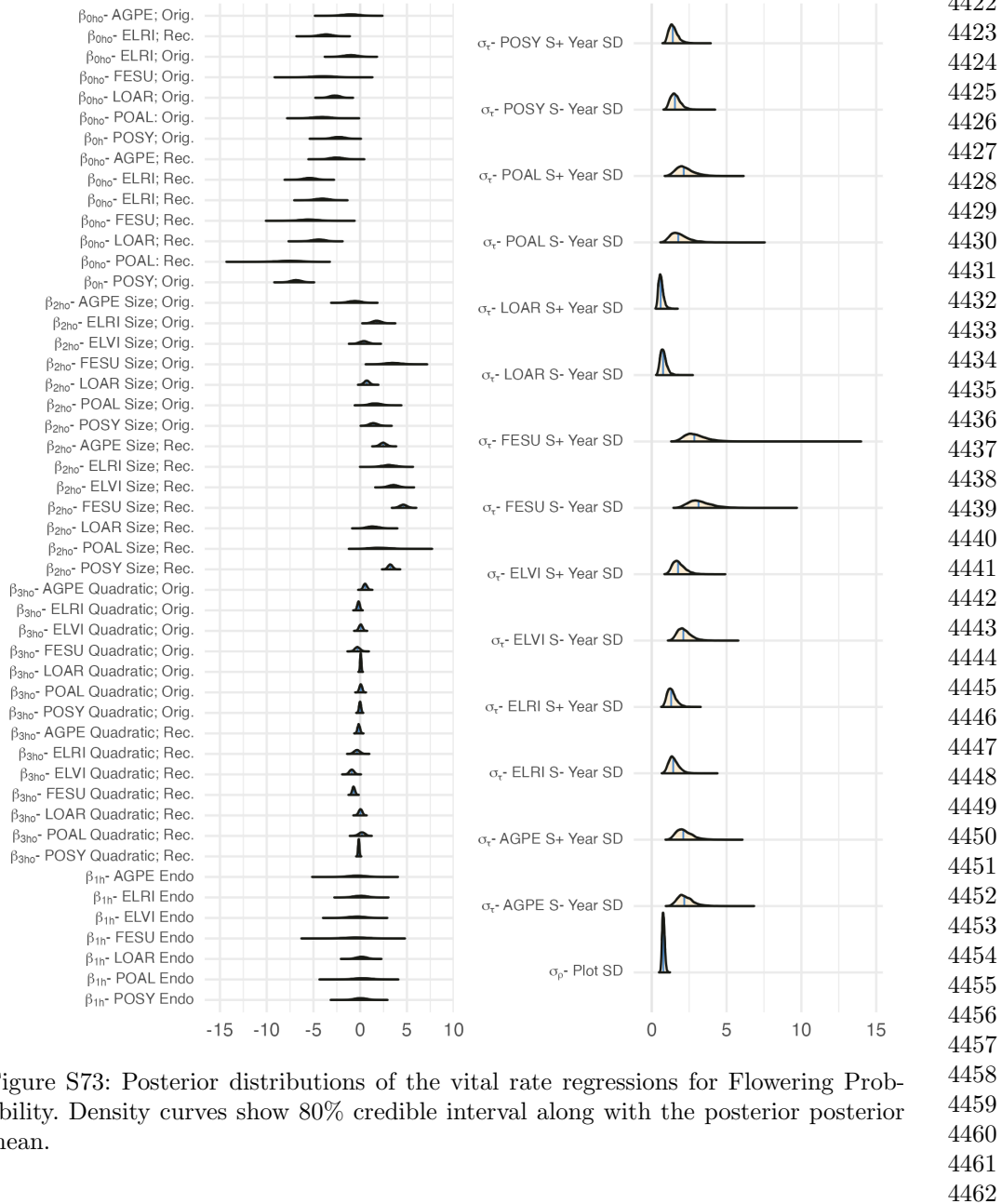


Figure S73: Posterior distributions of the vital rate regressions for Flowering Probability. Density curves show 80% credible interval along with the posterior posterior mean.

4463 Infl. Production

4464 Posterior mean with 80% credible intervals

4465

4466

4467

4468

β_{0ho} - AGPE; Orig.

4469 β_{0ho} - ELRI; Rec.

4470 β_{0ho} - ELRI; Orig.

4471 β_{0ho} - FESU; Orig.

4472 β_{0ho} - LOAR; Orig.

4473 β_{0ho} - POAL; Orig.

4474 β_{0ho} - POSY; Orig.

4475 β_{0ho} - AGPE; Rec.

4476 β_{0ho} - ELRI; Rec.

4477 β_{0ho} - FESU; Rec.

4478 β_{0ho} - LOAR; Rec.

4479 β_{0ho} - POAL; Rec.

4480 β_{0ho} - POSY; Rec.

4481 β_{2ho} - AGPE Size; Orig.

4482 β_{2ho} - ELRI Size; Orig.

4483 β_{2ho} - ELVI Size; Orig.

4484 β_{2ho} - FESU Size; Orig.

4485 β_{2ho} - LOAR Size; Orig.

4486 β_{2ho} - POAL Size; Orig.

4487 β_{2ho} - POSY Size; Orig.

4488 β_{3ho} - AGPE Quadratic; Orig.

4489 β_{3ho} - ELRI Quadratic; Orig.

4490 β_{3ho} - ELVI Quadratic; Orig.

4491 β_{3ho} - FESU Quadratic; Orig.

4492 β_{3ho} - LOAR Quadratic; Orig.

4493 β_{3ho} - POAL Quadratic; Orig.

4494 β_{3ho} - POSY Quadratic; Orig.

4495 β_{3ho} - AGPE Quadratic; Rec.

4496 β_{3ho} - ELRI Quadratic; Rec.

4497 β_{3ho} - ELVI Quadratic; Rec.

4498 β_{3ho} - FESU Quadratic; Rec.

4499 β_{3ho} - LOAR Quadratic; Rec.

4500 β_{3ho} - POAL Quadratic; Rec.

4501 β_{3ho} - POSY Quadratic; Rec.

4502 β_{1h} - AGPE Endo

4503 β_{1h} - ELRI Endo

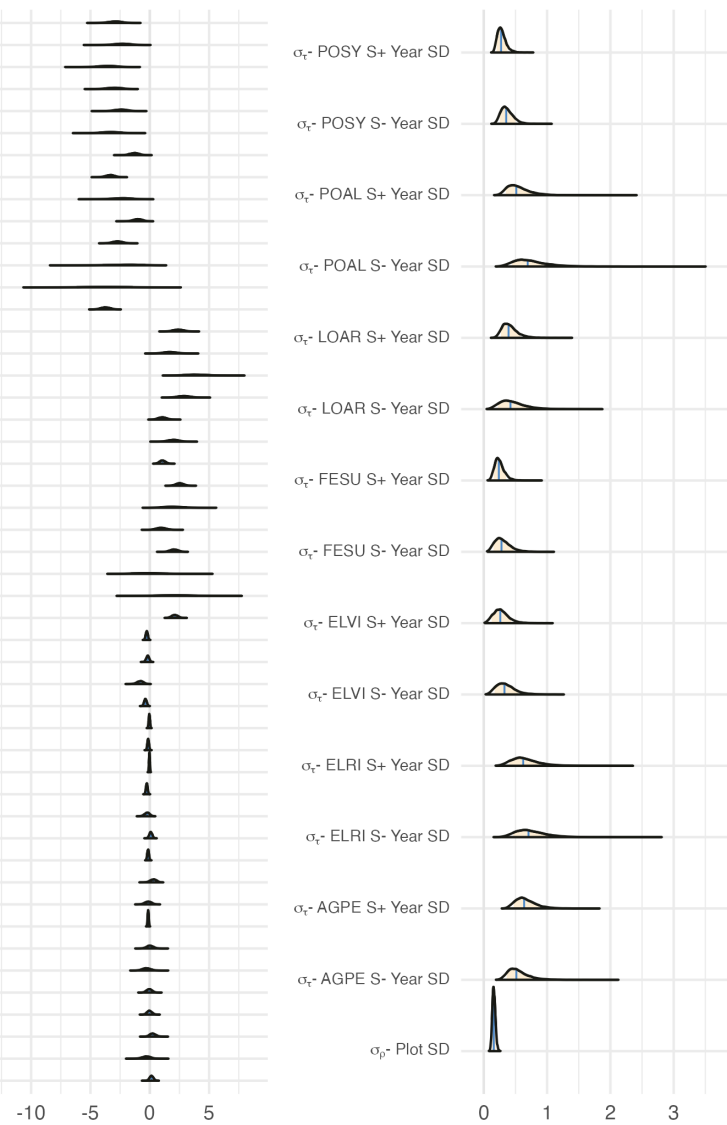
4504 β_{1h} - ELVI Endo

4505 β_{1h} - FESU Endo

4506 β_{1h} - LOAR Endo

4507 β_{1h} - POAL Endo

4508 β_{1h} - POSY Endo



4504 Figure S74: Posterior distributions of the vital rate regressions for Inflorescence Production. Density curves show 80% credible interval along with the posterior posterior mean.

4507

4508

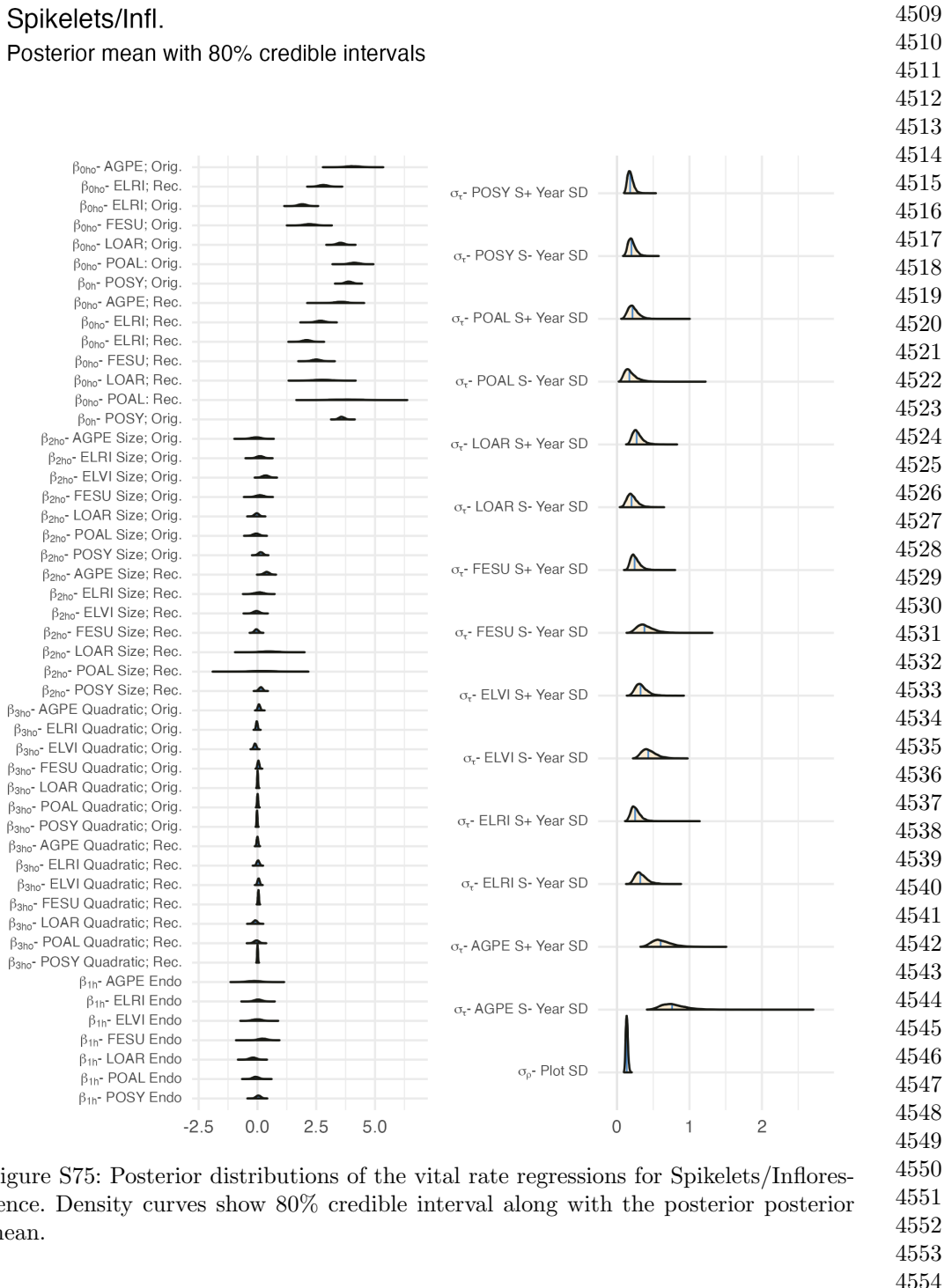
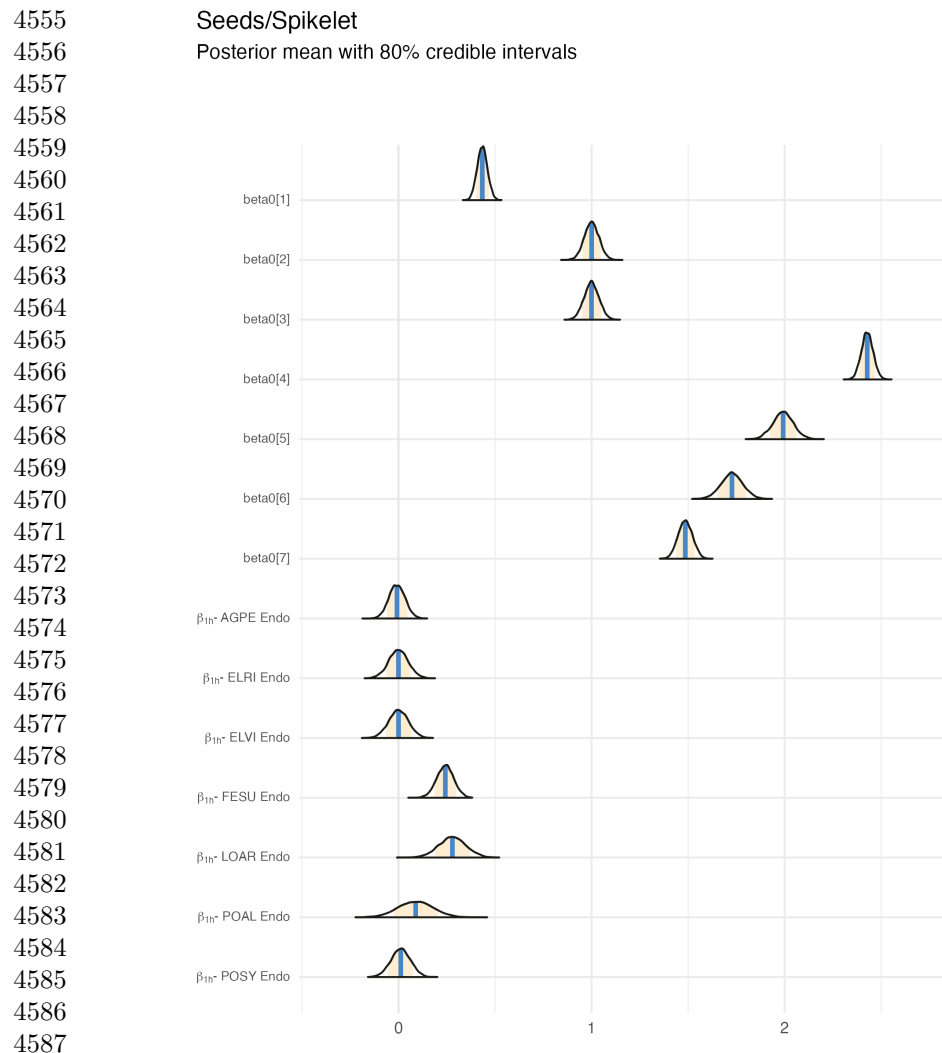


Figure S75: Posterior distributions of the vital rate regressions for Spikelets/Inflorescence. Density curves show 80% credible interval along with the posterior posterior mean.



4588 Figure S76: Posterior distributions of the vital rate regressions for Seeds/Spikelet.
 4589 Density curves show 80% credible interval along with the posterior posterior mean.

4590
 4591
 4592
 4593
 4594
 4595
 4596
 4597
 4598
 4599
 4600

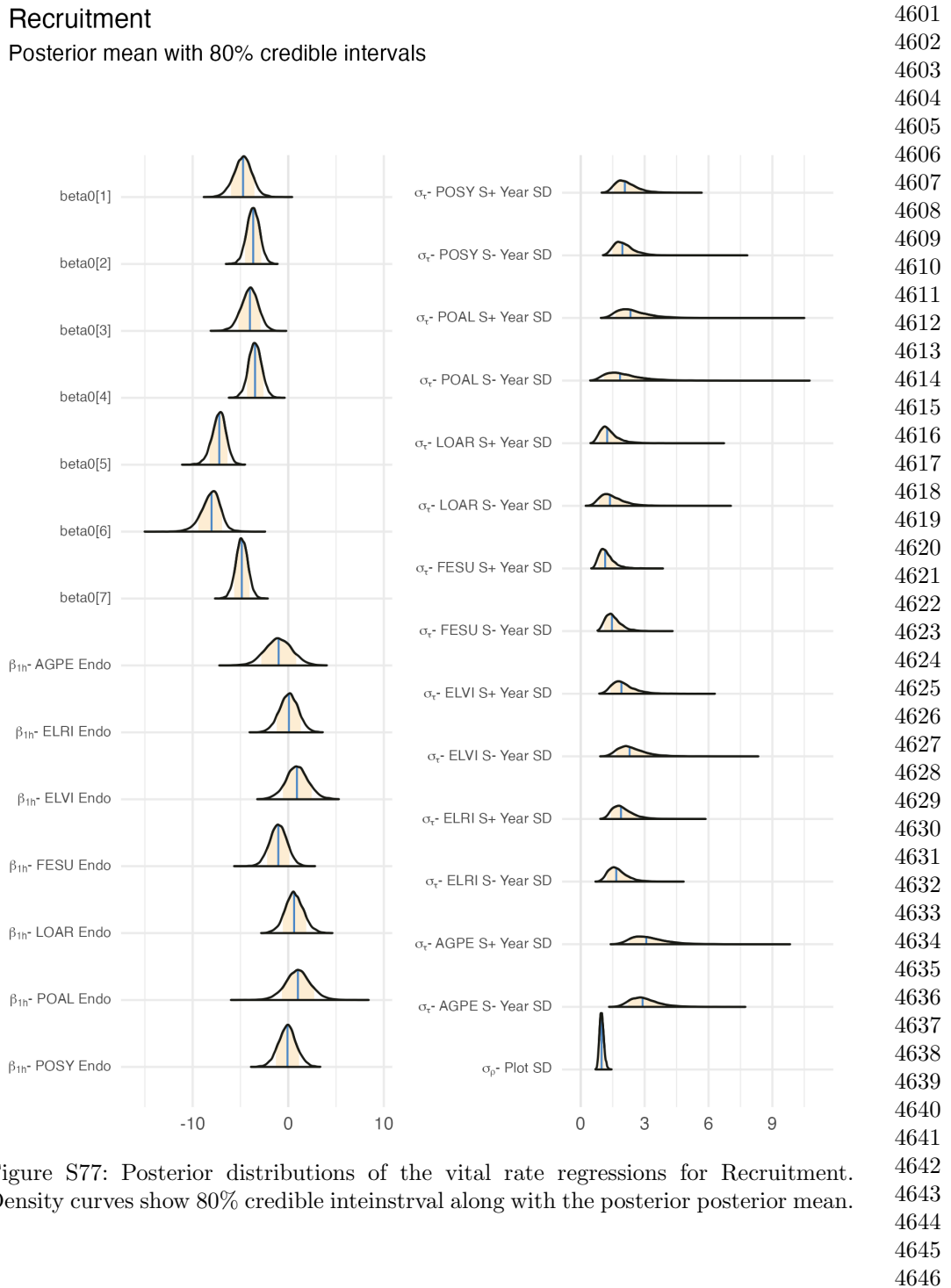
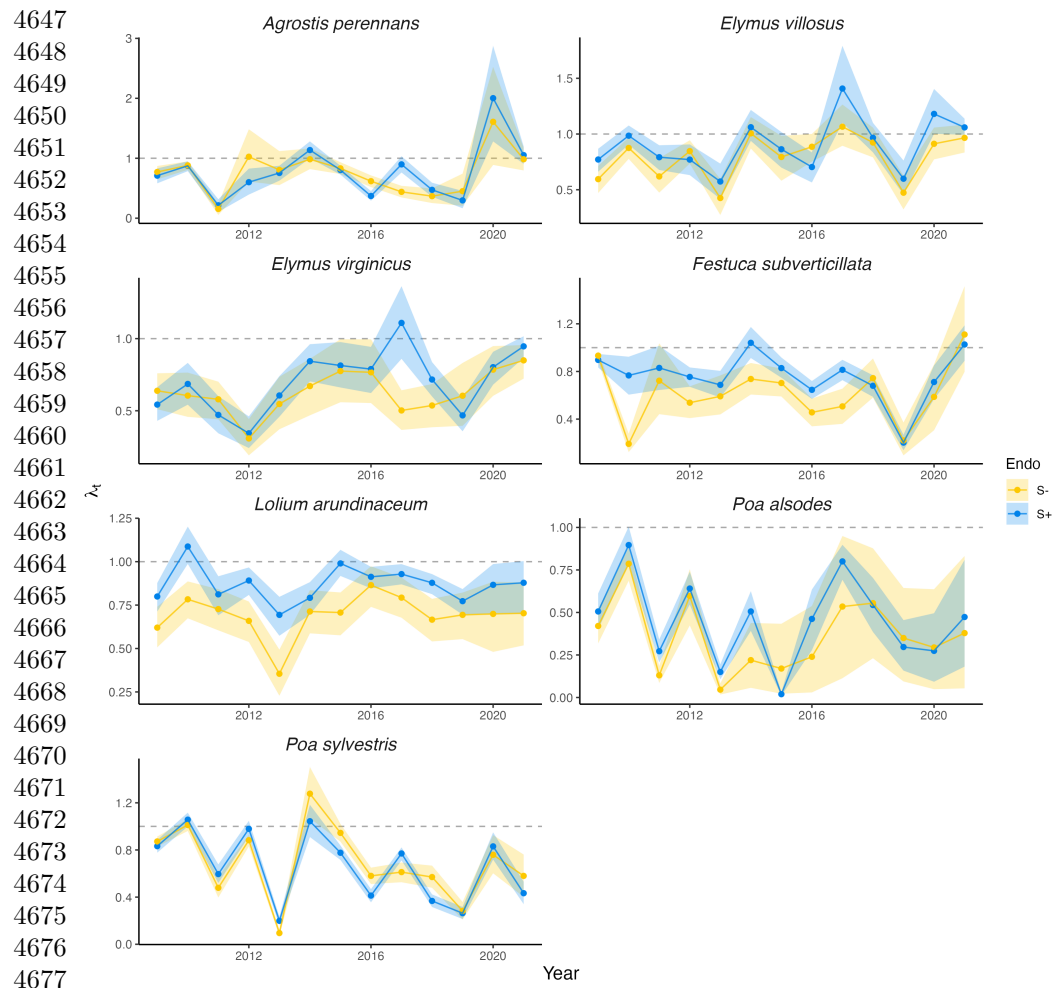


Figure S77: Posterior distributions of the vital rate regressions for Recruitment. Density curves show 80% credible interval along with the posterior mean.



4678 Figure S78: Annual growth rate values (λ_t) over thirteen years. Mean values for symbiotic (blue) and symbiont-free (yellow) population growth rates are shown along with 4679 80% credible intervals. Dashed line at $\lambda_t = 1$ indicates stable population growth rate. 4680 All values are calculated from matrix models representing recruit plants.

4681
4682
4683
4684
4685
4686
4687
4688
4689
4690
4691
4692

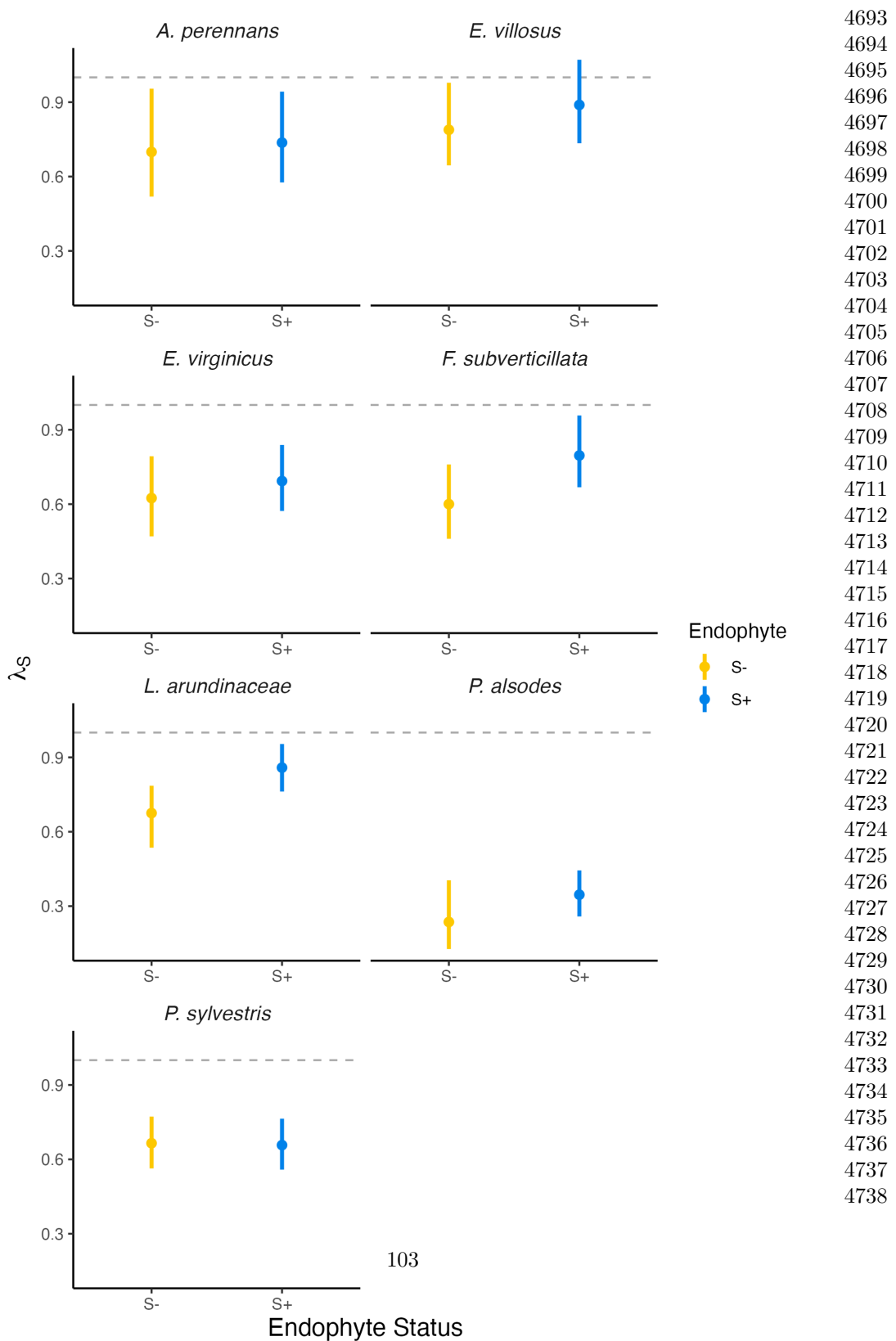
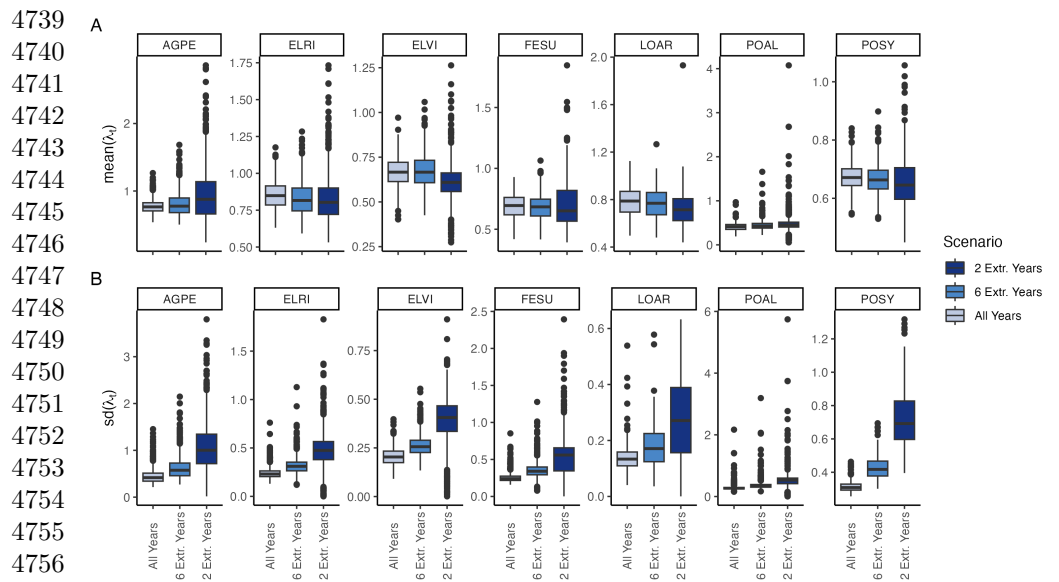


Figure S79: Stochastic population growth rates (λ_S) for symbiotic (blue) and symbiont-free (yellow) populations. Points show posterior medians along with the 95% credible interval and posterior medians. All values are calculated from matrix models representing recruit plants.



4758 Figure S80: (A) Mean and (B) standard deviation of annual growth rate values during
 4759 simulation scenarios. Each scenario selects from observed transition matrixes, increasing
 4760 the variance by selecting either all observed years, or a set (6 or 2 years) that have
 4761 the highest and lowest growth rates for symbiont-free populations.

4762
 4763
 4764
 4765
 4766
 4767
 4768
 4769
 4770
 4771
 4772
 4773
 4774
 4775
 4776
 4777
 4778
 4779
 4780
 4781
 4782
 4783
 4784

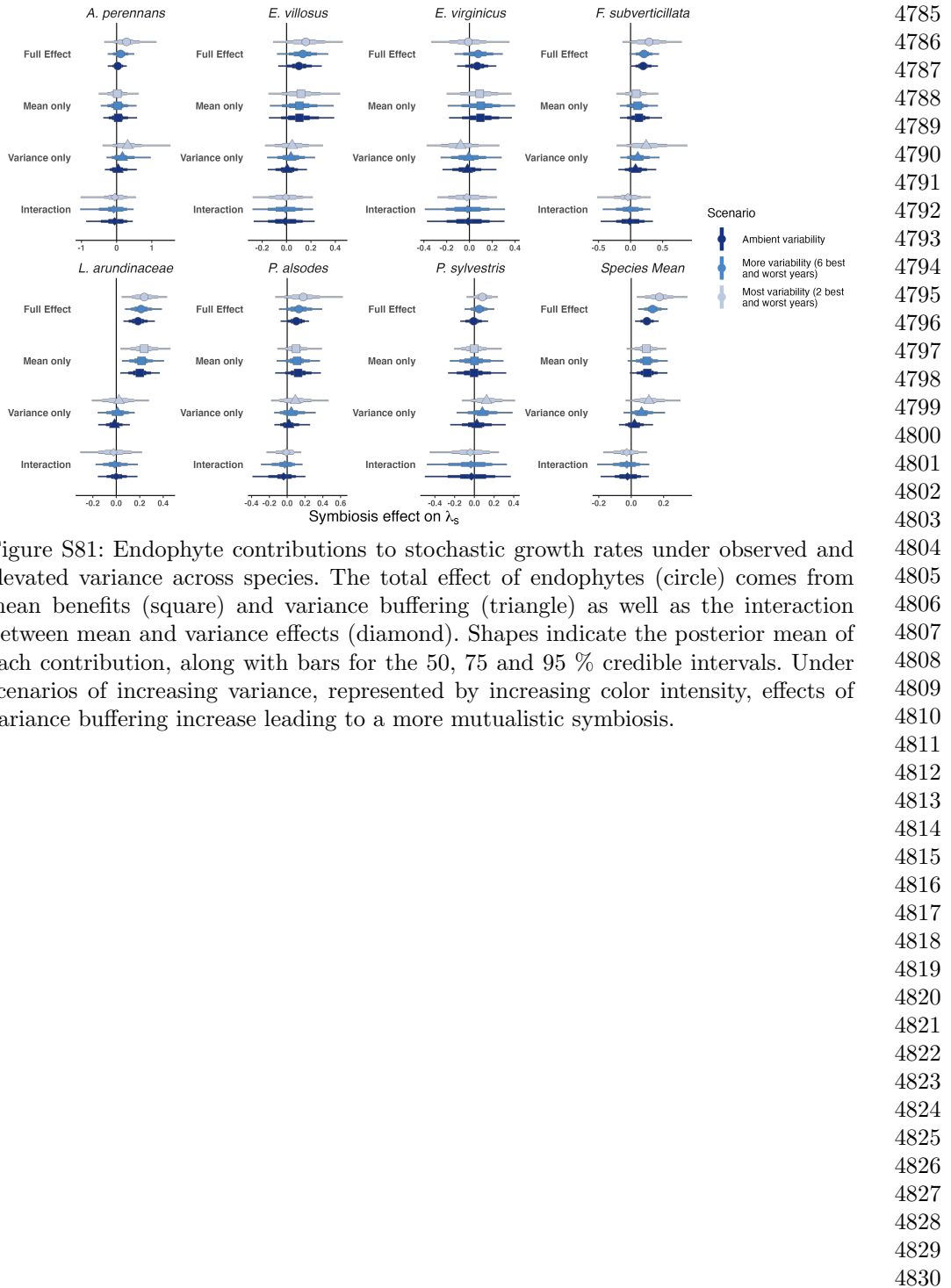
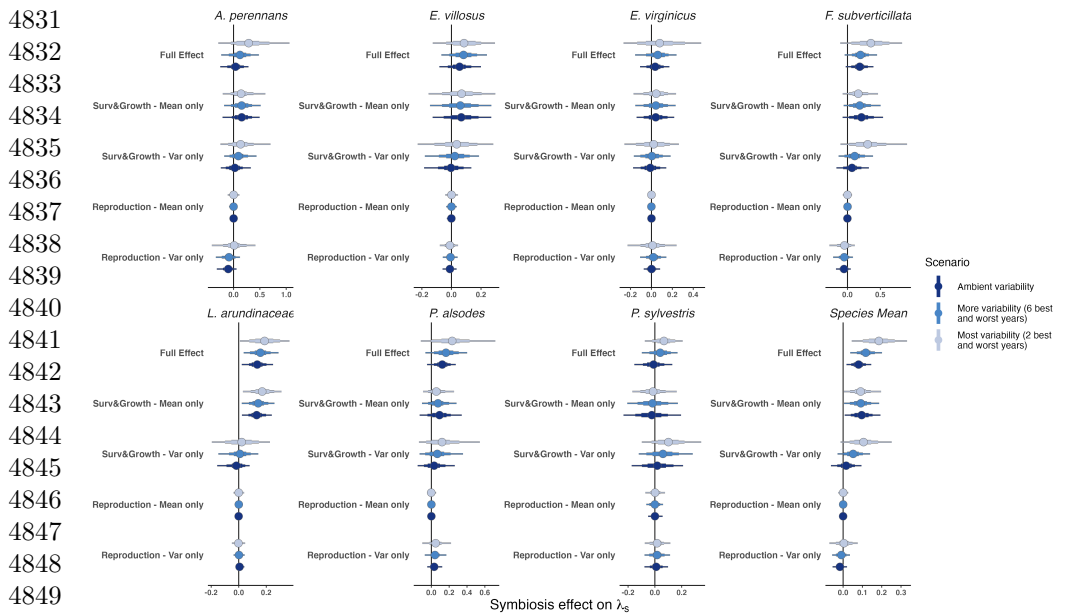


Figure S81: Endophyte contributions to stochastic growth rates under observed and elevated variance across species. The total effect of endophytes (circle) comes from mean benefits (square) and variance buffering (triangle) as well as the interaction between mean and variance effects (diamond). Shapes indicate the posterior mean of each contribution, along with bars for the 50, 75 and 95 % credible intervals. Under scenarios of increasing variance, represented by increasing color intensity, effects of variance buffering increase leading to a more mutualistic symbiosis.



4831
4832
4833
4834
4835
4836
4837
4838
4839
4840
4841
4842
4843
4844
4845
4846
4847
4848
4849
4850
4851
4852
4853
4854
4855
4856
4857
4858
4859
4860
4861
4862
4863
4864
4865
4866
4867
4868
4869
4870
4871
4872
4873
4874
4875
4876

Figure S82: Vital rate decomposition of endophyte contributions to stochastic growth rates under observed and elevated variance across species. The total effect of endophytes comes from mean and variance effects across vital rates, but are primarily driver by effect on survival and growth, rather than vital rates associated with reproduction. Circles indicate the posterior mean of each contribution, along with bars for the 50, 75 and 95 % credible intervals. Under scenarios of increasing variance, represented by increasing color intensity, effects of variance buffering increase leading to a more mutualistic symbiosis.

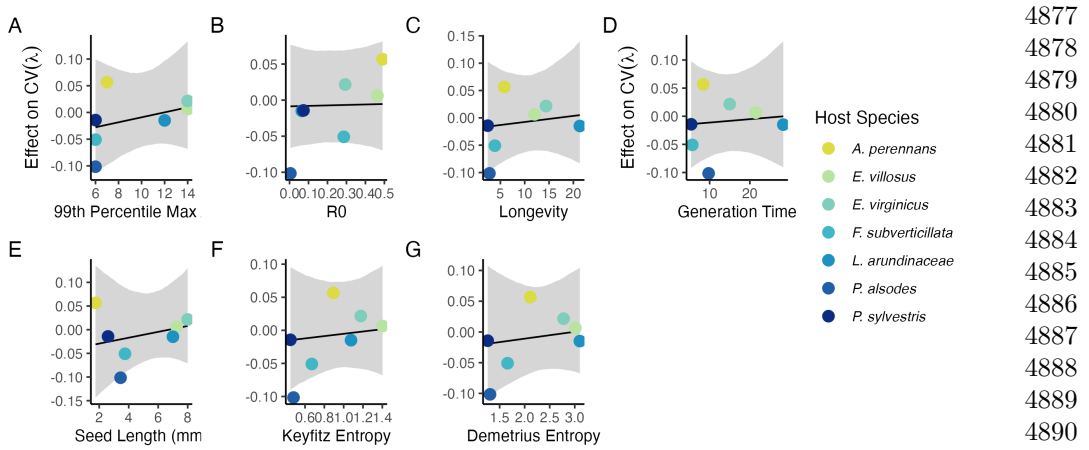


Figure S83: Relationship between variance buffering and life history traits describing the fast-slow life history continuum accounting for phylogenetic covariance between grass host species. Regressions between life history traits describing the fast-slow life history continuum ((A) 99th percentile maximum age observed during long term censuses in years; (B) Net reproductive rate; (C) Longevity; (D) Generation time in years; (G) Seed size) and the effect of endophyte symbiosis on the coefficient of variation in population growth rate (λ). Each panel shows the fitted mean relationship (line) along with the 95% credible interval.

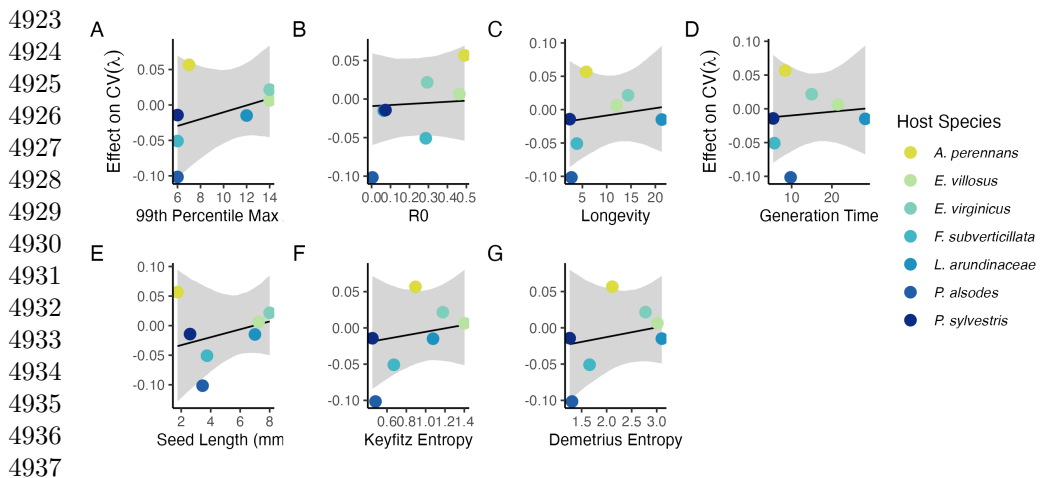


Figure S84: Relationship between variance buffering and life history traits describing the fast-slow life history continuum accounting for phylogenetic covariance between *Epichloë* symbionts. Regressions between life history traits describing the fast-slow life history continuum ((A) 99th percentile maximum age observed during long term censuses in years; (B) Net reproductive rate; (C) Longevity; (D) Generation time in years; (G) Seed size) and the effect of endophyte symbiosis on the coefficient of variation in population growth rate (λ). Results are similar to regressions accounting for host plant phylogeny (Fig. S83), however symbionts are all within a single genus. Each panel shows the fitted mean relationship (line) along with the 95% credible interval.

4938
4939
4940
4941
4942
4943
4944
4945
4946
4947
4948
4949
4950
4951
4952
4953
4954
4955
4956
4957
4958
4959
4960
4961
4962
4963
4964
4965
4966
4967
4968

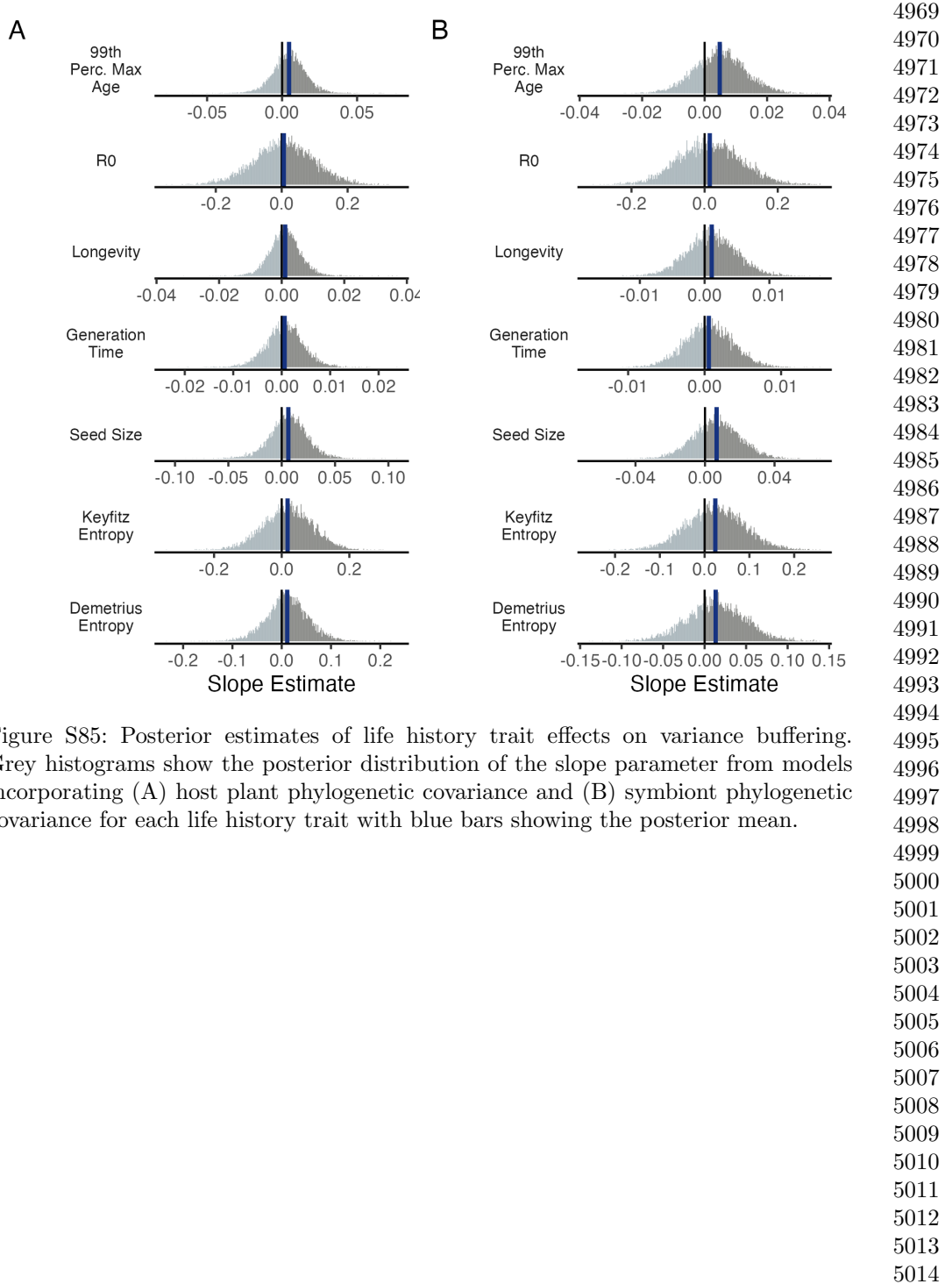
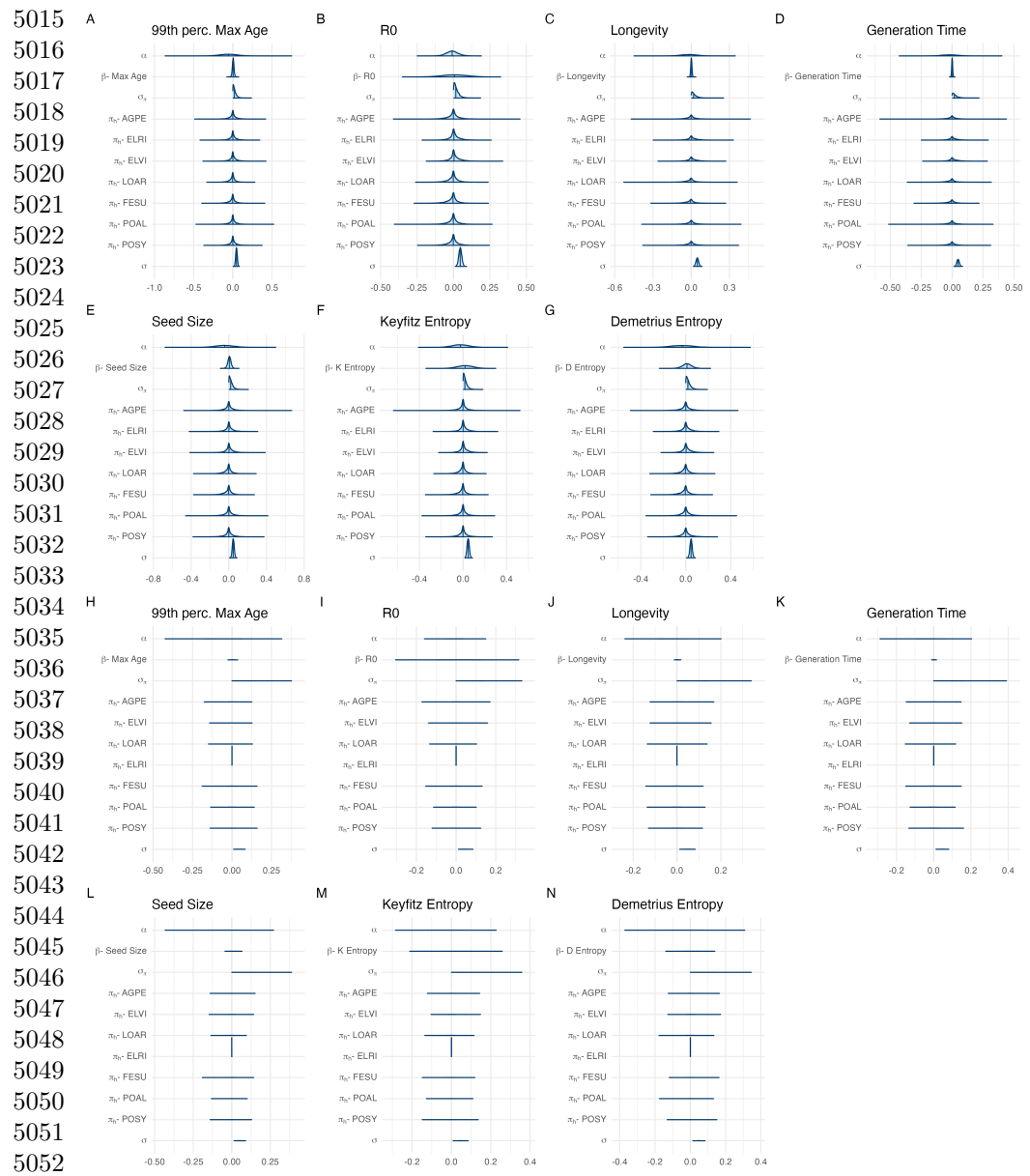


Figure S85: Posterior estimates of life history trait effects on variance buffering. Grey histograms show the posterior distribution of the slope parameter from models incorporating (A) host plant phylogenetic covariance and (B) symbiont phylogenetic covariance for each life history trait with blue bars showing the posterior mean.



5053 Figure S86: Posterior distributions of the life history trait regressions. Panels show
5054 parameter estimates from phylogenetic models incorporating host phylogenetic covari-
5055 ance (A-G) and for symbiont phylogenetic covariance (H-N). Density curves show 80%
5056 credible interval along with the posterior mean.

5057
5058
5059
5060

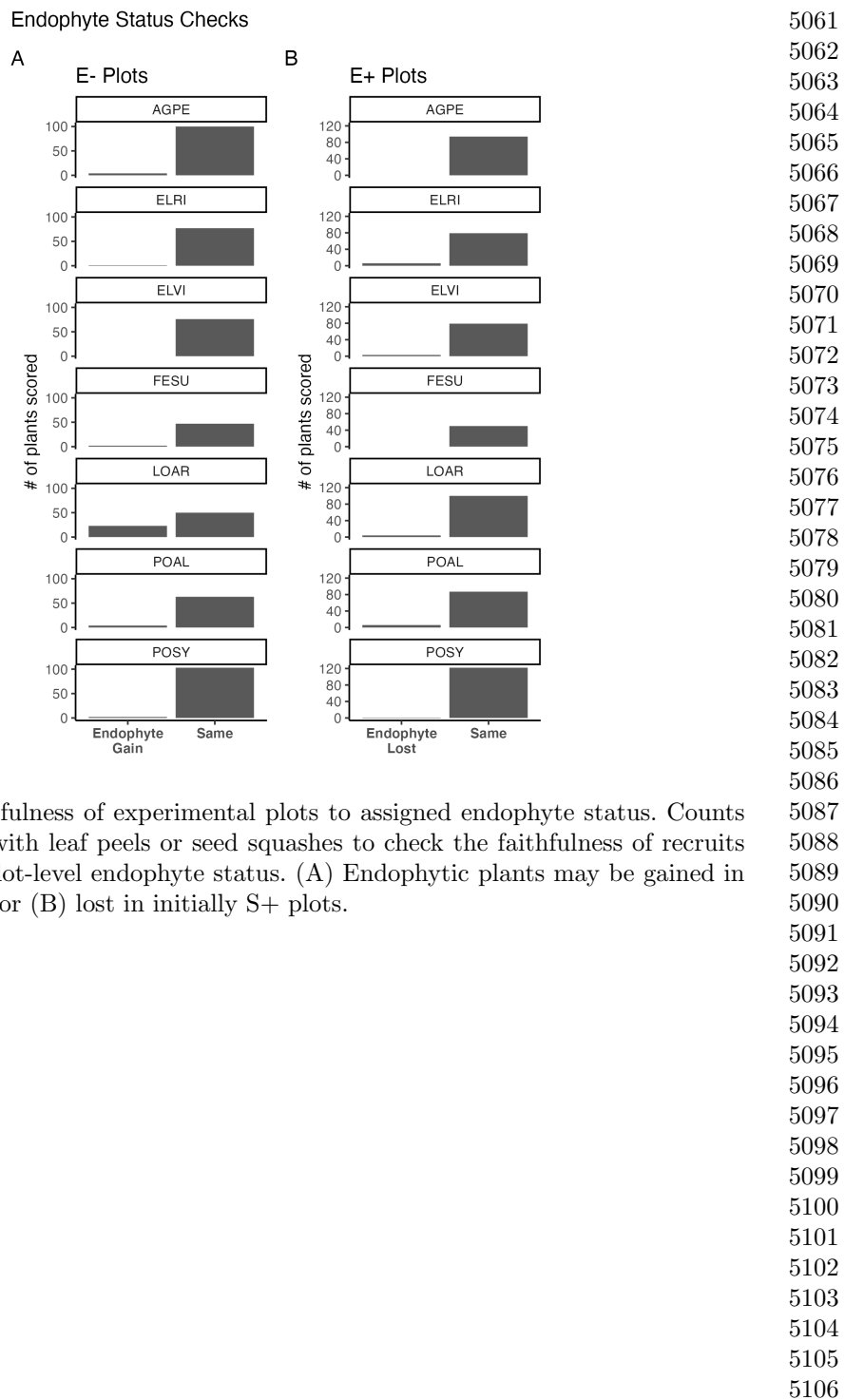
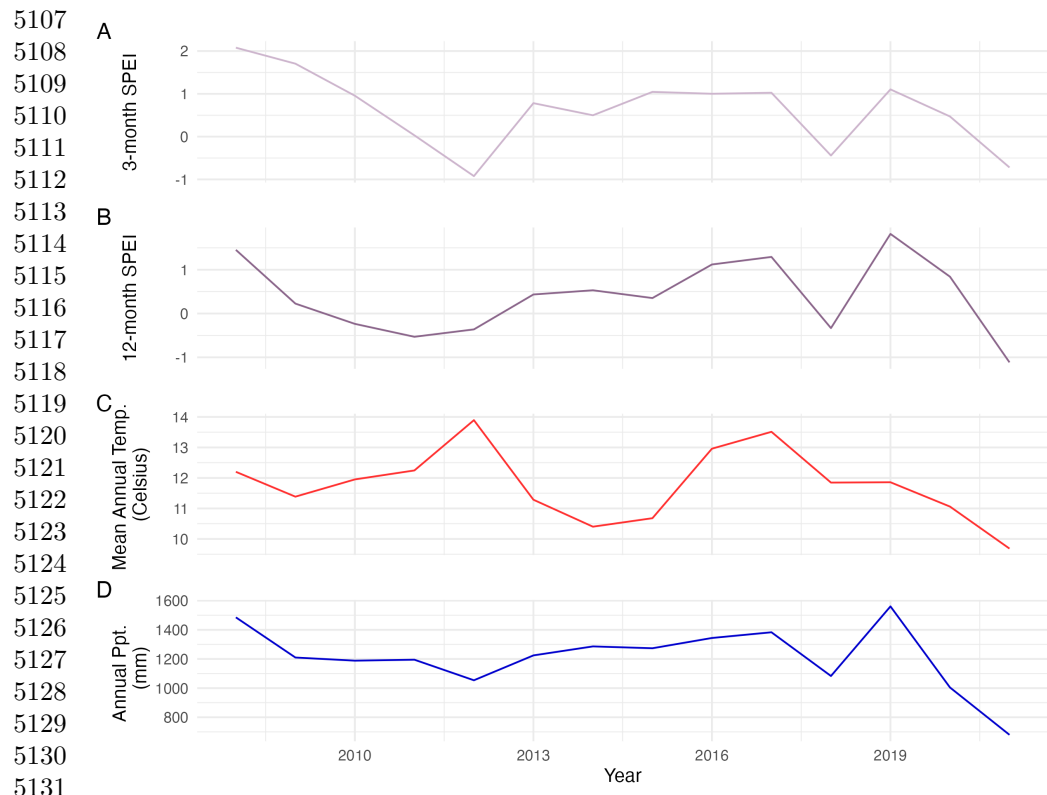


Figure S87: Faithfulness of experimental plots to assigned endophyte status. Counts of plants scored with leaf peels or seed squashes to check the faithfulness of recruits to the assigned plot-level endophyte status. (A) Endophytic plants may be gained in initially S- plots, or (B) lost in initially S+ plots.



5132 Figure S88: Weather station time-series for Bloomington, IN. The Seasonal
 5133 Precipitation-Evapotranspiration Index (SPEI) calculated for the (A) three month
 5134 growing season and (B) annually from daily weather station observations of (C)
 5135 average temperatures and (D) cumulative precipitation. Climatic data shown are
 5136 determined by the census year centered on the month of July.

5137
 5138
 5139
 5140
 5141
 5142
 5143
 5144
 5145
 5146
 5147
 5148
 5149
 5150
 5151
 5152

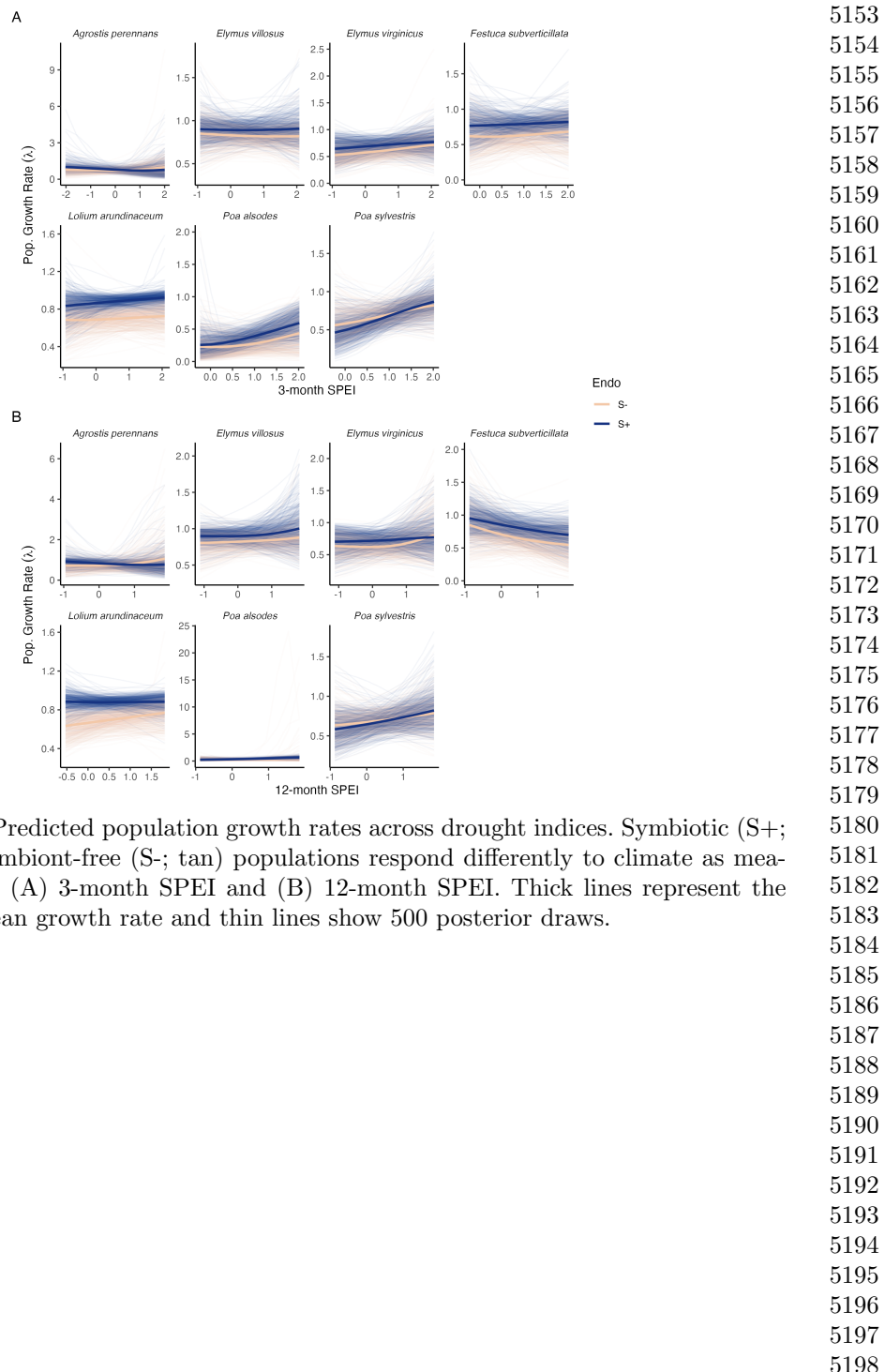


Figure S89: Predicted population growth rates across drought indices. Symbiotic (S+; blue) and symbiont-free (S-; tan) populations respond differently to climate as measured by the (A) 3-month SPEI and (B) 12-month SPEI. Thick lines represent the predicted mean growth rate and thin lines show 500 posterior draws.

5199	Supplemental Tables S1-S3
5200	
5201	
5202	
5203	
5204	
5205	
5206	
5207	
5208	
5209	
5210	
5211	
5212	
5213	
5214	
5215	
5216	
5217	
5218	
5219	
5220	
5221	
5222	
5223	
5224	
5225	
5226	
5227	
5228	
5229	
5230	
5231	
5232	
5233	
5234	
5235	
5236	
5237	
5238	
5239	
5240	
5241	
5242	
5243	
5244	

Table S1: Summary of host-endophyte propositing and transplant methods

Host Species	Symbiont Species	Heat treatment duration (Temp.)	Transplant date
<i>Agrostis perennans</i>	<i>E. amarillans</i>	12 min. hot water bath (60 °C)	April 2008 (10 plots)
<i>Elymus villosus</i>	<i>E. elymi</i>	6 days drying oven (60 °C)	April 2008 (10 plots)
<i>Elymus virginicus</i>	<i>E. elymi</i> or <i>EviTG-1</i>	6 days drying oven (60 °C)	April 2008 (10 plots)
<i>Festuca subverticillata</i>	<i>E. starrii</i>	6 days drying oven (60 °C)	April 2008 (10 plots)
<i>Lolium arundinaceum</i>	<i>E. coenophiala</i>	6 days drying oven (60 °C)	Sept. 2007 (10 plots)
<i>Poa alsodes</i>	<i>E. alsodes</i>	7 days drying oven (60 °C)	Sept. 2007 (8 plots)/April 2008 (10 plots)
<i>Poa sylvestris</i>	<i>E. PsytTG-1</i>	7 days drying oven (60 °C)	Sept. 2007 (8 plots)/April 2008 (10 plots)
			5245
			5246
			5247
			5248
			5249
			5250
			5251
			5252
			5253
			5254
			5255
			5256
			5257
			5258
			5259
			5260
			5261
			5262
			5263
			5264
			5265
			5266
			5267
			5268
			5269
			5270
			5271
			5272
			5273
			5274
			5275
			5276
			5277
			5278
			5279
			5280
			5281
			5282
			5283
			5284
			5285
			5286
			5287
			5288
			5289
			5290

5291
 5292
 5293
 5294
 5295
 5296
 5297
 5298
 5299
 5300
 5301
 5302
 5303
 5304
 5305
 5306
 5307
 5308
 5309
 5310
 5311
 5312
 5313
 5314
 5315
 5316
 5317
 5318
 5319
 5320
 5321
 5322
 5323
 5324
 5325
 5326
 5327
 5328
 5329
 5330
 5331
 5332
 5333
 5334
 5335
 5336

Table S2: Summary of focal life history traits

Host Species	Observed max age (years)	99th percentile max age (years)	Generation time (years)	R_0	Longevity (years)	Seed length (mm.)	Keyfitz Entropy	Demetrios Entropy	Imperfect transmission rate (%)	Observed Stromata (% of individ. per species)
<i>Agrostis perennans</i>	11	7	7.6	0.58	6.4	1.75	0.9	2.1	69.8	0.0
<i>Elymus villosus</i>	14	14	20.7	0.35	9.8	7.25	1.3	2.9	100	4.6
<i>Elymus virginicus</i>	14	14	13.4	0.25	12.5	8	1.1	2.6	100	0.6
<i>Festuca subverticillata</i>	9	6	6.6	0.28	4.3	3.75	0.8	1.8	42.7	0.0
<i>Lolium arundinaceum</i>	12*	12*	27.4	0.08	21.3	7	1.1	3.1	100	0.0
<i>Poa alsodes</i>	8	6	9.2	0.003	2.6	3.45	0.5	1.2	99.9	0.0
<i>Poa sylvestris</i>	12	6	8.0	0.14	3.2	2.6	0.7	1.8	16.6	0.1
Pagei's λ -host	—	0.23	0.22	0.19	0.23	0.23	0.19	0.22	—	—
Pagei's λ -host (90% CI)	—	(0-0.8)	(0-0.8)	(0-0.7)	(0-0.8)	(0-0.8)	(0-0.8)	(0-0.8)	—	—
Pagei's λ -symbiont	—	0.57	0.56	0.56	0.56	0.56	0.55	0.58	—	—
Pagei's λ -symbiont(90% CI)	—	(0-0.9)	(0-0.9)	(0-0.9)	(0-0.9)	(0-0.9)	(0-0.9)	(0-0.9)	—	—

*Censuses for *L. arundinaceum* plots stopped after year 12 of the experiment.

Table S3: Summary of host-endophyte drought sensitivities

Host Species	Effect on CV(λ)	Effect on Mean(λ)	$\frac{\Delta\lambda^-}{\Delta SPEI_3}$	$\frac{\Delta\lambda^+}{\Delta SPEI_3}$	3 month S- to S+ ratio	$\frac{\Delta\lambda^-}{\Delta SPEI_{12}}$	$\frac{\Delta\lambda^+}{\Delta SPEI_{12}}$	12 month S- to S+ ratio
<i>Agrostis perennans</i>	0.0475	0.0513	-0.06	0.05	0.83	-0.05	0.119	2.34
<i>Elymus villosus</i>	0.0105	0.0710	0.00	-0.01	5.89	0.05	0.03	0.74
<i>Elymus virginicus</i>	0.031	0.0913	0.04	0.06	1.56	0.02	0.06	2.41
<i>Festuca subverticillata</i>	-0.1524	0.1386	0.02	0.03	1.15	-0.09	-0.11	1.20
<i>Lolium arundinaceum</i>	-0.0799	0.1872	0.02	0.01	0.47	-0.00	0.05	111.
<i>Poa alsodes</i>	-0.6859	0.1079	0.10	0.09	0.62	0.14	0.11	0.79
<i>Poa sylvestris</i>	-0.0164	-0.0211	0.18	0.12	0.64	0.09	0.06	0.64

5337
5338
5339
5340
5341
5342
5343
5344
5345
5346
5347
5348
5349
5350
5351
5352
5353
5354
5355
5356
5357
5358
5359
5360
5361
5362
5363
5364
5365
5366
5367
5368
5369
5370
5371
5372
5373
5374
5375
5376
5377
5378
5379
5380
5381
5382

5383
5384
5385
5386
5387
5388
5389
5390
5391
5392
5393
5394
5395
5396
5397
5398
5399
5400
5401
5402
5403
5404
5405
5406
5407
5408
5409
5410
5411
5412
5413
5414
5415
5416
5417
5418
5419
5420
5421
5422
5423
5424
5425
5426
5427
5428